

**Standard Title Page - Report on Federally Funded Project**

1. Report No. FHWA/VTRC 05-CR20		2. Government Accession No.		3. Recipient's Catalog No.	
4. Title and Subtitle Investigation of Long-Term Prestress Losses In Pretensioned High Performance Concrete Girders				5. Report Date June 2005	
				6. Performing Organization Code	
7. Author(s) T. E. Cousins				8. Performing Organization Report No. VTRC 05-CR20	
9. Performing Organization and Address  Virginia Transportation Research Council 530 Edgemont Road Charlottesville, VA 22903				10. Work Unit No. (TRAIS)	
				11. Contract or Grant No. 59300	
12. Sponsoring Agencies' Name and Address  Virginia Department of Transportation      FHWA 1401 E. Broad Street                              P.O. Box 10249 Richmond, VA 23219                                Richmond, VA 23240				13. Type of Report and Period Covered Final Report August 2001 through June 2005	
				14. Sponsoring Agency Code	
15. Supplementary Notes					
16. Abstract <p>Effective determination of long-term prestress losses is important in the design of prestressed concrete bridges. Over-predicting prestress losses results in an overly conservative design for service load stresses, and under-predicting prestress losses, can result in cracking at service loads. Creep and shrinkage produce the most significant time-dependent effect on prestress losses, and research has shown that high performance and high strength concretes (HPC and HSC) exhibit less creep and shrinkage than conventional concrete. For this reason, the majority of traditional creep and shrinkage models and methods for estimating prestress losses, over-predict the prestress losses of HPC and HSC girders.</p> <p>Nine HPC girders, with design compressive strengths ranging from 8,000 psi to 10,000 psi, and three 8,000 psi lightweight HPC (HPLWC) girders were instrumented to determine the changes in strain and prestress losses. Several creep and shrinkage models were used to model the instrumented girders. For the HPLWC, each model over-predicted the long-term strains, and the Shams and Kahn model was the best predictor of the measured strains. For the normal weight HPC, the models under-estimated the measured strains at early ages and over-estimated the measured strains at later ages, and the B3 model was the best-predictor of the measured strains. The PCI-BDM model was the most consistent model across all of the instrumented girders.</p> <p>Several methods for estimating prestress losses were also investigated. The methods correlated to high strength concrete, the PCI-BDM and NCHRP 496 methods, predicted the total losses more accurately than the methods provided in the AASHTO Specifications. The newer methods over-predicted the total losses of the HPLWC girders by no more than 8 ksi, and although they under-predicted the total losses of the normal weight HPC girders, they did so by less than 5 ksi.</p>					
17 Key Words Prestress, bridge, girders, high-performance concrete, lightweight concrete, shrinkage, creep			18. Distribution Statement No restrictions. This document is available to the public through NTIS, Springfield, VA 22161.		
19. Security Classif. (of this report) Unclassified		20. Security Classif. (of this page) Unclassified		21. No. of Pages 70	22. Price

**FINAL CONTRACT REPORT**

**INVESTIGATION OF LONG-TERM PRESTRESS LOSSES IN PRETENSIONED  
HIGH PERFORMANCE CONCRETE GIRDERS**

**T. E. Cousins, Associate Professor  
Via Department of Civil and Environmental Engineering  
Virginia Polytechnic Institute & State University**

*Project Manager*

Jose P. Gomez, Ph.D., P.E., Virginia Transportation Research Council

Contract Research Sponsored by  
Virginia Transportation Research Council

Virginia Transportation Research Council  
(A Cooperative Organization Sponsored Jointly by the  
Virginia Department of Transportation and  
the University of Virginia)

Charlottesville, Virginia

June 2005  
VTRC 05-CR20

## **NOTICE**

The project that is the subject of this report was done under contract for the Virginia Department of Transportation, Virginia Transportation Research Council. The contents of this report reflect the views of the author, who is responsible for the facts and the accuracy of the data presented herein. The contents do not necessarily reflect the official views or policies of the Virginia Department of Transportation, the Commonwealth Transportation Board, or the Federal Highway Administration. This report does not constitute a standard, specification, or regulation.

Each contract report is peer reviewed and accepted for publication by Research Council staff with expertise in related technical areas. Final editing and proofreading of the report are performed by the contractor.

Copyright 2005 by the Commonwealth of Virginia.

## ABSTRACT

Effective determination of long-term prestress losses is important in the design of prestressed concrete bridges. Over-predicting prestress losses results in an overly conservative design for service load stresses, and under-predicting prestress losses, can result in cracking at service loads. Creep and shrinkage produce the most significant time-dependent effect on prestress losses, and research has shown that high performance and high strength concretes (HPC and HSC) exhibit less creep and shrinkage than conventional concrete. For this reason, the majority of traditional creep and shrinkage models and methods for estimating prestress losses, over-predict the prestress losses of HPC and HSC girders.

Nine HPC girders, with design compressive strengths ranging from 8,000 psi to 10,000 psi, and three 8,000 psi lightweight HPC (HPLWC) girders were instrumented to determine the changes in strain and prestress losses. Several creep and shrinkage models were used to model the instrumented girders. For the HPLWC, each model over-predicted the long-term strains, and the Shams and Kahn model was the best predictor of the measured strains. For the normal weight HPC, the models under-estimated the measured strains at early ages and over-estimated the measured strains at later ages, and the B3 model was the best-predictor of the measured strains. The PCI-BDM model was the most consistent model across all of the instrumented girders.

Several methods for estimating prestress losses were also investigated. The methods correlated to high strength concrete, the PCI-BDM and NCHRP 496 methods, predicted the total losses more accurately than the methods provided in the AASHTO Specifications. The newer methods over-predicted the total losses of the HPLWC girders by no more than 8 ksi, and although they under-predicted the total losses of the normal weight HPC girders, they did so by less than 5 ksi.

## INTRODUCTION

In recent years, long-term durability has become a major concern in the design and specification of bridge structures. As a result, high performance concrete (HPC) has gained popularity and has achieved widespread use throughout the United States. HPC is generally defined as any concrete that is more durable than conventional concrete. The Federal Highway Administration (FHWA) defines HPC as concrete that has been designed to be more durable and, if necessary, stronger than conventional concrete, while the American Concrete Institute (ACI) defines HPC as concrete meeting special combinations of performance and uniformity requirements that cannot always be achieved routinely with conventional constituents and normal mixing, placing, and curing practices.

The increased durability and strength of HPC are generally achieved through the use of chemical and mineral admixtures. The primary admixtures used in HPC in Virginia are water reducers, air entrainers, and pozzolanic and supplemental cementitious materials such as fly ash, ground granulated blast furnace slag, and microsilica. The water reducers (normal and high range) allow a reduction in the water-to-cementitious materials ratio to increase the concrete strength without sacrificing the fluidity and workability of the concrete mix. Air entrainers form microscopic bubbles in the cement paste during mixing, which improves the freeze-thaw durability of the hardened cement paste. The pozzolanic materials have the general effect of densifying the cement paste resulting in increased strength, reduced void ratio and permeability, and increased long-term durability.

Virginia has undertaken several projects to investigate the advantages of HPC and high strength concrete (HSC). These projects included the design and construction of two bridges. The Richlands Bridge (Ozyildirim and Gomez, 1999) demonstrated the use of normal weight HPC, while the Chickahominy River Bridge (Nassar, 2002) demonstrated the use of lightweight HPC. These projects examined several of the design and implementation issues relating to HPC; however, prestress losses were generally ignored and design recommendations for conventional concrete were applied to these bridges for determination of prestress losses.

This study investigates the long-term losses for two bridges in Virginia constructed utilizing normal weight HPC and one bridge utilizing lightweight HPC. The measured long-term losses are compared to losses determined from the AASHTO Standard (AASHTO, 1996) and LRFD (AASHTO, 1998) Specifications, the PCI Bridge Design Manual (BDM) (PCI-1997), PCI Committee on Prestress Losses (PCI, 1975), and NCHRP Report 496 (Tadros et al., 2003), as well as several creep and shrinkage models including ACI-209 (ACI, 1992), CEB-FIP MC90 (CEB, 1990), PCI-BDM, B3 (Bazant and Baweja, 1995a, b, c), GL2000 (Gardner and Lockman, 2001), AFREM (Le Roy et al., 1996), AASHTO LRFD, Shams and Kahn (2000), and NCHRP Report 496. These specification and model comparisons are then used to provide design recommendations for the determination of prestress losses for Virginia's HPC. In conjunction with this project, creep and shrinkage studies of the HPC mixes used in the three bridges of this project were conducted at Virginia Tech. The results from these studies are also used in modeling prestress losses to aid in the determination of a correlation between standard creep and shrinkage results and field performance.

## **Motivations**

Effective determination of long-term prestress losses is an integral part of the design of prestressed concrete bridges. Elimination of cracking at service loads controls the design of many prestressed girders, and prestress losses directly influence the service load stresses. An over-prediction in prestress losses results in an overly conservative design for service load stresses, while an under-prediction in prestress losses, depending on the severity of the under-prediction, could result in significant cracking at service loads. An over-prediction of prestress losses can also cause further design inefficiencies by limiting the span length of a girder, and by requiring a larger initial prestressing force to resist the applied loads, which, in turn, produces excessive camber.

Initial research studies have shown that HPC tends to exhibit less creep and shrinkage than does conventional concrete. The reduced creep and shrinkage tends to reduce the total long-term prestress losses below that exhibited by conventional concrete. The current creep and shrinkage models used by the AASHTO Specifications were developed for conventional concrete; therefore, they should be unreliable in predicting the creep and shrinkage characteristics, and in turn, the long-term prestress losses of HPC. This study aims to determine if this is true and to provide recommendations for the determination of prestress losses for HPC girders in Virginia.

## **Prestress Losses**

Prestress losses are a reduction in the initial prestressing force in the strands (the jacking force) and can be grouped into two general categories, instantaneous losses and long-term losses. Instantaneous losses occur quickly upon release of the tendons and include anchorage slip, elastic shortening, and friction. Time-dependent losses occur more slowly over the life of the girder and include steel relaxation and concrete creep and shrinkage.

For the pretensioned girders investigated in this research, elastic shortening is the only instantaneous loss of significant importance. When the prestressing force is transferred from the end blocks of the casting bed to the girder after the concrete has sufficiently hardened, the concrete undergoes elastic shortening. This shortening, in turn, reduces the force in the prestressing strands. Elastic shortening losses are easily determined by applying the prestressing force at the time of release (the jacking force minus the appropriate amount of steel relaxation) to the transformed girder section. This is accomplished without directly calculating the transformed girder properties using a mechanics of materials approach resulting in the following equations presented in the PCI Bridge Design Manual (PCI, 1997):

$$f_{po} = \frac{f_{pi} + \frac{E_p M_{sw} \cdot e_{net}}{E_{ci} I_{cnet}}}{1 + \alpha} \quad \text{Eq. 1}$$

$$\alpha = \frac{E_p A_p}{E_{ci} A_{cnet}} \left( 1 + \frac{A_{cnet} \cdot e_{net}^2}{I_{cnet}} \right) \quad \text{Eq. 2}$$

where  $f_{po}$  is the stress in the strand after elastic shortening losses in ksi,  $f_{pi}$  is the stress in the strand at the time of release in ksi,  $E_p$  is the elastic modulus of the prestressing steel in ksi,  $E_{ci}$  is the chord elastic modulus of the concrete at the time of release in ksi,  $M_{sw}$  is the self-weight moment of the girder at midspan in k-in.,  $e_{net}$  is the eccentricity of the prestressing force at midspan relative to the centroid of the net section in in.,  $I_{cnet}$  is the net moment of inertia of the concrete girder in  $\text{in.}^4$ ,  $A_p$  is the area of the prestressing steel in  $\text{in.}^2$ , and  $A_{cnet}$  is the net cross-sectional area of the concrete girder in  $\text{in.}^2$ . This method of determining the elastic shortening losses is used throughout the research, regardless of the creep and shrinkage model being investigated.

The time-dependent losses of steel relaxation and concrete creep and shrinkage are all of significant importance in pretensioned girders. However, since the rate and extent of steel relaxation is dependent only on the type of prestressing strand used and time, a single model for steel relaxation, expressed as a function of time, is used throughout the research. The phenomenon of steel relaxation is generally well understood and is characterized by the following equation for the low-relaxation strands used in the girders in this study:

$$\Delta f_{rel} = f_{pi} \left( \frac{\log(t_n) - \log(t_r)}{45} \right) \left( \frac{f_{pi}}{f_{py}} - 0.55 \right) \quad \text{Eq. 3}$$

where  $\Delta f_{rel}$  is the loss in stress due to relaxation in ksi,  $t_n$  is the time at the end of the desired interval in hr,  $t_r$  is the time at the beginning of the desired interval in hr,  $f_{pi}$  is the strand stress at the beginning of the desired interval in ksi, and  $f_{py}$  is the yield stress of the strand in ksi. It should be noted that this equation is only valid for  $f_{pi}/f_{py}$  greater than 0.55.

## Concrete Creep

Concrete creep and shrinkage produce the most significant time-dependent effect on prestress losses. When subjected to a sustained stress concrete first deforms elastically then continues to deform for a prolonged period of time. This prolonged deformation under a sustained stress is called creep. Concrete creep may be separated into two components, basic creep and drying creep. Basic creep is the continued deformation that occurs in a sealed specimen subjected to a hydro-equilibrium environment. An unsealed specimen, one that is free to exchange moisture with the environment, experiences greater creep because of the addition of drying creep, which results from drying induced stress. In a prestressed girder, creep results in a

prolonged shortening of the girder. The prolonged shortening of the girder reduces the stress in the strands and results in a loss of prestress.

Compressive creep of concrete has been the focus of a great deal of research for quite some time, and this research has resulted in several models for concrete creep, several of which are presented later. The extent and rate of creep depends not only on time, but also on the maturity of the concrete when the load is first applied, the magnitude of the applied stress, the ambient relative humidity, the curing conditions, and the mixture proportions including the amount and type of cement, the aggregate properties, and the water-to-cement ratio.

The maturity of the concrete at the application of the applied load influences the creep characteristics of the concrete. The more mature a concrete specimen is at the application of the applied load, the better able that specimen is to resist creep. In particular, researchers have observed that HSC is more sensitive to early-age loading than is normal strength concrete (Kahn, et al., 1997).

The magnitude of the applied stress also influences the creep characteristics of concrete. ACI-209 (ACI, 1992) suggests that the amount of creep is proportional to the applied stress level for applied stresses up to 40% of the concrete strength at the time the load is applied. Other researchers (Smadi et al., 1987) have suggested that the limit of proportionality for HSC is as high as 65%. Still others (Shams and Kahn, 2000) have suggested that the creep strains are proportional to the applied stress for stresses up to 60% of the compressive strength. The maximum allowable compressive stress according the AASHTO LRFD Specifications (AASHTO, 1998) is 60% of the compressive strength of the concrete at the time of load application; therefore, the creep of HSC is generally taken as proportional to the applied stress.

The ambient relative humidity affects the amount of drying creep, and in turn, the total creep of a concrete specimen. ACI-209 (ACI, 1992) and the AASHTO LRFD Specification (AASHTO, 1998) indicate that at an ambient relative humidity of 40%, the ultimate creep coefficient is 36% higher than the ultimate creep coefficient at 80% relative humidity.

The curing conditions also affect the creep characteristics of concrete. The common practice of steam curing can reduce creep by 30% to 50% by accelerating the hydration of the cement (Neville, 1970). Kahn et al. (1997) found that air-cured specimens exhibit higher creep strains than mist-cured specimens, and Mokhtarzadeh and French (2000) found that specimens cured at higher temperatures exhibit more creep than specimens cured at lower temperatures as a result of increased porosity and internal cracking.

The concrete mixture proportions and components also significantly affect creep. The majority of concrete creep occurs in the cement paste surrounding the aggregate; therefore, the cement type significantly affects creeps. Rapid-hardening cements (Type III) exhibit less creep than slower-hardening cements because the cement matrix gains stiffness more quickly and is better able to resist creep at earlier ages (Neville, 1970). The inclusions of supplemental cementitious materials, such as ground granulated blast furnace slag (GGBFS) and microsilica also influences creep. The inclusion of GGBFS slightly decreases basic creep but increases drying creep, resulting in an increase in total creep (Chern and Chan, 1989). Conversely, the

inclusion of microsilica, in proportions below 10% by weight, decreases the total creep (Wiegrink et al., 1996).

Aggregate properties, including stiffness, size, absorption, and surface roughness also affect creep. The aggregate stiffness influences creep as the cement paste deforms and load is transferred to the aggregate. Stiffer aggregates resist more load as it is transferred from the cement paste and thus reduce creep (Alexander, 1996). Collins (1989) examined the effect of aggregate size on creep and found that concrete mixtures with 1.5 in. aggregates exhibit 15% less creep after 90 days than similar concrete mixtures with 0.75 in. aggregates. Aggregate absorption can affect creep by influencing the moisture movement in the concrete if the aggregate is not fully saturated during mixing. In this case, the aggregate may absorb water from the cement paste, increasing the amount of creep (Neville, 1970). Finally, the surface roughness of the aggregate affects creep because the aggregate-paste interface influences the aggregates' ability to resist deformation. As the cement paste creeps, load is transferred more efficiently to aggregates with a rougher surface; therefore, rougher-surface aggregates have a tendency to reduce creep (Mokhtarzadeh and French, 2000).

The ratio of water-to-cementitious materials (w/cm) in a concrete mixture significantly influences creep. Lower w/cm ratios reduce the volume of the hydrates and also reduce the free water in the concrete. Both of these characteristics have the effect of reducing creep deformations (Neville, 1970). Since the majority of the creep models were developed empirically from studies of conventional concrete mixtures, they tend to over-predict the creep associated with HPC and HSC mixtures because of the lower w/cm ratios of the HPC and HSC mixtures needed to achieve higher strength.

## **Concrete Shrinkage**

The volumetric change in a concrete specimen in the absence of load is called shrinkage. Shrinkage consists of three components, drying shrinkage, autogenous shrinkage, and carbonation. Drying shrinkage occurs when water not consumed during hydration diffuses into the environment, resulting in a decrease in the volume of the concrete specimen. Autogenous shrinkage is a result of the hydration of cement. The volume of the hydrated cement paste is smaller than the solid volume of the unhydrated cement and water. Finally, carbonation occurs when carbon dioxide from the atmosphere reacts with the calcium hydroxide in the cement paste in the presence of moisture, resulting in a decrease in the volume of the concrete specimen. Shrinkage, like creep, causes the girder to shorten over time, thus reducing the stress in the strands and causing prestress losses.

Shrinkage has been the focus of a great deal of research along with creep, and several shrinkage models have also been published. The ambient relative humidity, curing conditions, the size and shape of the specimen, and mixture proportions affect the rate and extent of shrinkage. Drying shrinkage occurs when the ambient relative humidity is less than the internal relative humidity of the concrete, as a result of water loss to the environment. Therefore, a lower ambient relative humidity will increase shrinkage. ACI-209 (ACI, 1992) and the AASHTO

LRFD Specification (AASHTO, 1998) indicate that shrinkage will increase 67% at 40% relative humidity compared to 80% relative humidity.

Researchers have found that accelerated curing using high temperatures reduces the observed shrinkage. When compared with standard curing, Mak et al. (1997) found specimens cured using heat to accelerate the curing process exhibit 75% less shrinkage, and Mokhtarzadeh and French (2000) found that specimens cured at 150 °F exhibit less shrinkage than specimens cured at 120 °F.

Since drying shrinkage is the result of water loss, the size and shape of a specimen also influence the amount of shrinkage. Thicker specimens and those with larger volume-to-surface area ratios lose less moisture to the environment than do thinner specimens or specimens with smaller volume-to-surface ratios. This is because the water near the surface of the specimen is lost quite easily; while the water in the interior of the specimen must first diffuse through the concrete before it can be lost to the environment. Therefore, larger specimens exhibit both a slower rate and a lower magnitude of shrinkage when compared to smaller specimens (Shah and Ahmad, 1994).

Finally, the mixture proportions, most notably the water content and w/cm ratio, also influence shrinkage. Lower w/cm ratios result in less free water in the concrete and, therefore, reduce drying shrinkage (Shah and Ahmad, 1994). Lower water contents result in fewer pores in the mature cement, which, in turn, results in increased rigidity of the solid matrix and lower shrinkage deformations (Smadi et al., 1987). Since many of the shrinkage models were developed empirically from data for conventional concrete mixtures, they tend to over-predict shrinkage of HPC mixtures, which typically have lower w/cm ratios.

## **LITERATURE REVIEW**

Prestress losses and the effects of concrete creep and shrinkage have been studied since the earliest days of prestressed concrete. Recently, the prediction of prestress losses, especially the models that account for the effects of creep and shrinkage have been questioned in their application to high performance and high strength concrete (HPC and HSC). Several studies have shown that the current models tend to over-predict the long-term prestress losses associated with these concretes. This over-prediction is not desired because the models are designed to predict the mean behavior of the concrete, and the design specifications do not rely on over-predicted prestress losses to insure the overall safety of the structure. In the following sections, a summary of relevant projects that have measured prestress losses for HPC or HSC are presented along with the various models for prestress losses and creep and shrinkage currently in the literature. Further details of these projects and models can be found in work by Waldron (Waldron, 2004).

### **Prestress Losses and High Performance Concrete**

Creep, shrinkage, and prestress losses in girders utilizing HPC, HSC, and normal strength concrete have been investigated in several states, including Georgia, Nebraska, New Hampshire,

Texas, Washington, Pennsylvania, Ohio, Illinois, Louisiana, and Minnesota. These projects have compared both creep and shrinkage measured in the laboratory and prestress losses measured in the field to losses determined from several creep and shrinkage models and several methods for estimating prestress losses. A summary of the projects discussed in this section and how the measured losses compare to the losses calculated using various methods for estimating prestress losses is presented in Table 1.

Several projects have investigated prestress losses in HPC, HPLWC, and HSC. In general, the losses predicted by the AASHTO Specifications, the ACI-209 committee recommendations, and the CEB-FIP recommendations over-predict the losses associated with these concretes. However, new methods are being developed, most recently that of Tadros et al. (2003), to better estimate the creep and shrinkage characteristics and, therefore, the prestress losses associated with HPC and HSC.

### **Prestress Loss Recommendations**

The following section presents the recommendations for estimating prestress losses included in the AASHTO Standard (AASHTO, 1996) and LRFD (AASHTO, 1998) Specifications, and the PCI Bridge Design Manual (PCI, 1997), as well as the recommendations of the PCI Committee on Prestress Losses (PCI, 1975), and the recommendations of NCHRP Report 496 (Tadros et al., 2003). A summary of the methods for determining prestress losses discussed in this section is presented in Table 2. In addition to listing the various methods discussed in this section, the summary indicates whether or not each method determines loss components individually or in a lump sum fashion, at what times prestress losses can be determined using the particular method, and the section in which the associated creep and shrinkage model is located, if it is required for the determination of prestress losses.

**Table 1 – Summary of Projects Investigating Prestress Losses**

Researcher	Project Location		Concrete Strength Release / Cast Deck psi	Ratio of Calculated Prestress Losses to Measured Prestress Losses						
				AASHTO LRFD Refined	AASHTO LRFD Lump Sum	AASHTO Standard	PCI 1975	PCI BDM	NCHRP 496 Est.	NCHRP 496 Refined
Shams and Kahn (2000)	Georgia (Type II)	Grade 2 HPC	12,380 / 13,430	1.58	1.65	--	--	--	--	--
		Grade 4 HPC	14,400 / 16,110	1.74	1.67	--	--	--	--	--
	Georgia (Rect. beam)	Grade 2 HPC	12,380 / 13,430	1.68	1.52					
		Grade 4 HPC	14,400 / 16,110	2.01	1.43					
Lopez et al. (2003)	Georgia (test girders)	8,000 psi LWC	7,465 / 9,084	1.42	0.93	--	--	--	--	--
		10,000 psi LWC	9,040 / 10,590	1.75	1.13	--	--	--	--	--
Tadros et al. (2003)	Albion, NE		6,250 / 9,025	1.55	1.49	--	--	1.11	1.20	1.16
	Rollinsford, NH		5,790 / 10,050	1.27	1.18	--	--	0.93	0.97	0.97
	Harris County, TX		7,230 / 10,670	2.07	1.93	--	--	1.27	1.35	1.09
	Clark County, WA		7,530 / 10,280	1.63	1.29	--	--	0.99	0.93	0.96
Greuel et al. (2000)	Cincinnati, OH		5,892 / 10,410	1.23	0.85	--	--	0.91	0.95	1.00
Pessiki et al. (1996)	Philadelphia, PA		4,772 / 7,476	1.30	1.39	--	--	1.17	0.97	0.95
Mossiossian and Gamble (1972)	Douglas County, IL		3,690 / 5,781	1.36	1.54	--	--	1.01	1.07	1.04
Kebraei et al. (1997)	Sarpy County, NE		7,856 / 12,307	1.52	1.62	--	--	0.98	0.99	0.98
Shenoy and Frantz (1991)	Eat Hartford, CT		3,380 / 5,296	1.26	1.31	--	--	1.48	1.28	1.46
Stanton et al. (2000)	Kent, WA		5,000 / 10,000	1.02	1.21	--	--	0.78	0.79	0.93
			7,400 / 10,000	1.01	0.87	--	--	0.64	0.61	0.62
Seguirant and Anderson (1998)	WA		4,436 / 6,306	1.35	1.39	--	--	1.19	0.98	1.21
Gross and Burns (1999)	Louetta, TX		7,700 / 11,600	1.98	1.56	--	--	1.22	1.23	1.05
	San Angelo, TX	Eastbound	8,050 / 13,500	1.96	1.22	--	--	1.02	1.16	0.93
		Westbound	5,770 / 7,850	1.82	1.79	--	--	1.25	1.44	1.15
Ahlborn et al. (1995)	Minnesota (test girders)	Limestone	9,300 / 12,100	--	--	0.94	1.22	--	--	--
		Gravel	10,400 / 11,300	--	--	1.19	1.50	--	--	--
Roller et al. (1995)	Louisiana (test girders)		7,940 / 9,380	--	--	1.91	--	--	--	--

**Table 2 – Summary of Prestress Loss Recommendations**

Method		How Components are Determined	When Losses can be Determined	Required Creep and Shrinkage Model
AASHTO Standard	General	Individually	End of Service	--
	Lump Sum	Lump Sum	End of Service	--
AASHTO LRFD	Refined	Individually	Any Time	Section 2.3.4
	General	Individually	End of Service	--
	Lump Sum	Lump Sum	End of Service	--
PCI-BDM		Individually	Any Time	Section 2.3.2
PCI – 1975		Individually	Any Time	Included in loss recommendations
NCHRP 496	Detailed	Individually	Any Time	Section 2.3.6
	Approximate	Lump Sum	End of Service	--

### Creep and Shrinkage Models

In conjunction with the prestress loss recommendations presented in the previous section, the creep and shrinkage models described in this section will be used to determine the creep and shrinkage losses associated with each bridge. A summary of the creep and shrinkage models discussed in this section is presented in Table 3. The summary not only lists each creep and shrinkage model but also indicates the input parameters used for the determination of creep and shrinkage in each model. The creep and shrinkage losses are then combined with the elastic shortening losses and steel relaxations losses previously described to determine the total loss of prestress. These calculated losses and girder strains will then be compared to the recorded girder strains.

**Table 3 – Summary of Creep and Shrinkage Models**

Model	Input Parameter											
	Loading Age	Humidity	Size	Strength	Concrete Composition							
					Slump	FA%	Air	Cement Content	Water Content	w/c	a/c	Cement Type
ACI-209 (ACI, 1992)	Creep	Creep Shrinkage	Creep Shrinkage	--	Creep Shrinkage	Creep Shrinkage	Creep Shrinkage	Shrinkage	--	--	--	--
PCI-BDM (PCI, 1997)	Creep	Creep Shrinkage	Creep Shrinkage	Creep Shrinkage	--	--	--	--	--	--	--	--
CEB-FIP-90 (CEB, 1993)	Creep	Creep Shrinkage	Creep Shrinkage	Creep Shrinkage	--	--	--	--	--	--	--	Shrinkage
AASHTO LRFD (AASHTO, 1998)	Creep	Creep Shrinkage	Creep Shrinkage	Creep	--	--	--	--	--	--	--	--
Shams and Kahn (2000)	Creep	Creep Shrinkage	Creep Shrinkage	Creep	--	--	--	--	--	--	--	--
NCHRP 496 (Tadros et al., 2003)	Creep	Creep Shrinkage	Creep Shrinkage	Creep Shrinkage	--	--	--	--	--	--	--	--
B3 (Bazant and Baweja, 1995a,b,c)	Creep	Creep Shrinkage	Creep Shrinkage	Creep Shrinkage	--	--	--	--	Shrinkage	Creep	Creep	Shrinkage
GL2000 (Gardener and Lockman, 2001)	Creep	Creep Shrinkage	Creep Shrinkage	Shrinkage	--	--	--	--	--	--	--	Shrinkage
AFREM (LeRoy et al., 1996)	--	Creep* Shrinkage	Creep* Shrinkage	Creep Shrinkage	--	--	--	--	--	--	--	--

\*Humidity and member size are input parameters for shrinkage, which is used to calculate drying creep.

## RESEARCH METHODS

Girders from three bridges in Virginia containing HPC girders were instrumented with strain gages to determine the long-term prestress losses associated with HPC, and a summary of the three bridges and instrumented girders is presented in Table 4. The concrete strain at the level of centroid of the prestressing force was recorded and was used to determine the long-term prestress losses for each bridge. The strains from the three bridges were compared with the strains estimated using the creep and shrinkage models presented in Table 3, and the prestress losses calculated from the measured strains were compared with the prestress losses calculated utilizing the methods presented in Table 2.

**Table 4 – Summary of Research Bridges**

Bridge	Girder ID	Casting Date	Interior or Exterior	Girder Type	Design $f'_c$ Release / 28-day psi	Girder Span	Girder Spacing
Chickahominy River (LWC)	1	Mar. 12, 2001	Exterior	AASHTO Type IV	4,500 / 8,000	82' – 10"	10' – 0"
	2		Interior			81' – 10"	
	3						
Pinner's Point	F	Sept. 12, 2002	Interior	AASHTO Type V	6,400 / 8,000	85' – 4"	8' – 8"
	T		Exterior			86' – 2"	7' – 11"
	U					86' – 9"	
	G	Sept. 17, 2002	Interior	AASHTO Type V	8,000 / 10,000	86' – 0"	8' – 8"
	H		Exterior			86' – 8"	
	J					87' – 4"	
Dismal Swamp	B	Aug. 18, 2003	Interior	PCBT-45	4,000 / 8,700	63' – 2"	9' – 2"
	A	Sept. 9, 2003	Exterior				
	C						

In addition to the instrumentation and monitoring of the bridge girders, a study of the concrete mixtures used in the three bridges was completed under laboratory controlled conditions. The concrete compressive strength, tensile strength, elastic modulus, and creep and shrinkage characteristics were all analyzed in the laboratory.

### Chickahominy River Bridge

The Chickahominy River Bridge is located on Virginia Route 106 in Charles City County, near Richmond, and is a three-span structure, made continuous for live-loads, that carries two lanes of traffic. The two end spans are 81 ft 10 in. long, and the center span is 82 ft 10 in. long. Each span consists of five AASHTO Type IV high performance, lightweight concrete (HPLWC) girders prestressed with 38, 0.5 in. diameter, grade 270, low relaxation prestressing strands with eight strands harped 8 ft 3 in. on either side of midspan. The girders are transversely spaced 10 ft on-center and are topped with an 8.5 in. 4,000 psi lightweight concrete

(LWC), composite deck. The complete superstructure and girder details are provided on select sheets from the bridge plans in Appendix A. The bridge was constructed in the spring of 2001 and is the first bridge in Virginia to utilize HPLWC, prestressed girders and a LWC Deck.

### **Laboratory Testing**

A study of the mechanical properties, including the creep and shrinkage characteristics, of the HPLWC mixture used in the Chickahominy River Bridge was conducted by Edward Vincent at Virginia Tech in 2002, and a complete description of the testing procedures is available in his Master's Thesis (Vincent, 2003). It should be noted, however, that all of the concrete specimens in this study were made from concrete mixed in the laboratory at Virginia Tech, utilizing the same materials as were used in the bridge girders, and were cured utilizing the Sure-Cure system with a temperature profile matching the curing of instrumented girders.

### **Girder Instrumentation**

Three girders from the Chickahominy River Bridge were instrumented to determine the long-term changes in strain in the girder. The girders were cast at Bayshore Concrete Products in Cape Charles, Virginia, in March of 2001. Girder 1 was an exterior girder in the center span, and Girders 2 and 3 were interior girders in the end spans. Each girder was instrumented with three vibrating wire gages placed inline at midspan, at the level of the centroid of the prestressing force. Each vibrating wire gage also contained a thermistor so that the raw strain measurements could be corrected for the difference between the coefficient of thermal expansion of the vibrating wire gage and the concrete eliminating thermal strains from the vibrating wire gage readings.

The strain and temperature measured by each gage were recorded every two hours, using a Campbell Scientific CR10X datalogger, throughout the detensioning of the girders and the storage of the girders at the precasting yard. Recording of the data from the gages was then suspended while the girders were moved from the precasting yard to the bridge site and resumed once the girders were placed in the bridge. Strains and temperatures were then again recorded at a two hour frequency through the placing of the deck, and for over two years following the placing of the deck.

In addition to the three girders from the Chickahominy River Bridge, three identical test girders were cast in May of 2000 and instrumented in the same fashion as the bridge girders. These girders were part of a study conducted at Virginia Tech (Nassar, 2002), prior to the construction of the Chickahominy River Bridge, to determine the feasibility of constructing girders utilizing HPLWC. The three test girders never left the precasting yard and never had any additional dead load (i.e. deck weight) placed on them. These girders were monitored in the same fashion as the Chickahominy River Bridge girders, with data recorded every two hours, for almost two years.

## **Pinner's Point Bridge**

The Pinner's Point Bridge is a twin bridge structure that carries Virginia Route 164 over the Western Branch of the Elizabeth River to U.S. Route 58, bypassing downtown Portsmouth. The bridge utilizes AASHTO Type V and Type VI Modified girders and connects to an existing concrete bridge at the west end and a new steel girder bridge at the east end interchange with U.S. 58. The instrumented girders are located in the eastbound structure, in the two spans adjacent to the new steel superstructure, denoted as spans 1E and 2E in the plans. Construction on the superstructure for this section of the bridge began in the summer of 2003 and was completed in the summer of 2004. These spans are part of a four span unit that is made continuous for live load with continuity diaphragms placed in conjunction with the 8.5 in., 4,000 psi composite, concrete deck. Spans 1E and 2E consist of nine AASHTO Type V girders, each prestressed with 37 or 40, 0.5 in. diameter, grade 270, low-relaxation prestressing strands with either 9 or 12 strands harped 9 ft on either side of midspan. The six instrumented girders utilize the 40 strand pattern and range in length from 85 ft 4 in. to 87 ft 3 in. with a transverse spacing varying from 8 ft 7.5 in. on-center at the east end of span 1E to 7 ft 11 in. on-center at the west end of span 2E.

### **Laboratory Testing**

A study of the mechanical properties, including the creep and shrinkage characteristics, of the 8,000 psi HPC mixture used in the Pinner's Point Bridge was completed at Virginia Tech in 2003, and a complete description of the testing procedures is available in Brad Townsend's Master's Thesis (2003). The concrete in this study was mixed in the laboratory utilizing the same materials as were used in the bridge girders, and the concrete specimens were cured using the Sure-Cure system with a temperature profile matching the curing of the bridge girders.

### **Girder Instrumentation**

Six girders from the Pinner's Point Bridge were cast at Bayshore Concrete Products in Cape Charles, Virginia, in September of 2002 and instrumented to determine the long-term strain change in the girder. Girders F, T, and U were cast with an 8,000 psi HPC, and Girders G, H, and J were cast with a 10,000 psi HPC. Girders F, G, H, and J were placed side-by-side in the span 1E, with Girder J as the exterior girder in that span, and Girders T and U were placed side-by-side in the adjacent span (2E), with Girder U as the exterior girder in that span.

Each of the six girders was instrumented with three vibrating wire gages, placed in-line at the centroid of the prestressing force at midspan. In addition to the vibrating wire gages, Girders T, U, H, and J were instrumented with a series of thermocouples. These thermocouples were added to provide a profile of the temperature gradient through the girder, so the raw strains recorded by the vibrating wire gages could be more accurately corrected for the changes in temperature in the girder.

During casting and detensioning of the girders, the vibrating wire gages in all six girders and the thermocouples in girders J and T were connected to a Campbell Scientific CR10X

datalogger, and strain and temperature readings were logged every 15 minutes. After detensioning, the girders were disconnected from the datalogger and moved into storage at the precasting yard, at which time the vibrating wire gages in all six girders and the thermocouple in girders J and T were again connected. The girders remained in storage for approximately six months during which time the girder strains and temperatures were logged every two hours.

In the summer of 2003, the six girders were disconnected from the datalogger, shipped to the bridge site, and erected. Once access to the bridge site was granted by the contractor, three additional thermocouples were placed in the deck at midspan, over-top of girder J, as indicated in the gage plan (Figure 6), and two thermocouples were placed along-side girder J at midspan to measure the ambient air temperature at the top and bottom of the girder. The vibrating wire gages in all six girders, the five thermocouples in girder J, and the five new thermocouples in the deck over-top of girder J and along-side girder J at midspan were connected to the datalogger, which continued to log data every two hours.

### **Dismal Swamp Bridge**

The Dismal Swamp Bridge, located on U.S. 17, in Chesapeake, Virginia, was constructed in the summer of 2004 and is the first bridge in Virginia to utilize prestressed concrete bulb-T (PCBT) girders. The bridge is a twin bridge structure composed of three, five span units in each bridge, made continuous for live load. Each span is composed of five PCBT-45 girders spanning 62 ft. 2 in. and prestressed with 26, 0.5 in. diameter, grade 270, low-relaxation prestressing strands with six strands harped at 40% of the girder length. The girders are transversely spaced 9 ft 2.25 in. on-center and are topped with an 8.5 in., composite, concrete deck with a design compressive strength of 4,400 psi.

### **Laboratory Testing**

A study of the mechanical properties, including the creep and shrinkage characteristics, of the 8,700 psi HPC mixture used in the Pinner's Point Bridge was completed at Virginia Tech in 2003, and a complete description of the testing procedures is available in Chris Waldron's dissertation (2004). The concrete in this study was mixed in the field utilizing the same materials as were used in the bridge girders, and the concrete specimens were cured using the Sure-Cure system with a temperature profile matching the curing of the bridge girders.

### **Girder Instrumentation**

Three girders from the Dismal Swamp Bridge were instrumented with vibrating wire gages and thermocouples to determine the long-term changes in strain in the girders. The three girders were cast by Bayshore Concrete Products at their Chesapeake, Virginia plant on two different days. Girder B, an interior girder, was cast on August 18, 2003, and girders A and C, both exterior girders, were cast on September 9, 2003. The girders were to be placed at the southern-most span of the southbound bridge. However, due to confusion between the contractor and the casting yard, girder B was placed at the southern end of the middle unit of the bridge, 328 ft from its intended location.

The girders were instrumented with three vibrating wire gages, at midspan, across the bottom flange of the girder, at the level of the centroid of the prestressing force, one at the girder centroid, and one in the top flange of the girder. Each girder also contained an embedment type electrical resistance gage at midspan at the centroid of the prestressing force. Additionally, girders A and B were instrumented with thermocouples at midspan to determine the temperature profile through the girders.

During casting, curing, and detensioning of girder B, the vibrating wire gages were connected to a Campbell Scientific CR-10X datalogger, with readings taken every two hours. The electrical resistance gage and the thermocouples were not connected at this time due to problems with the datalogger. Readings from the vibrating wire gages were also taken, at a two hour frequency, between the casting of girder B and girders A and C. During casting, curing, and detensioning of girders A and C, the vibrating wire gages and the electrical resistance gages of girders A and C, as well as the two thermocouples at the top of girder A were connected to the datalogger, and readings were taken every 15 minutes. Once girders A and C were moved to storage, all the vibrating wire gages and electrical resistance gages in girders A, B, and C, along with the top two thermocouples in girder A were monitored, and measurements were recorded every two hours for approximately 8 months.

After approximately 8 months in storage, in the spring of 2004, the datalogger was disconnected so that the girders could be shipped to the bridge site and placed in the bridge. In August of 2004, the vibrating wire gages and electrical resistance gages in girders A and C, along with the top two thermocouples in girder A were again connected to the datalogger, and readings were recorded every two hours. However, because girder B was placed in a different span than was intended, 328 ft from its intended location, as discussed in previously, it was not possible for it to be connected to the datalogger.

### Time-Step Modeling

To compare the various creep and shrinkage models discussed in Chapter 2 with the strains recorded in the bridge girders, a time-step analysis of the girders was conducted using each of the creep and shrinkage models. The superposition method, developed by McHenry (1943) by modifying Boltzmann's principle of superposition for viscoelastic materials to include the aging effect of concrete, is one of the most common methods utilized for performing a time-step analysis of creep under a varying state of stress. Boltzmann stated that the strain produced at any time  $t$  by a stress applied at time  $t'$ , which is less than  $t$ , is independent of the effects of any stress applied earlier or later. Therefore, McHenry surmised, superposition of the creep curves for loads applied at different times, accounting for the aging effect of concrete, can be used to determine the state of strain at any time  $t$  under a varying state of stress. To account for the aging effect of concrete a new creep function must be determined for each time at which new load, or a change in load is applied. The total strain at any time  $t$  is then given by:

$$\varepsilon(t) = \frac{\sigma(t')}{E(t')} [1 + \phi(t, t')] + \sum_{i=1}^n \frac{\Delta\sigma(t_i)}{E(t_i)} [1 + \phi(t, t_i)] + \varepsilon_{sh}(t, t') \quad \text{Eq. 4}$$

where  $t'$  is the time at which the initial stress is applied and drying begins,  $\sigma(t')$  is the initially applied stress,  $E(t')$  is the concrete modulus of elasticity at time  $t'$ ,  $\phi(t, t')$  is the creep coefficient

at time  $t$  for a load applied at time  $t'$ ,  $t_i$  is a time between  $t'$  and  $t$  when a change in stress is applied,  $\Delta\sigma(t_i)$  is a change in stress applied at time  $t_i$  due either to an applied load or the change in prestress over the preceding time interval,  $E(t_i)$  is the concrete modulus of elasticity at time  $t_i$ ,  $\phi(t, t_i)$  is the creep coefficient at time  $t$  for a load applied at time  $t_i$ , and  $\epsilon_{sh}(t, t')$  is the shrinkage occurring between time  $t'$  and  $t$ . Therefore, the first term in equation 4 accounts for the elastic and creep strains due to the initial prestressing force over all time intervals, the second term accounts for the elastic and creep strains due to the changes in the prestressing force resulting from prestress losses over each time interval and any changes in the applied loads at the start of each time interval, and the third term accounts for the shrinkage of the girder.

This method of determining the strain at any time  $t$  through the superposition of creep curves for loads applied at different times agrees well with experimental data for increasing stresses and slightly decreasing stresses (Neville et al., 1983). However, for a complete removal of load, the creep recovery is overestimated. For a typical precast, pretensioned, concrete beam, the complete removal of load is unusual. Instead, the beam typically shows a slow decreasing state of stress due to the continuous loss of prestress, and another slight loss in stress due to the application of superimposed dead load. Therefore, this method is widely used for the time-step analysis of precast, pretensioned, concrete beams.

For a member subjected to a continually varying state of stress, as is the case for a prestressed beam undergoing a loss of prestress due to creep and shrinkage, equation 4 must be evaluated numerically with the loss of prestress over each time step being applied as a change in stress at the beginning of the next time step. The accuracy of the solution, therefore, depends on the number of time steps undertaken in the analysis in addition to the accuracy of the creep and shrinkage models. Each time step added to the analysis, while increasing the accuracy of the result for a given creep and shrinkage model, also makes the analysis more complicated, as a new creep curve must be determined for each time step. Since the incremental stresses applied at each time step must be applied using a different creep curve, this method is not very well suited to analysis using a spreadsheet, having short time steps over a long period. Therefore, it was desired to try to simplify the time step analysis without losing significant accuracy.

For the time-step analyses in this research, the following procedure, modeled after the recommendations of the PCI Committee on Prestress Losses (PCI, 1975) was used:

1. The steel relaxation prior to detensioning is determined and subtracted from the jacking force to determine the initial prestressing force.
2. The initial prestressing force is used with Equations 1 and 2 to determine the prestressing force after elastic shortening, which is then used to determine the stress and strain in the concrete at the centroid of the prestressing force at midspan using the net section properties of the girder.
3. The change in strain due to creep and shrinkage over the first time step is determined using the desired model. Strain compatibility is used to determine the associated loss in prestress. A strand modulus of 28,500 ksi was used to convert strains to prestress losses, and changing the strand modulus from 27,000 ksi to 29,000 ksi (the generally accepted range for strand modulus) results in less than a 1 ksi difference in the estimated losses at 750 days.

4. The change in tendon stress due to steel relaxation over the first time step is determined using Equation 3.
5. The nominal loss in prestress over the time step is then determined as the sum of the losses due to creep, shrinkage, and steel relaxation.
6. The change in strain at the centroid of the prestressing force at midspan due to the nominal loss in prestress (elastic rebound of concrete due to prestress losses) is determined as is the associated small gain in prestress.
7. The total change in strain and the total prestress loss over the time step is calculated by summing the effects of creep, shrinkage, steel relaxation, and elastic rebound.
8. The total change in strain is added to the strain in the concrete at the beginning of the time step to determine the strain in the concrete at the end of the time step.
9. The prestress force and concrete strain at the end of the time step become the inputs for the next time step, and steps 3 through 8 are repeated for each time step until the superimposed dead load is placed on the bridge.
10. Once the deck is placed on the bridge, step 3 through 8 are repeated using the composite girder properties to determine the changes in stress and strain in the concrete caused by changes in prestress (step 6), and the effect of the superimposed dead load is modeled separately and added to the effect of the prestressing force.

At the application of the superimposed dead load, the time step method is altered to account for the application of this load on a more mature concrete and the effect of differential shrinkage between the deck and girder concrete. The procedure for determining the changes in prestressing force and concrete strain due to the superimposed dead load is as follows:

1. A new creep model is determined for loads applied at the time of application of the superimposed dead load.
2. The change in prestressing force and the stress and strain at the centroid of the prestressing force, at midspan, due to the superimposed dead loads are determined.
3. The change in strain over the time step due to creep caused by the superimposed dead load (tensile creep) is determined using the appropriate creep model.
4. The prestress gain associated with the creep caused by the superimposed dead loads is determined using strain compatibility.
5. The elastic strain of the concrete due to the prestress gain is determined using the composite girder properties and is used to determine the associated prestress loss.
6. The total prestress gain due to creep resulting from the superimposed dead loads for the time step is determined by combining the prestress gain resulting from creep with the prestress loss resulting from elastic deformation due to the prestress gain.
7. The total strain in the concrete at the end of time step is determined from the creep strain over the time step and the elastic strain due to the gain in prestress.
8. The gain in prestress and strain at the end of the time step become the change in prestress and strain used at the beginning of the next time step, and step 3 through 7 are repeated for each time step.

A similar approach is used to account for differential shrinkage of the deck and girder concrete. This approach is well suited for the short time steps used in the modeling of the girders in this research, but is not suited to large time steps:

1. The horizontal force in the deck due to differential shrinkage for the first time interval is estimated as the shrinkage strain of the deck for the time interval times the area of the deck associated with one girder times the modulus of the deck for the interval.
2. The creep of the deck is determined as the creep coefficient for the time interval times the strain in the deck due to the horizontal force determined in step 1 for the first time step and step 9 for all other time steps. The reduction in the horizontal force in the deck due to creep is the creep strain times the area of the deck associated with a single girder times the modulus of the deck for the time interval. The net horizontal force in the deck for the time interval is then the horizontal force calculated in step 1 for the first time step or step 9 for all other time steps minus the reduction in the horizontal force due to creep.
3. The change in prestressing force and the stress and strain at the centroid of the prestressing force, at midspan, due to the horizontal force located at the centroid of the deck are determined using the net (or transformed) composite properties of the deck/girder system.
4. The change in strain in the girder over the time step due to creep caused by the forces associated with differential shrinkage is determined using the creep model for the girder for loads applied at the time of deck placement.
5. The prestress gain associated with the creep caused by the forces associated with differential shrinkage is determined using strain compatibility.
6. The elastic strain of the concrete due to the prestress gain is determined using the composite girder properties and is used to determine the associated prestress loss.
7. The total prestress gain at the end of the time step is determined by combining the elastic prestress gain associated with the horizontal deck force, the prestress gain associated with creep in the girder due to the horizontal deck force, and the prestress loss associated with elastic deformation due to the prestress gain.
8. The total strain in the concrete at the end of time step is determined by combining the elastic strain due to the horizontal deck force, the creep strain over the time step, and the elastic strain due to the gain in prestress.
9. The additional horizontal force in the deck for the next time step is determined from the shrinkage strain for the time step as was done in step 1. This force is then added to the reduced horizontal force from the previous time step to determine the total horizontal force for the time step.
10. Finally, steps 2 through 8 are repeated for each time step.

Once the changes in the prestressing force and concrete strain due to the creep associated with the superimposed dead loads and differential shrinkage are determined, the total changes in the prestressing force and concrete strain for each time step can be determined using superposition. The changes in prestressing force and concrete strain due to the creep associated with the initially applied prestressing force, the shrinkage of the girder, steel relaxation of the tendons, and the elastic gain due to prestress losses are added to the tensile creep and elastic losses associated with the superimposed dead loads and the elastic strains and creep associated with differential shrinkage to determine the total strain at the end of each time step. Using this method, plots of the prestressing force and concrete strain, at the centroid of the prestressing force, at midspan, versus time can be created for each creep and shrinkage model. These plots

can then be compared to the data recorded from each bridge to determine the best model for predicting prestress losses of Virginia's HPC.

This method is better suited to a spreadsheet analysis using short time steps over a long period than is the method of superposition proposed by McHenry because only two creep functions are needed, one for loads applied at detensioning and one for loads applied at the time of deck placement. The two methods differ by no more than 2% when using the same time steps for the 8,000 psi Pinner's Point girders. Similar results were obtained for the other girders in this study. Therefore, since accuracy is improved by increasing the number of time steps, and the method described above is easier to implement with many short time steps over a long period, this method is used throughout this research.

## **RESULTS AND DISCUSSION**

As discussed in the previous section, three HPC bridges were instrumented to determine the long-term changes in strain and the associated prestress losses. Two of the bridges utilized normal-weight HPC with design strengths ranging from 8,000 to 10,000 psi and the third bridge utilized a lightweight HPC with a design strength of 8,000 psi. In the following sections, the measured strains are presented and are compared with the predicted strains and prestress losses determined using the previous recommendations and the creep and shrinkage models previously discussed.

### **Chickahominy River Bridge**

Three girders from the Chickahominy River Bridge and two similar test girders were instrumented by Adil Nassar (2002). The three bridge girders were monitored for almost 900 days with the exception of approximately 2 months during the bridge construction while the girders were shipped to the bridge site and erected and while the bridge site was not accessible. The test girders were monitored for approximately 200 days as part of the study conducted by Nassar, after which recording was suspended for approximately 200 days. The girders were then again monitored for approximately 300 days, providing data spanning almost 2 years. The results for the test girders will not be discussed here but these results can be found in the dissertation by Chris Waldron (2004) and the thesis by Adil Nassar (2002).

#### **Bridge Girder Predicted Strains and Model Residuals**

Figures 1 through 6 show the strains predicted by the creep and shrinkage models for the Chickahominy River Bridge girders and the residuals between the predicted and measured strains. The girder properties and model parameters used in this analysis are given in Appendices B and C, respectively. Figures 1 and 2 show the strains predicted by the ACI-209, PCI-BDM, and CEB-FIP MC90 models. As was the case with the test beams, each of these models over-predicts the measured strains throughout the observed period, and predicts compressive strains outside the range of two standard deviations of the measured data, shown by the error bars on the plots. Each model shows too rapid an increase in compressive strain between loading and the deck placement at 120 days. However, after 150 days the ACI-209 and

PCI-BDM models show a fairly consistent residual indicating that the shape of the model curve after deck placement is similar to the measured strain, but at the wrong magnitude due to the over-prediction of compressive strains prior to deck placement. The ACI-209 model over-predicts the measured compressive strain by 360 to 460 microstrain and the PCI-BDM model over-predicts the measured strain by 240 to 320 microstrain between 150 and 890 days. The residual for the CEB-FIP MC90 model, however, continues to increase throughout the modeled period indicating that the shape of the model does not mirror the measured strains before or after deck placement. Between 150 and 890 days, the residual for the CEB-FIP MC90 model steadily increases from 400 to 610 microstrain.

Figures 3 and 4 show the predicted and residual strains, respectively, for the AASHTO LRFD, Shams and Kahn, and NCHRP 496 models. The AASHTO LRFD and Shams and Kahn models under-predict the compressive strains for early ages and over-predict the strains after approximately 30 days. Both models predict within the error bars, for the first 200 days, and the Shams and Kahn model continues to predict within the error bars for the remainder of the modeled period. The maximum residual for the Shams and Kahn model is approximately 160 microstrain and occurs near the end of the modeled period. The residuals for the AASHTO LRFD method increase throughout the modeled period reaching a peak of 370 microstrain at 890 days, indicating that the shape of the modeled curve does not accurately mirror the shape of the measured strains. The NCHRP 496 model over-predicts the measured strains for the entire modeled period. The residuals for the NCHRP method remain consistently between 340 and 420 microstrain after 150 days indicating that after deck placement, the shape of the NCHRP 496 curve mirrors the measured strains, and that the majority of the difference between the model and the measured strains occurs prior to the placement of the deck.

Figures 5 and 6 show the predicted and residual strains, respectively, for the B3, GL2000, AFREM, and PCI-1975 models. Only the PCI-1975 model predicts within the error bars for the measured strains, predicting near the upper limit for the majority of the modeled period. Between 150 and 900 days the PCI-1975 model over-predicts the measured strains by 60 to 200 microstrain. The B3 and AFREM models are very similar and both over-predict the compressive strains early and show a consistent residual after deck placement, indicating that after deck placement the shape of the B3 and AFREM models is similar to the measured data, but at the wrong magnitude. After 150 days, the B3 and AFREM models over-predict the strains by 260 to 390 microstrain. The GL2000 model over-predicts the measured strains by the largest magnitude. Prior to the girders being moved from the casting yard at 60 days, the GL2000 model over-predicts the measured strains by as much as 790 microstrain. After deck placement the residual between the measured strains and the GL2000 modeled strains continues to increase reaching a maximum of over 1,000 microstrain at 890 days.

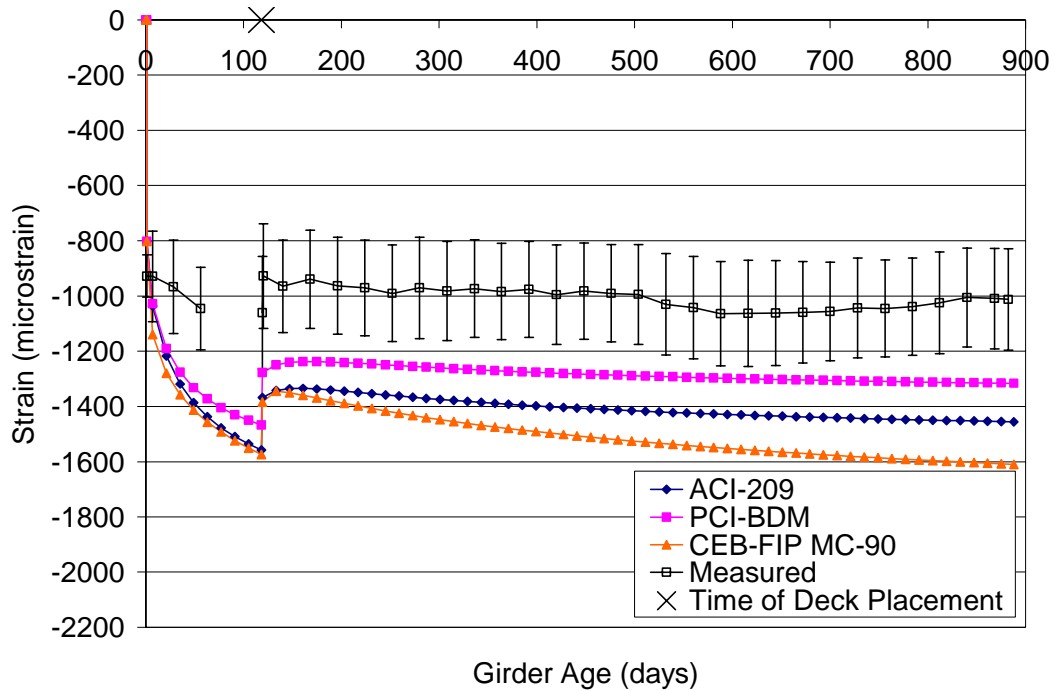


Figure 1 – HPLWC Bridge Girder Predicted Strains for the ACI-209, PCI-BDM, and CEB-FIP MC90 Models

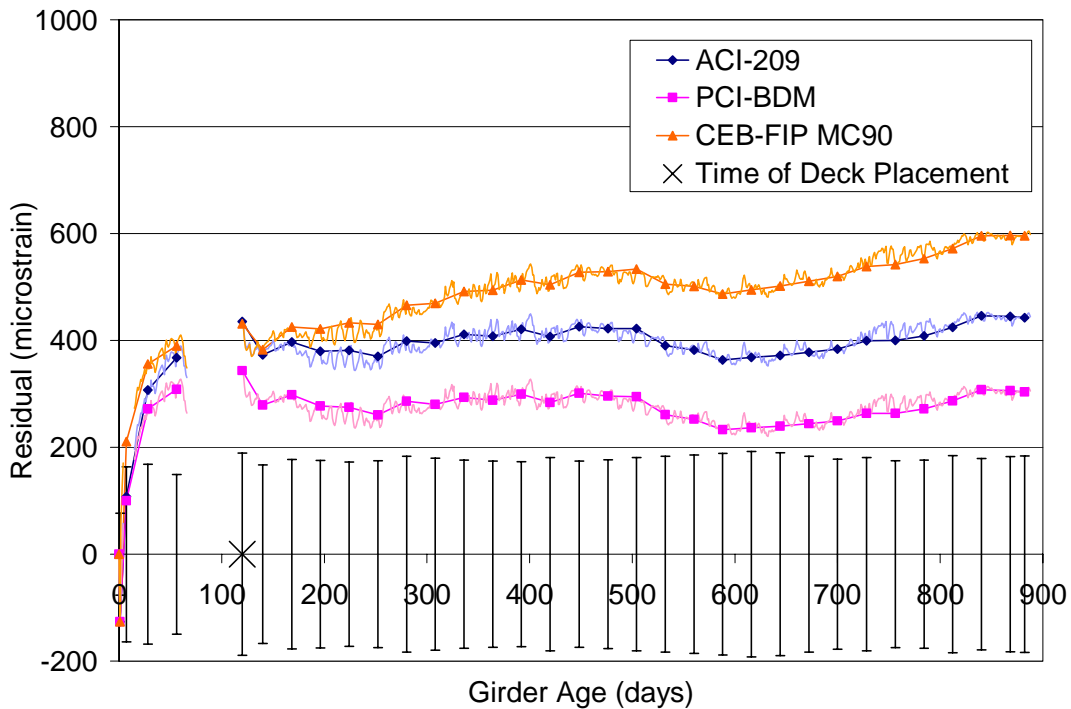


Figure 2 – HPLWC Bridge Girder Residual Strains for the ACI-209, PCI-BDM, and CEB-FIP MC90 Models

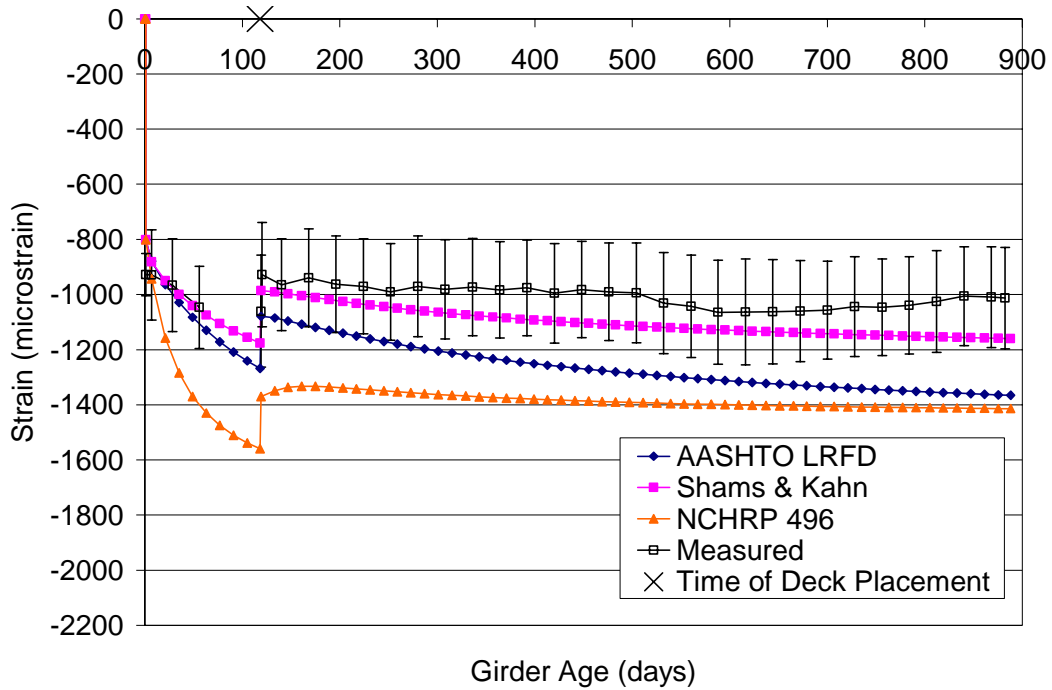


Figure 3 - HPLWC Bridge Girder Predicted Strains for the AASHTO LRFD, Shams and Kahn, and NCHRP 496 Models

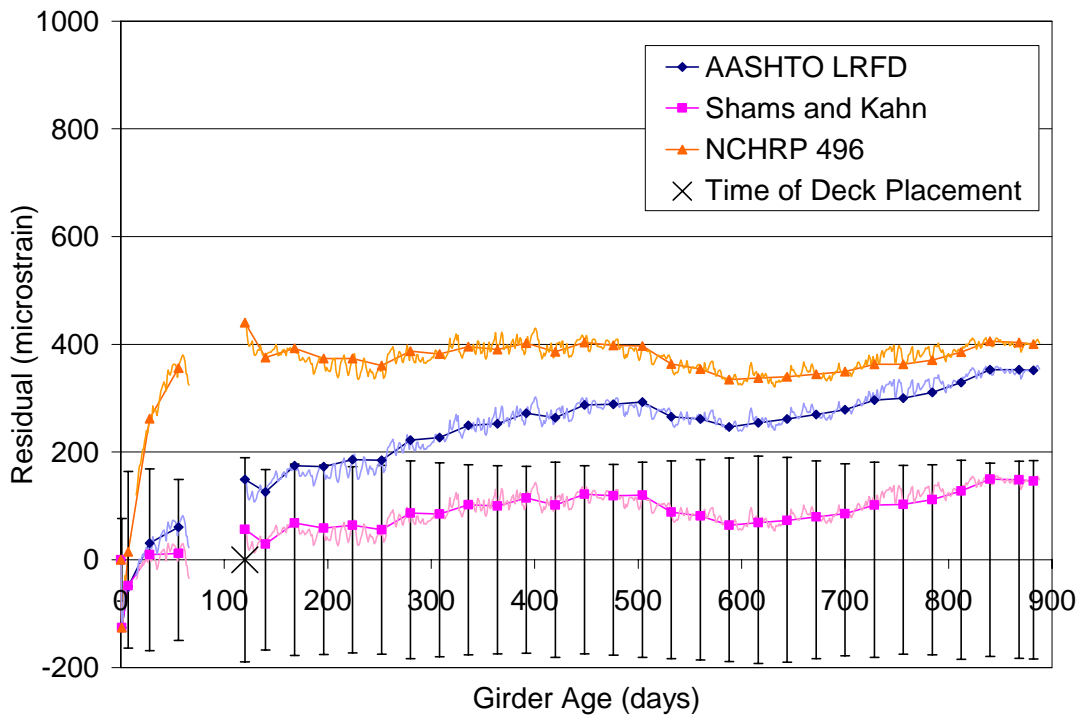


Figure 4 - HPLWC Bridge Girder Residual Strains for the AASHTO LRFD, Shams and Kahn, and NCHRP 496 Models

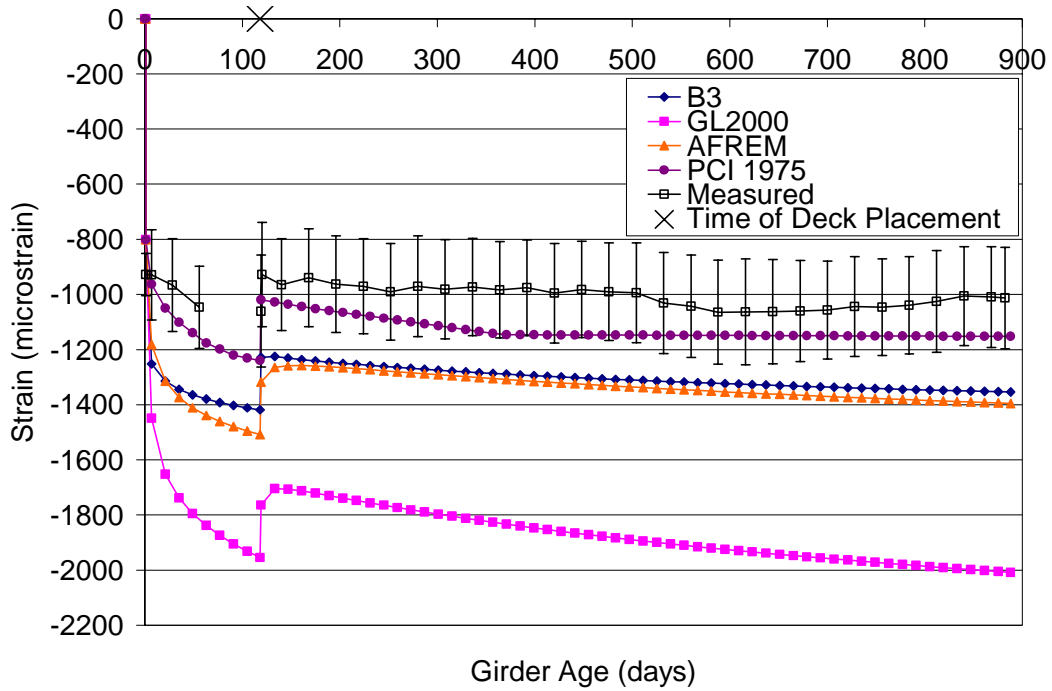


Figure 5 - HPLWC Bridge Girder Predicted Strains for the B3, GL2000, AFREM, and PCI-1975 Models

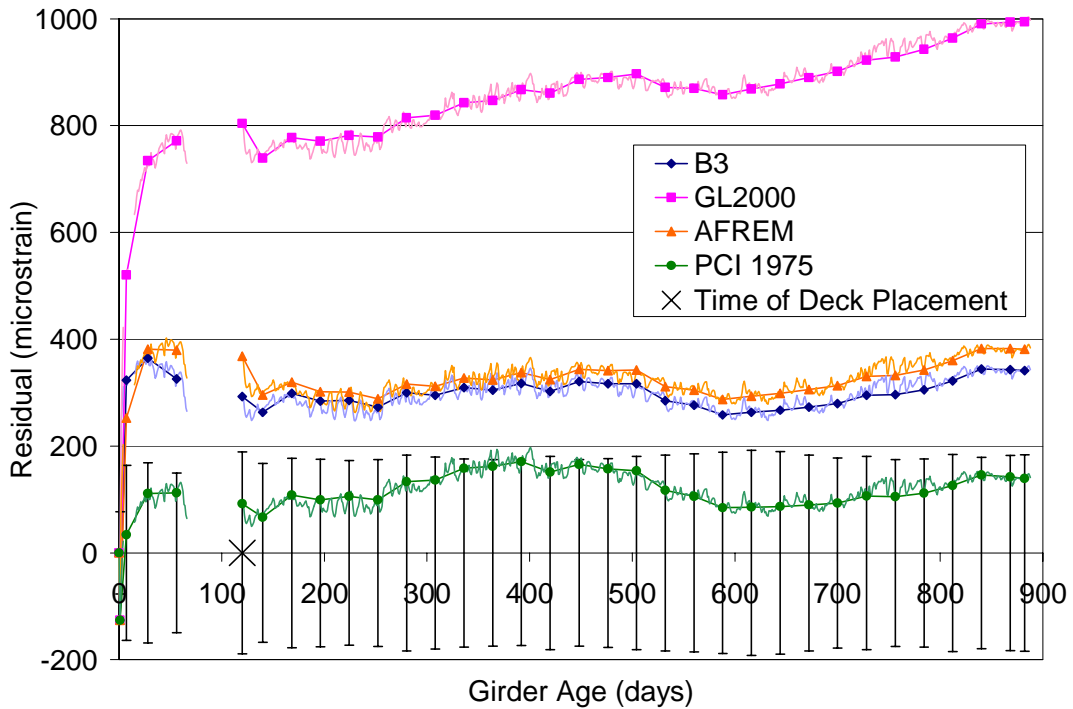


Figure 6 - HPLWC Bridge Girder Residual Strains for the B3, GL2000, AFREM, and PCI-1975 Models

Finally, the models developed from the creep and shrinkage testing performed on the HPLWC, Equations 7 and 8, were used with the correction factors for relative humidity and

specimen size given in the ACI-209 and AASHTO LRFD models to compare the laboratory measured creep and shrinkage properties to the measured compressive strains of the bridge girders. Figures 7 and 8 show the predicted and residual strains, respectively for these models. The models based on the laboratory data over-predict the compressive strains measured in the bridge girders throughout the observed period. The model using the AASHTO LRFD corrections for non-standard conditions predicts within the error bars until just before deck placement. This model exhibits residual strains that are consistently increasing, indicating that the shape of the model does not accurately mirror the compressive strains measured in the bridge beams. From 150 to 890 days, the residual for this model increases from 200 to 430 microstrain. The model corrected using the ACI-209 factors for non-standard conditions predicts outside the range of the error bars for the entire observed period. This model does, however, exhibit generally consistent residuals after deck placement between 350 and 450 microstrain.

As was the case with the HPLWC test girder, the poor correlation between the laboratory measured creep and shrinkage characteristics and the measured compressive strains of the Chickahominy River Bridge girders has at least three possible causes. Either the laboratory prepared concrete mixture and the mixture prepared at the casting yard are significantly different, the correction factors for non-standard conditions do not accurately represent the changes in the behavior of concrete specimens of differing sizes under varying environmental conditions, or the strain measurements were not accurate. The differences between the laboratory concrete and the casting yard concrete were discussed previously, and the primary difference was in the 28 day compressive strength. The 28 day compressive strength of the laboratory concrete was 6,400 psi, while the 28 day compressive strength of the casting yard concrete was 8,110 psi. Applying this difference in strength to the correction factor for strength given in the AASHTO LRFD model results in a reduction in the ultimate creep coefficient of 12% and a reduction in the predicted strain at 890 days of only 70 microstrain, which reduces the residual from 430 to 360 microstrain. Therefore, difference in the two concrete mixtures cannot account for the difference between the models and the data alone indicating that the correction factors likely do not accurately represent the changes in the creep and shrinkage properties due to varying sizes and environments. Vibrating wire gages are widely used and trusted by bridge researchers, however, one explanation for the poor correlation is inaccuracies in the vibrating gage data. It is recommended that in future research projects an additional (or verification) method of measuring prestress force be employed.

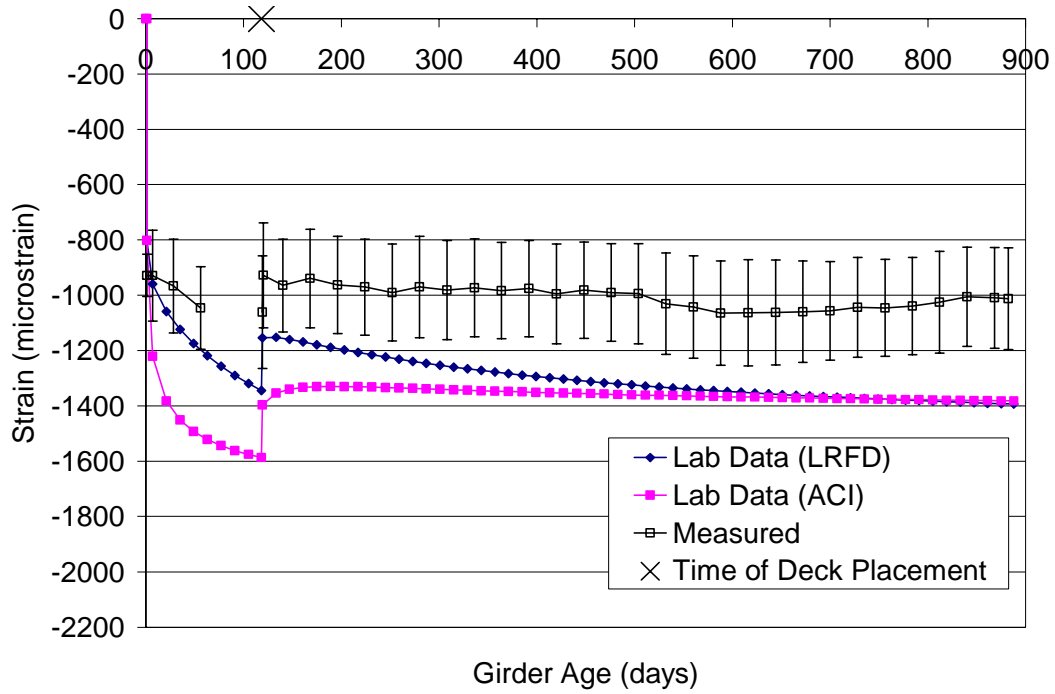


Figure 7 – HPLWC Bridge Girder Predicted Strains for the Models Correlated to the Measured Creep and Shrinkage Properties of the HPLWC

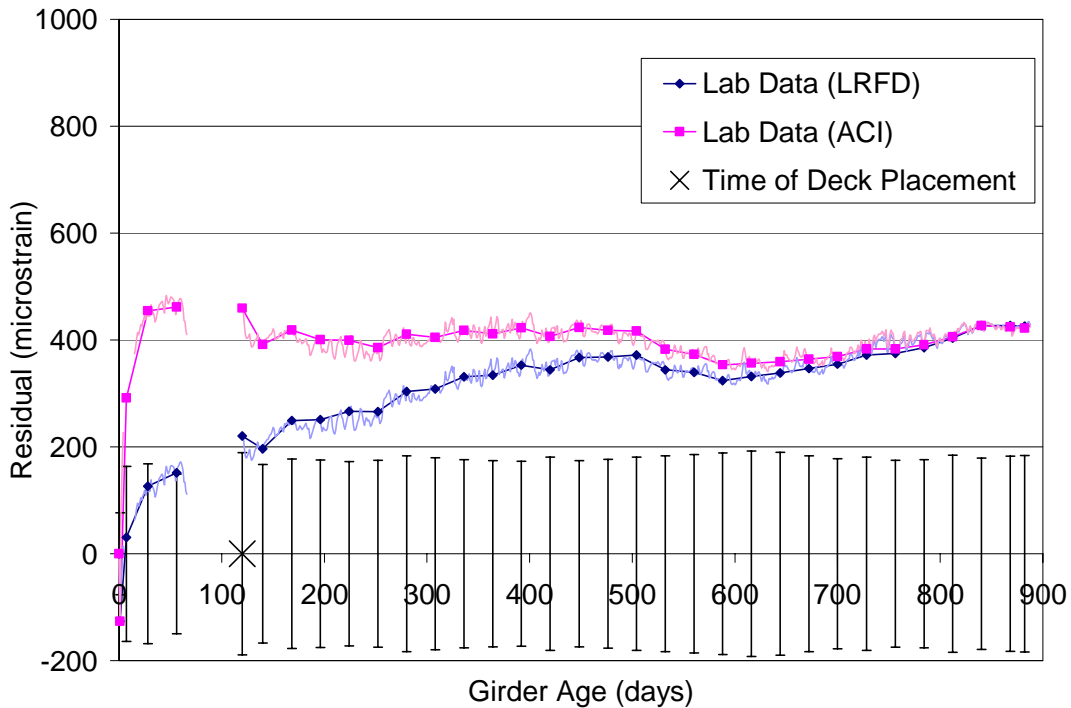


Figure 8 - HPLWC Bridge Girder Residual Strains for the Models Correlated to the Measured Creep and Shrinkage Properties of the HPLWC

## Bridge Girder Residuals Squared Analysis and Model Ranking

Again, to determine which model is the best predictor of strain for the Chickahominy River Bridge girders a residuals squared analysis was performed. Table 5 shows the resulting ranking of the models, and the models with similar sums are ranked equally. The PCI-1975 and Shams and Kahn models predict within the error bars for the entire observed period. The Shams and Kahn model most accurately predicts the mean response of the bridge girders, over-predicting the measured strains by a maximum of approximately 160 microstrain, and the PCI-1975 model provides a good upper bound on the measured compressive strains, over-predicting by a maximum of approximately 200 microstrain during the observed period.

**Table 5 – Bridge Girder Model Ranking**

Ranking	Model
1	Shams and Kahn
1	PCI-1975
2	AASHTO LRFD
2	PCI-BDM
2	B3
3	AFREM
3	Lab Data – ACI
3	Lab Data – LRFD
4	NCHRP 496
4	ACI-209
5	CEB-FIP MC90
6	GL2000

## Prestress Loss Calculations

In addition to the analysis carried out using the creep and shrinkage models, prestress losses were calculated for the Chickahominy River Bridge girders. Table 2, connects the methods for estimating prestress losses that use a creep and shrinkage model to the appropriate model. In addition, only the PCI-1975 and AASHTO LRFD Lump Sum methods account for lightweight concrete in the determination of prestress losses. Prestress loss calculations were not carried out for the HPLWC test girder since the methods for determining prestress losses, especially the simplified methods, are calibrated for bridge girders that experience the application of a significant amount of dead load during their design life. The lack of any significant dead load on the test girders, therefore, renders many of the prestress loss calculation methods highly inaccurate. Furthermore, although it is beneficial to compare the creep and shrinkage models against the test girders using a time-step method to determine their accuracy in predicting creep and shrinkage effects, predicting the prestress losses, especially using simplified methods, of a girder so differently loaded than a typical bridge girder is much less beneficial. The total prestress losses predicted using the given methods and a comparison of those losses to the bridge girders is presented in the following sections.

## Predicted Prestress Losses

The predicted total prestress losses, including both instantaneous losses and long-term losses, are presented in Table 6. The predicted total losses range from 44.4 ksi for the PCI-BDM method to 69.9 ksi for the AASHTO LRFD Standard Specification (AASHTO, 1996) Lump Sum method. This is a difference of over 56% showing the tremendous variation in the various prestress loss calculation methods. Also shown in Table 6 are the predicted girder strains at the end of service life due to the predicted prestress losses. These values are determined through strain compatibility using the portion of prestress loss due to elastic shortening, creep, and shrinkage, but neglecting the portion of the prestress losses due to strand relaxation since relaxation occurs in the strand at a constant strain. For example, for the NCHRP 496 refined method, the total losses are 44.8 ksi and the strand relaxation losses are 3.5 ksi. Therefore, the total losses that cause changes in strain at the centroid of the prestressing force are 41.3 ksi, and for an estimated strand modulus of 28,500 ksi, the strain at the centroid of the prestressing force is 1,450 microstrain.

**Table 6 – Predicted Prestress Losses for the Chickahominy River Bridge**

Method	Initial Losses		Long-Term Losses			Total	P/S Centroid Strain
	Initial Rel.	ES	Shrinkage	Creep	Add'l Rel.		
	ksi	ksi	ksi	ksi	ksi		
AASHTO Standard General	2.1	22.8	5.8	24.8	3.2	58.7	-1,870
AASHTO Standard Lump Sum			45.0			69.9	-2,270 <sup>#</sup>
AASHTO LRFD Refined			10.7	19.8	1.4	56.8	-1,870
AASHTO LRFD General			5.8	24.8	1.4	56.9	-1,870
AASHTO LRFD Lump Sum			35.5			60.4	-2,000*
PCI-BDM			6.6	11.2	1.1	43.8	-1,430
NCHRP 496 Refined**			5.4	13.1	1.4	44.8	-1,450
NCHRP 496 Approximate			21.7			46.6	-1,480 <sup>+</sup>
PCI-1975			8.6	9.0	2.5	45.0	-1,420

<sup>#</sup> - Additional steel relaxation losses of 3.2 ksi assumed per AASHTO Standard General method

\* - Additional steel relaxation losses of 1.4 ksi assumed per AASHTO LRFD General method

<sup>+</sup> - Additional steel relaxation losses of 2.4 ksi assumed per Tadros et al., 2003.

\*\* - NCHRP 496 Refined shrinkage losses include the prestress gain due to differential shrinkage, and the creep losses include the elastic gain due to the deck slab.

## Comparison of Predicted and Measured Prestress Losses

Table 7 presents a comparison of the predicted and measured prestress losses for the Chickahominy River Bridge. The losses are separated into losses occurring before and after deck placement for the models that allow the prediction of losses at any time (see Table 2). Also, the long-term prestress losses presented in Table 7 do not include steel relaxation losses since these occur at constant strain and cannot be directly determined for the instrumented girders. The measured losses are determined from the recorded strains assuming strain compatibility between the concrete and the prestressing strands. For the predicted total losses to be compared to the losses determined from the measured strains, the measured strains must be

adjusted to the end of service life of the bridge girders, which is estimated to be 75 years. Adjusting the measured girder strains to the end of service life is accomplished by fitting a logarithmic curve, which approximates the shape of time-dependent losses reasonably well, to the data and extrapolating an estimated value for the strain at 75 years. From this equation, the estimated strain in the Chickahominy River Bridge at the end of service life (75 years) is 1,210 microstrain, which correlates to a total prestress loss of 34.5 ksi, excluding relaxation losses.

**Table 7 – Comparison of Predicted and Measured Prestress Losses (excluding relaxation) for the Chickahominy River Bridge Girders**

Method	Elastic Shortening	Loss From Transfer To Deck	Elastic Gain Due To Deck	Loss After Deck	Total Long-Term Loss	Total Loss	Ratio of Predicted to Meas.
	ksi	ksi	ksi	ksi	ksi	ksi	
AASHTO Standard General	22.8	--	-5.4	--	30.6 <sup>+</sup>	53.4	1.55
AASHTO Standard Lump Sum		--		--	41.8 <sup>+</sup>	64.6	1.87
AASHTO LRFD Refined		16.7		19.2	30.5	53.3	1.54
AASHTO LRFD General		--		--	30.6 <sup>+</sup>	53.4	1.55
AASHTO LRFD Lump Sum		--		--	34.1 <sup>+</sup>	56.9	1.65
PCI-BDM		21.3		1.9	17.8	40.6	1.18
NCHRP 496 Refined		21.2		2.7	18.5	41.3	1.20
NCHRP 496 Approximate		--		--	19.3 <sup>+</sup>	42.1	1.22
PCI-1975		15.2		7.8	17.6	40.4	1.17
Measured		26.5		5.1	-5.1	8.0	8.0

<sup>+</sup> - The elastic gain due to the deck is implicitly included in the total long-term losses for these methods

The methods for estimating prestress losses shown in Table 7, over-predict the total losses of the Chickahominy River Bridge by 17% to 87%. In general, the newer methods, PCI-BDM and NCHRP 496, which are correlated to high strength concrete data, over-predict less than the methods presented in the AASHTO Specifications. This is indicative of the trend that higher strength concretes exhibit less creep and shrinkage than lower strength concrete due to their more dense structures and lower water-cement ratios. The exception to this is the PCI-1975 method, which predicts total losses similar to the more recent methods.

The PCI-1975 and PCI-BDM methods are the best predictors of the total prestress loss, excluding relaxation, over-predicting the total losses by 17% and 18%, respectively. However, each of the methods for estimating prestress losses over-predicts the total long-term losses of the bridge girders. The bridge girders exhibit total long-term losses of 8.0 ksi adjusted to the end of service life. This is less than half of the lowest total long-term losses predicted by the prestress loss estimates. The majority of the over-prediction in prestress loss occurs in the losses predicted before deck placement, where the measured losses of 5.1 ksi are approximately one third of the lowest estimated losses for this time period. A similar result is seen when comparing the creep and shrinkage models with the girder strains. The models over-predict the changes in strain prior to deck placement, but more accurately predict the changes in strain after deck placement. This indicates not only that the prestress loss estimates and creep and shrinkage models over-predict the total long-term losses, but also that the estimated losses accumulate too quickly at early ages.

Unlike the long-term losses, the elastic shortening losses observed in the Chickahominy River Bridge are under-predicted by the estimates. The estimate of elastic shortening losses is 86% of the measured elastic shortening loss, indicating that either the girder properties or prestressing force at release are not known with sufficient accuracy to provide a better estimate of the initial losses. A difference between the elastic modulus of the bridge girders and tested specimens is a likely cause of the differences between the measured and predicted elastic shortening losses. The elastic gain in the prestressing force due to the deck slab is slightly over-predicted by the estimate, with the estimated value being 1.06 times the measured value. According to ASTM C469 (2001), the expected variation for the elastic modulus, between concrete batches, is 5%. The variation in the deck weight due to construction tolerances is certainly more than 1%; therefore, the variation between the estimated and measured elastic gain in the prestressing force due to the deck placement is within the expected variation.

### **Pinner's Point Bridge**

Six girders from the Pinner's Point Interchange were instrumented with vibrating wire gages to determine the long-term changes in strain in the girders. Girders F, T, and U utilized an 8,000 psi HPC, while girders G, H, and J utilized a 10,000 psi HPC. The six girders were monitored for approximately 650 days with two periods of approximately 100 days each where no data was collected. The first gap in the data occurs between 200 and 300 days while the girders were shipped from the casting yard to the bridge site and while the girders and deck forms were erected. The second gap in the data occurs between 400 and 500 days when the data loggers were removed from the site to protect them from damage while the contractor completed work in the area where the data loggers were stored.

### **Measured Strains**

Strains were recorded at least every two hours throughout the duration of the monitoring period, and the strain readings from each day were averaged to reduce the data for analysis. As was performed for the Chickahominy River Bridge, the time-step modeling procedure presented was used with the creep and shrinkage models and the variation of creep and shrinkage with time recommended by PCI (1975) to determine the girder strain predicted by each model. These predicted strains were then compared to the measured strains presented in the preceding section to determine which model is the best predictor of the behavior of the 8,000 psi and 10,000 psi design compressive strength girders of the Pinner's Point Interchange.

### **Girders F, T, and U Predicted Strains and Model Residuals**

Figures 9 through 14 present the predicted strains and the residuals for the models compared to girders F, T, and U with the error bars representing plus and minus two standard deviations of the measured strains. Figures 9 and 10 show the predicted and residual strains, respectively, for the ACI-209, PCI-BDM, and CEB-FIP MC90 models. Each model under-predicts the strains before 30 days and over-predicts the strains after 30 days. None of the models accurately predict the trend of the measured strains. Before deck placement, the models increase in strain too slowly before 30 days and too quickly after 30 days. Soon after deck placement, the models each show a decrease in the compressive strain due to creep recovery and

differential shrinkage, while the measured strains exhibit a continued increase in compressive strain. After 500 days, the measured strains and the predicted strains all show only small changes in strain with the ACI-209 model over-predicting by 130 to 180 microstrain, the PCI-BDM model over-predicting by 30 to 80 microstrain, and the CEB-FIP MC 90 model over-predicting by 130 to 200 microstrain.

Figures 11 and 12 show the predicted and residual strains, respectively, for the AASHTO LRFD, Shams and Kahn, and NCHRP 496 models. Each of these models also under-predicts the measured compressive strains at early ages and over-predicts at later ages. The NCHRP 496 model under-predicts the measured strains for the first 40 days, the AASHTO LRFD model under-predicts for the first 110 days, and the Shams and Kahn model under predicts for the first 180 days. After deck placement, the Shams and Kahn model predicts consistently within the error bars, but again, none of the models accurately predict the trend of the measured strains. Each model shows too slow an increase in the compressive strains at very early ages and too rapid an increase at later ages before deck placement. Each model also shows a decrease in the compressive strains after deck placement, while the measured strains show a continued increase in the compressive strains. After 500 days, the NCHRP 496 and Shams and Kahn models bracket the measured strains. During this time frame, the NCHRP 496 model over-predicts the measured strains by 40 to 90 microstrain and the Shams and Kahn model under-predicts the measured strains by 20 to 80 microstrain. The AASHTO LRFD model over-predicts the measured strains by 50 to 110 microstrain after 500 days.

Figures 13 and 14 show the predicted and residual strains, respectively, for the B3, GL2000, AFREM, and PCI-1975 models. The PCI-1975 model under-predicts the measured strains by as much as 100 microstrain between 2 days and 40 days and over-predicts the measured strains by as much as 250 microstrain during the remainder of the observed period. The AFREM model under-predicts by as much as 100 microstrain between 2 days and 60 days and over-predicts by as much as 100 microstrain until shortly after deck placement. The AFREM model then predicts close to the measured strains for the remainder of the observed period, over-predicting by no more than 60 microstrain and under-predicting by no more than 30 microstrain. The B3 model predicts within the error bars between 2 days and 90 days and after deck placement. During this time, the B3 model over-predicts by no more than 50 microstrain and under-predicts by no more than 30 microstrain. Between 90 days and deck placement, the B3 model over-predicts the measured strains by 50 to 100 microstrain. The GL2000 model over-predicts the measured strains by as much as 520 microstrain between 2 days and 650 days.

Each of the models investigated over-estimates the creep recovery and differential shrinkage associated with the girders after deck placement, as evidenced by the constant or slightly decreasing compressive strains of the models, compared to the increasing compressive strains recorded in the bridge girders shortly after deck placement. The increasing strains of the bridge girders for the period following deck placement can be partially explained by the removal of the deck forms during that period, but it is unlikely that the dead load of the deck forms is equivalent to the dead load of the deck as would be necessary to account for the entire increase in compressive strain after deck placement. It is more likely that the girder experienced less creep recovery and differential shrinkage than is predicted by the models. However, the complete

nature of the increase in compressive strain after deck placement is not fully understood, considering the minimal changes in strain for the 100 days prior to deck placement.

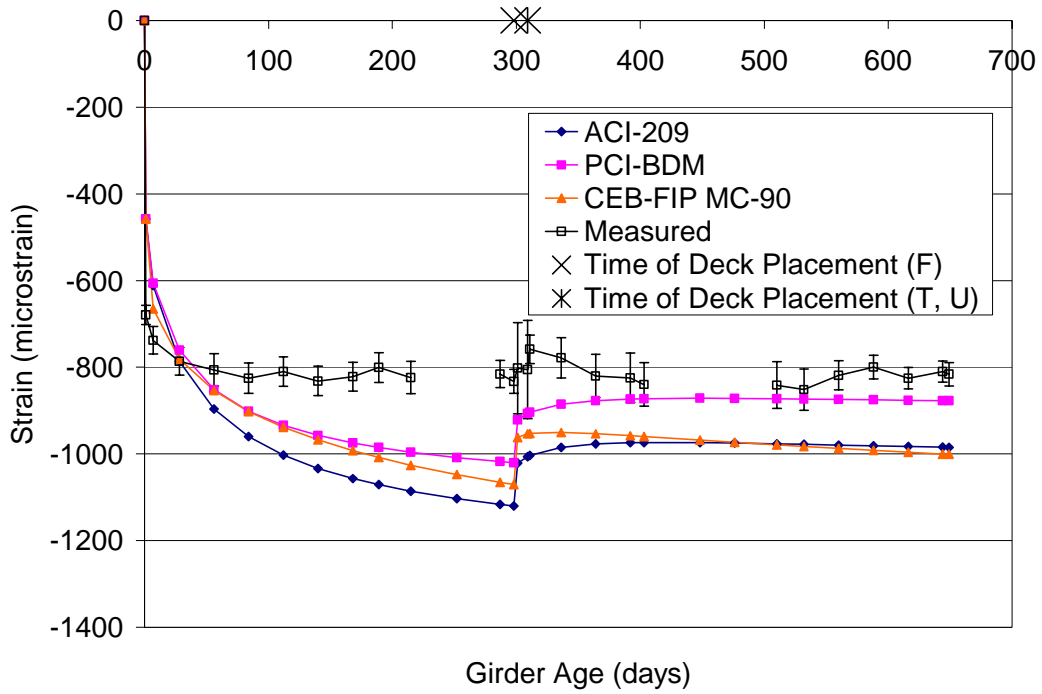


Figure 9 – Pinner’s Point Girders F, T, and U Predicted Strains for the ACI-209, PCI-BDM, and CEB-FIP MC90 Models

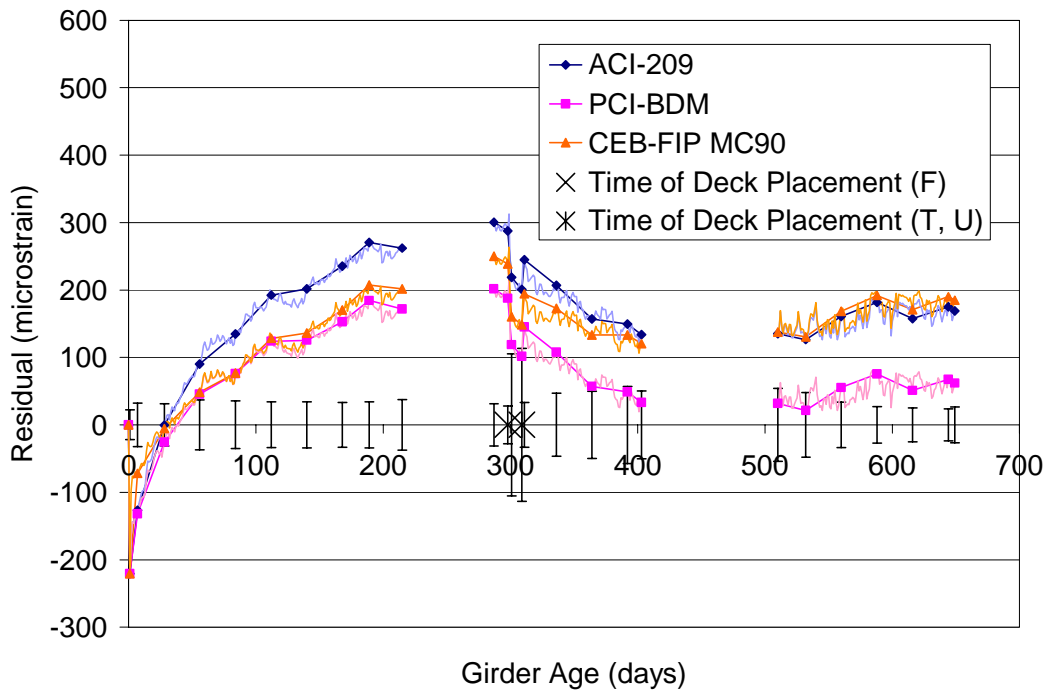


Figure 10 – Pinner’s Point Girders F, T, and U Residual Strains for the ACI-209, PCI-BDM, and CEB-FIP MC90 Models

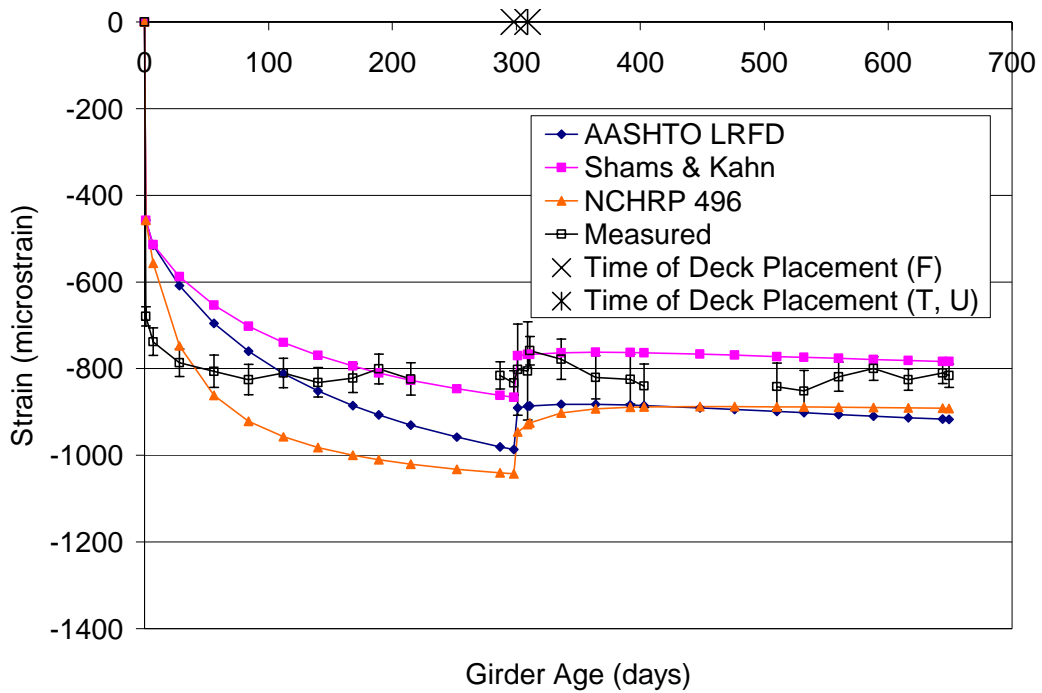


Figure 11 – Pinner’s Point Girder F, T, and U Predicted Strains for the AASHTO LRFD, Shams and Kahn, and NCHRP 496 Models

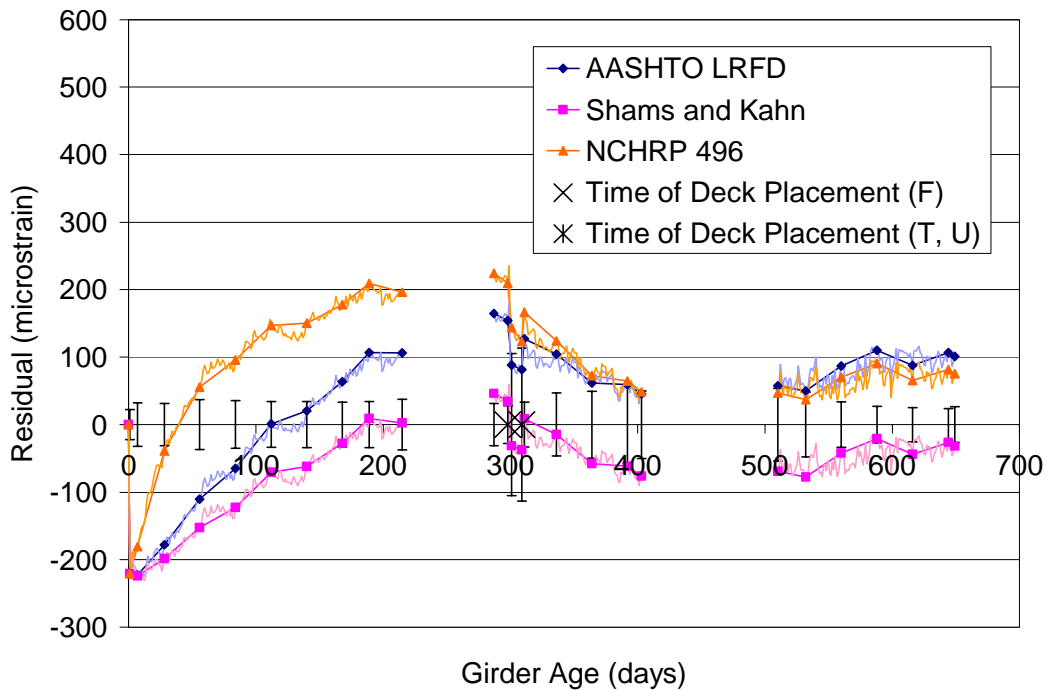


Figure 12 – Pinner’s Point Girders F, T, and U Residual Strains for the AASHTO LRFD, Shams and Kahn, and NCHRP 496 Models

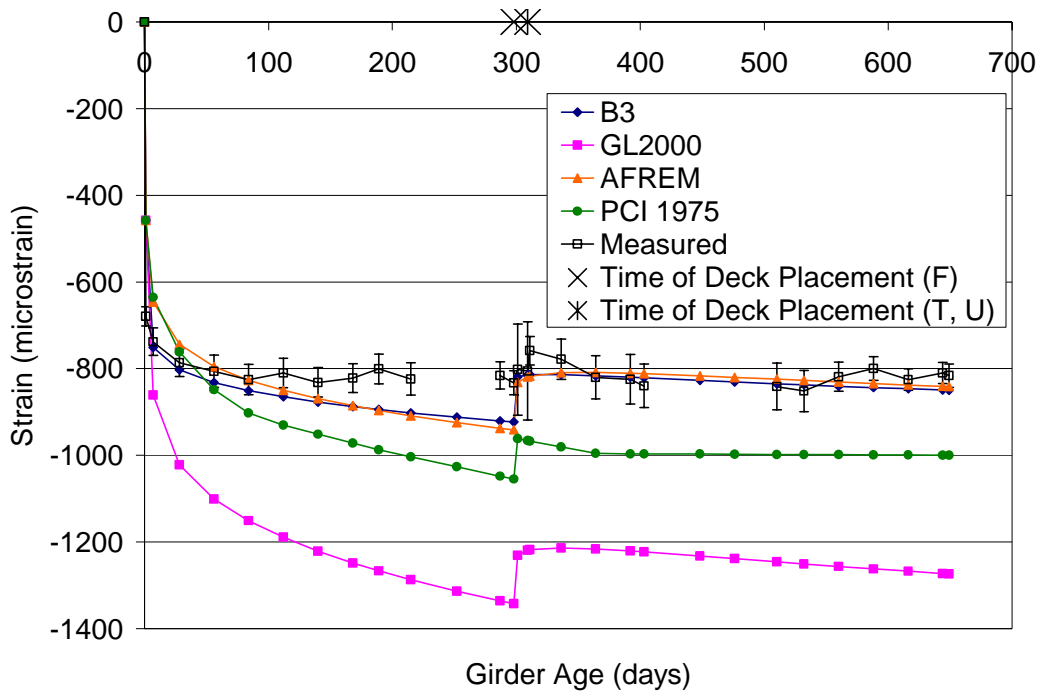


Figure 13 – Pinner’s Point Girders F, T, and U Predicted Strains for the B3, GL2000, AFREM, and PCI-1975 Models

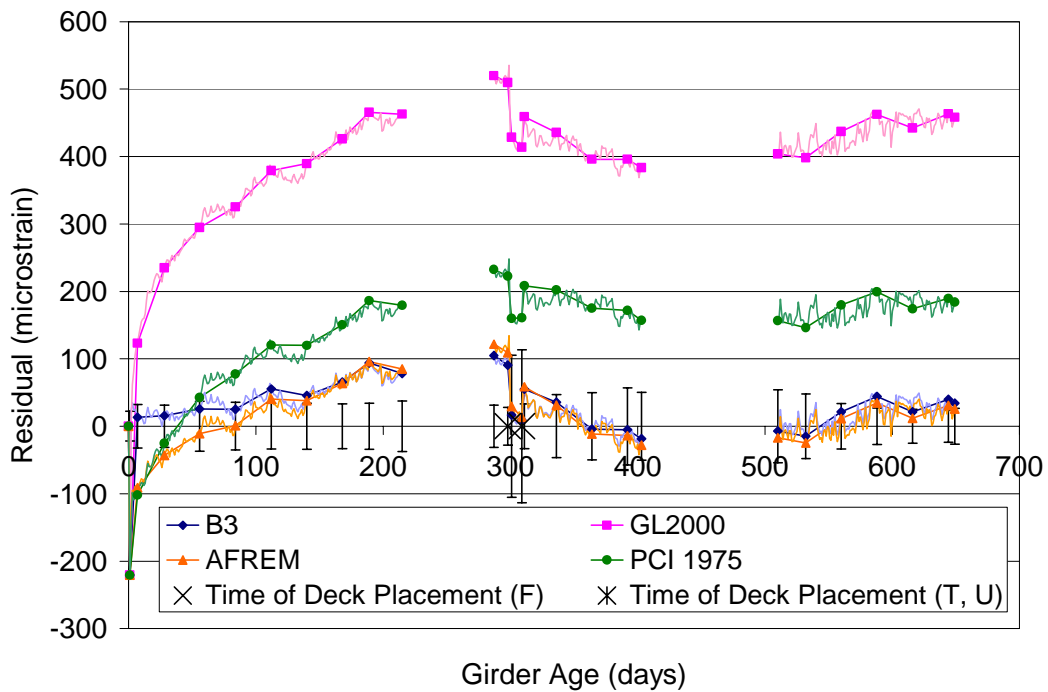


Figure 14 – Pinner’s Point Girders F, T, and U Residual Strains for the B3, GL2000, AFREM, and PCI-1975 Models

In addition to the existing creep and shrinkage models, models based on the results of the creep and shrinkage testing conducted by Townsend (2003) were constructed. These models were constructed by performing a nonlinear regression analysis on the laboratory creep coefficient and shrinkage strain to determine the parameters of Equations 5 and 6 that minimize the sum of the square of the residuals between the data and the model. The resulting models for the creep coefficient and shrinkage strain are given in Equations 9 and 10, respectively. When compared to the HPLWC, the ultimate creep coefficient for the Pinner's Point concrete is lower (1.18 vs. 2.27), but the ultimate shrinkage strain is higher, (596 vs. 527 microstrain) but by less than 15%. The higher ultimate creep coefficient of the HPLWC is expected since the lightweight aggregate is less stiff and less able to resist the loads transferred from the cement paste as a result of creep. The development of both creep and shrinkage with time are also slower for the Pinner's Point concrete, as indicated by the larger constants in the denominator of Equations 9 and 10 compared to Equations 7 and 8.

$$v_t = 1.18 \frac{t^{0.71}}{5.90 + t^{0.71}}, R^2 = 0.9929 \quad \text{Eq. 9}$$

$$(\epsilon_{sh})_t = 596 * (10^{-6}) \frac{t^{0.36}}{5.83 + t^{0.36}}, R^2 = 0.9905 \quad \text{Eq. 10}$$

The models established from the laboratory testing were used with the correction factors for humidity and size given by the ACI-209 and AASHTO LRFD models to predict the strains for Girders F, T, and U. Figures 15 and 16 show the predicted and residual strains, respectively, for these models. Both models under-predict the measured strains for the majority of the observed period. The model corrected using the ACI-209 factors predicts within the error bars between 100 days and deck placement, under-predicting by less than 50 microstrain and over-predicting by less than 20 microstrain during this period. Between 7 days and 100 days, the model under-predicts by as much as 110 microstrain, but the residual rapidly decreases becoming less than 50 microstrain after 50 days. The model corrected using the AASHTO LRFD factors only predicts within the error bars just prior to deck placement, and under-predicts by as much as 210 microstrain and as little as 50 microstrain between 7 days and deck placement. After deck placement, the two models follow a similar trend, under-predicting by as much as 160 microstrain.

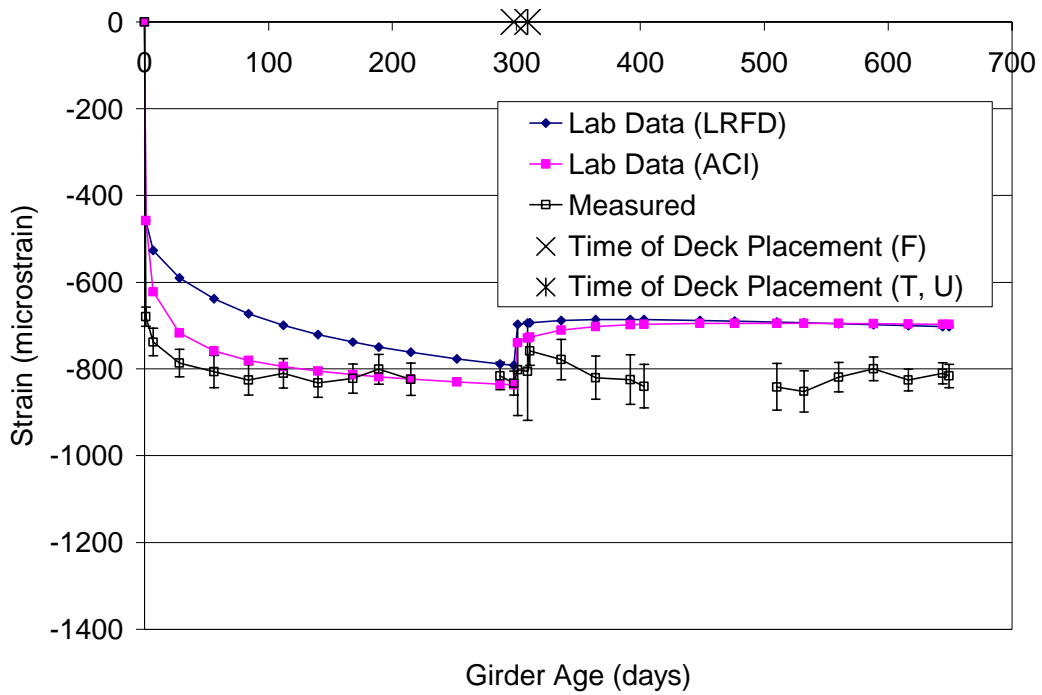


Figure 15 – Pinner’s Point Girders F, T, and U Predicted Strains for the Models Correlated to the Measured Creep and Shrinkage Properties

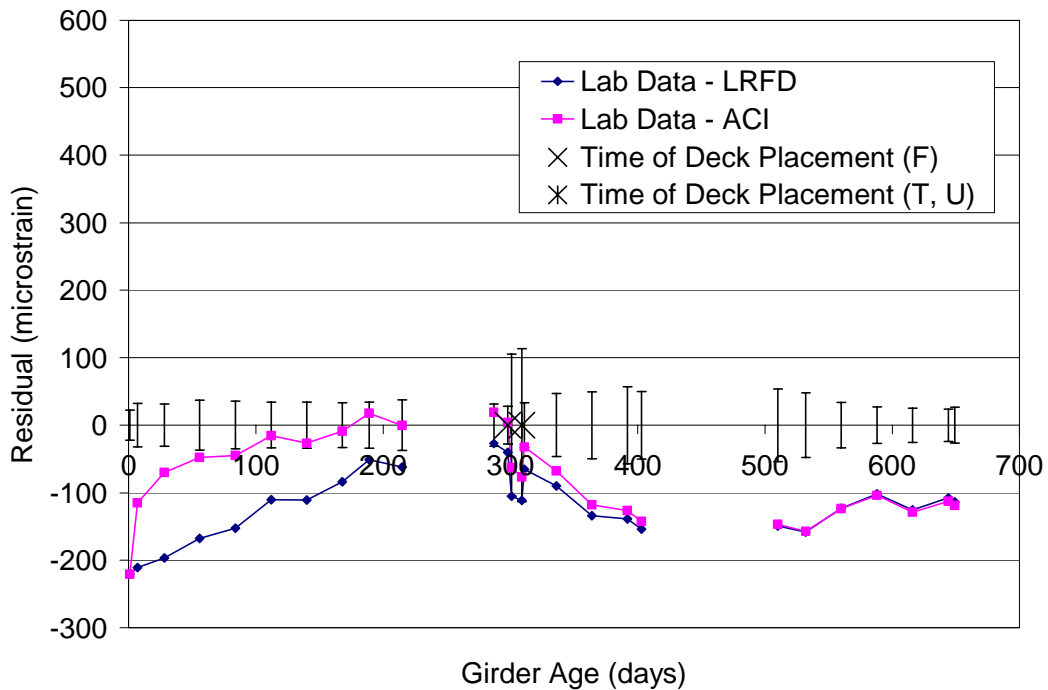


Figure 16 – Pinner’s Point Girders F, T, and U Residual Strains for the Models Correlated to the Measured Creep and Shrinkage Properties

The concrete produced in the laboratory for the creep and shrinkage study conducted by Townsend better represents the concrete used in the Pinner’s Point girders than was the case for the HPLWC study as indicated by the lower residuals of the laboratory data model for girders F, T, and U, as compared to the HPLWC girders. The most significant difference between the specimens prepared in the laboratory and girders F, T, and U is the observed compressive strength. The compressive strength at release for the laboratory specimens is 9,890 psi compared to 6,570 psi for the bridge girders. The 28 day compressive strength for laboratory specimens is 12,500 psi compared to 8,560 for the bridge girders. As expected, the measured moduli are also different, but are modeled well using the measured compressive strengths. Although not shown in Figure 48, applying the AASHTO LRFD correction factor for strength results in an increase in the ultimate creep coefficient and would increase the predicted long-term strains. However, with this adjustment made, the models would still under-predict the early strains of girders F, T, and U and the strains after deck placement, and the maximum under-prediction of the measured strains after deck placement would reduce from 160 to 130 microstrain. Therefore, the differences between the strengths of the laboratory specimens and bridge girders are not enough to fully account for the difference between the measured and modeled behavior. The correction factors for non-standard conditions, then, do not fully account for the differences in environmental and geometric conditions for these girders.

### **Girders F, T, and U Residuals Squared Analysis and Model Ranking**

The residual strains were squared and summed over the modeled period to rank the models with regard to their ability to predict the measured strains. Figure 50 shows the sums of the residuals squared, plotted on a logarithmic scale, and Table 8 shows the model rankings. Model with similar sums are again ranked equally. The B3 model is the best predictor of the measured strains, predicting within the error bars between 2 days and 80 days and after deck placement. The AFREM model also predicts within the error bars for a significant period, predicting within the error bars between 40 days and 140 days and between 300 days and 650 days.

**Table 8 –Girders F, T, and U Model Ranking**

Ranking	Model
1	B3
1	AFREM
2	Shams and Kahn
2	Lab Data – ACI
2	AASHTO LRFD
2	PCI-BDM
3	NCHRP 496
3	Lab Data – LRFD
4	CEB-FIP MC90
4	PCI-1975
5	ACI-209
6	GL2000

## **Girders G, H, and J Predicted Strains and Model Residuals**

Figures 17 through 22 show the predicted and residual strains for Pinner's Point Girders G, H, and J, which are the 10,000 psi design strength girders. As before, the error bars show two standard deviations above and below the average strains for the three girders. Figures 17 and 18 show the predicted and residual strains, respectively, for the ACI-209, PCI-BDM, and CEB-FIP MC90 models. The ACI-209 model for girders G, H, and J is similar to the ACI-209 model for girders F, T, and U since the concrete strength is not an input parameter for this model. The difference between the two models results from a difference in the modeled elastic moduli of the two sets of girders. The ACI-209 model under-predicts the measured strains by as much as 200 microstrain between 7 and 50 days and over-predicts by as much as 250 microstrain for the remainder of the period before the deck is cast. After the deck is cast, the model continues to over-predict the measured strains, over-predicting by 130 to 200 microstrain between 500 and 650 days. The PCI-BDM and CEB-FIP MC90 models predict similar strains prior to deck placement. Both models under-predict the measured strains before 115 days, but predict within the error bars between 55 and 170 days. Between 55 and 170 days, the models transition from under-predicting by 50 microstrain to over-predicting by 50 microstrain. After deck placement, the models diverge, and the PCI-BDM model again predicts within the error bars between 500 and 650 days, predicting within plus and minus 30 microstrain of the measured strains. The CEB-FIP MC90 model shows a more consistent residual between 300 and 650 days than do the other two models indicating that this model more closely mirrors the changes in strain of the bridge girders after deck placement. However, during this time, the absolute magnitude of the strains predicted by the CEB-FIP MC90 model over-predict the measured strains by 40 to 120 microstrain.

Figures 19 and 20 show the predicted and residual strains, respectively, for the AASHTO LRFD, Shams and Kahn, and NCHRP 496 models. The AASHTO LRFD and NCHRP 496 models under-predict the measured strains at early ages with the AASHTO LRFD model under-predicting by as much as 290 microstrain between 7 and 200 days and the NCHRP 496 model under-predicting by as much as 260 microstrain between 7 and 140 days. After deck placement, the AASHTO LRFD model over-predicts by 20 to 100 microstrain, and the Shams and Kahn model under-predicts by 20 to 100 microstrain. The NCHRP 496 model over-predicts the measured strains by as much as 80 microstrain immediately after deck placement and until approximately one year; however, after one year, the NCHRP model under-predicts by as much as 60 microstrain.

Figures 21 and 22 show the predicted and residual strains, respectively, for the B3, GL2000, AFREM, and PCI-1975 models. The B3 model under-predicts for the majority of the modeled period, predicting within the error bars after 150 days. After 150 days, the B3 model under-predicts by less than 50 microstrain and over-predicts by less than 20 microstrain. The AFREM model predicts similar strains to the B3 model under-predicting the measured strains with the exception of just before and shortly after deck placement. The AFREM model predicts within the error bars after 120 days, under- and over-predicting by less than 50 microstrain. The GL2000 model over-predicts the measured strains after 7 days, and over-predicts by as much as 420 microstrain during the modeled period. Finally, the PCI-1975 model under-predicts the measured strains for the first 50 days and over-predicts for the remainder of the modeled period. After deck placement, the PCI-1975 model most closely mirrors the changes in strain of the

bridge girders, as evidenced by the consistent residuals, and the model over-predicts by 180 to 250 microstrain.

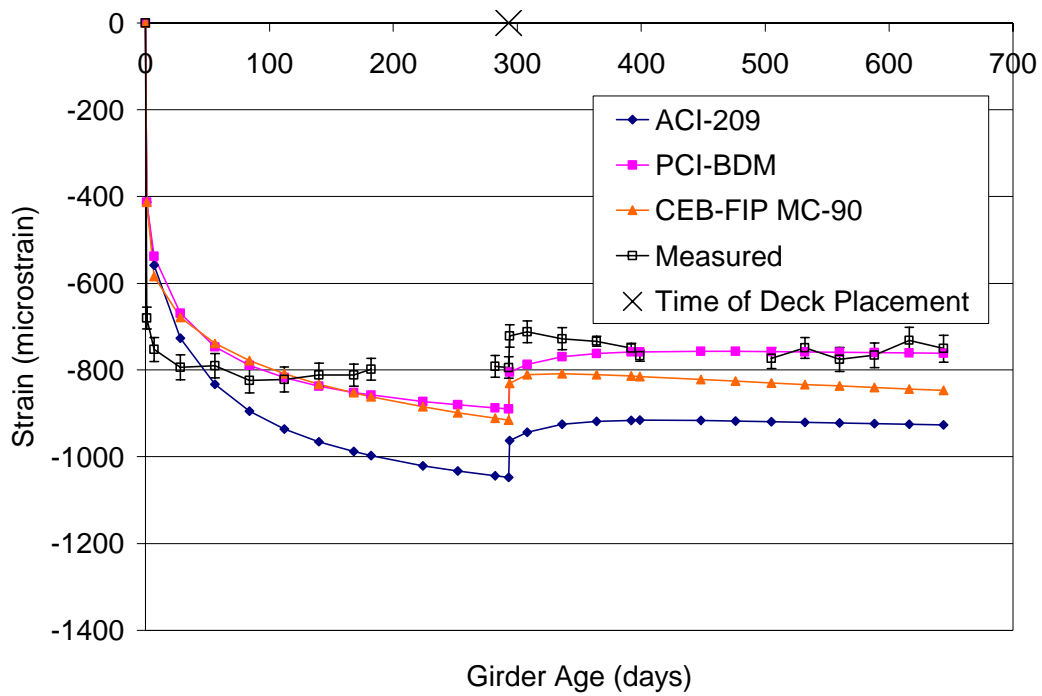


Figure 17 – Pinner’s Point Girders G, H, and J Predicted Strains for the ACI-209, PCI-BDM, and CEB-FIP MC90 Models

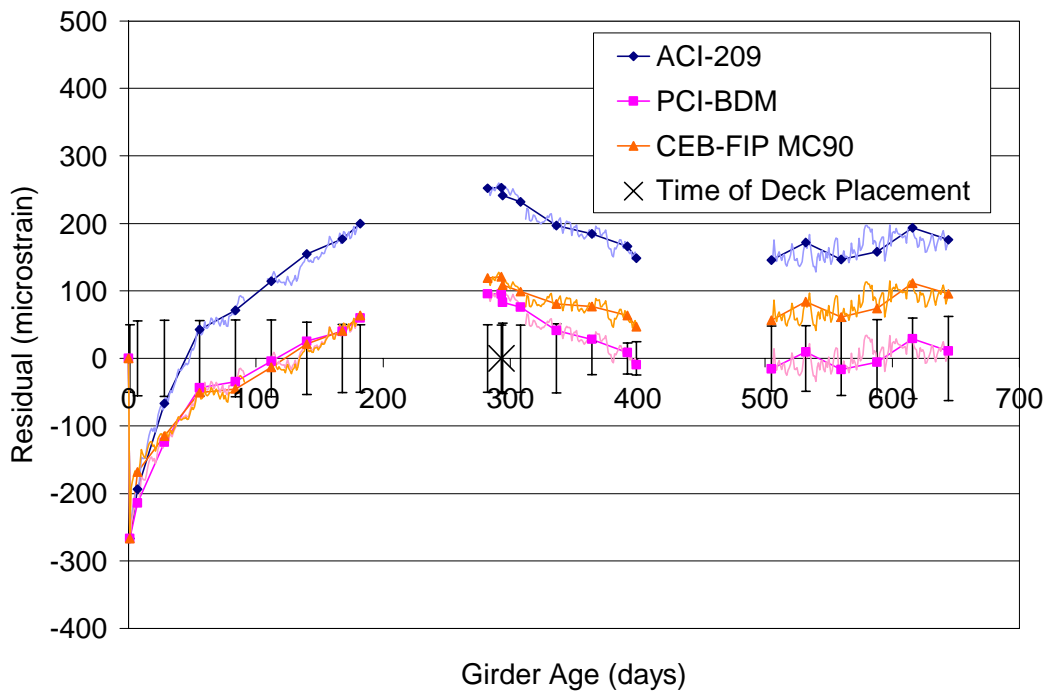


Figure 18 – Pinner’s Point Girders G, H, and J Residual Strains for the ACI-209, PCI-BDM, and CEB-FIP MC90 Models

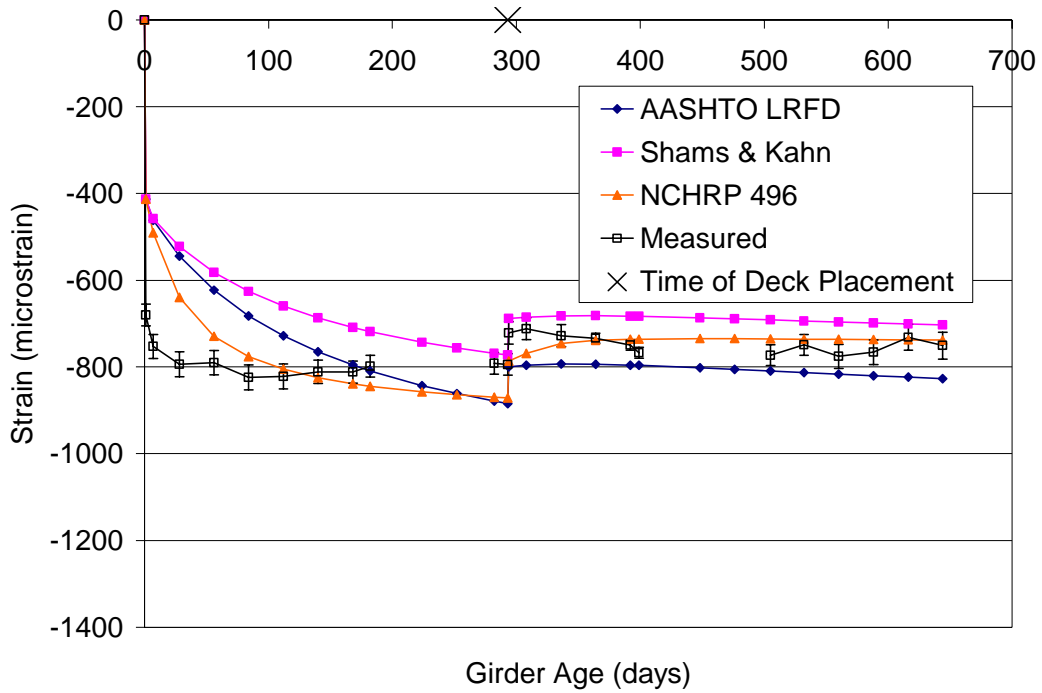


Figure 19 – Pinner’s Point Girders G, H, and J Predicted Strains for the AASHTO LRFD, Shams and Kahn, and NCHRP 496 Models

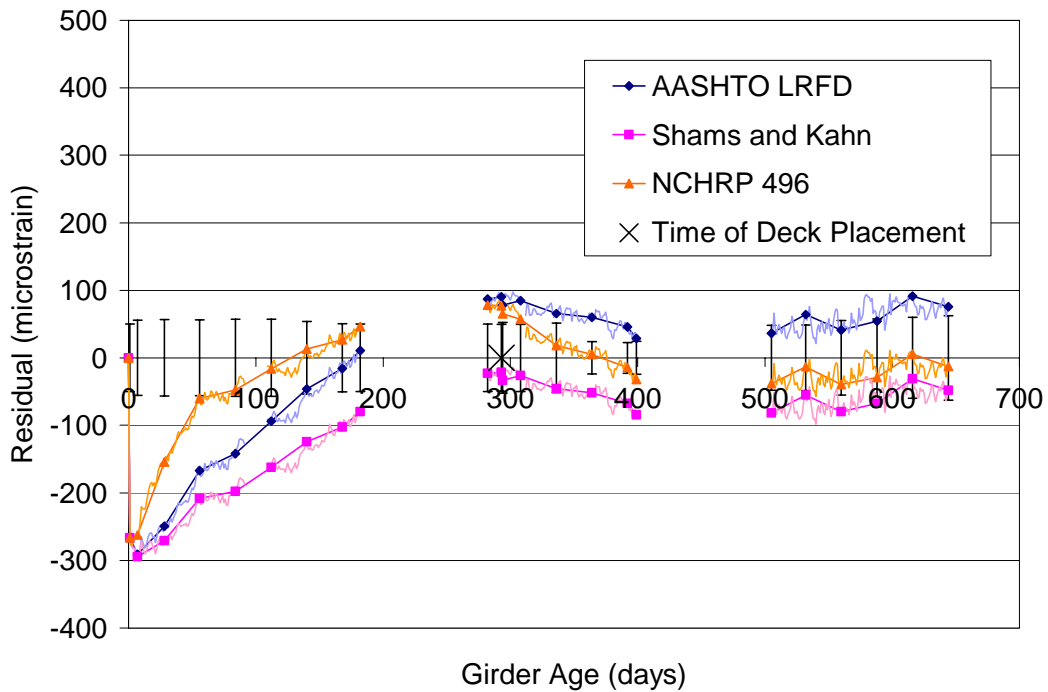


Figure 20 – Pinner’s Point Girders G, H, and J Residual Strains for the AASHTO LRFD, Shams and Kahn, and NCHRP 496 Models

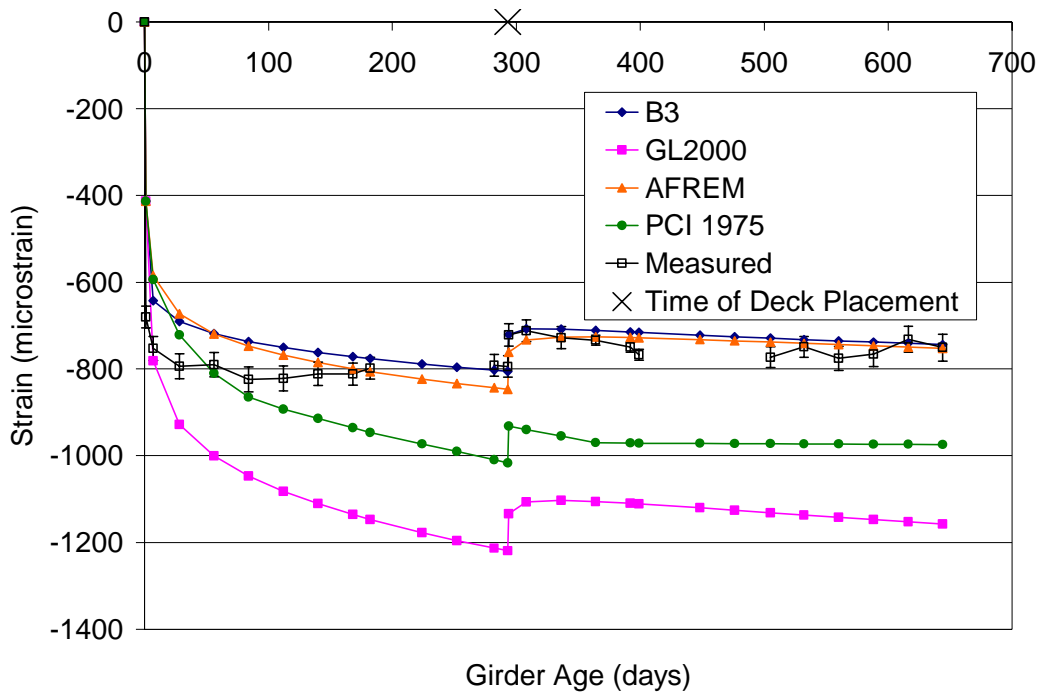


Figure 21 – Pinner’s Point Girders G, H, and J Predicted Strains for the B3, GL2000, AFREM, and PCI-1975 Models

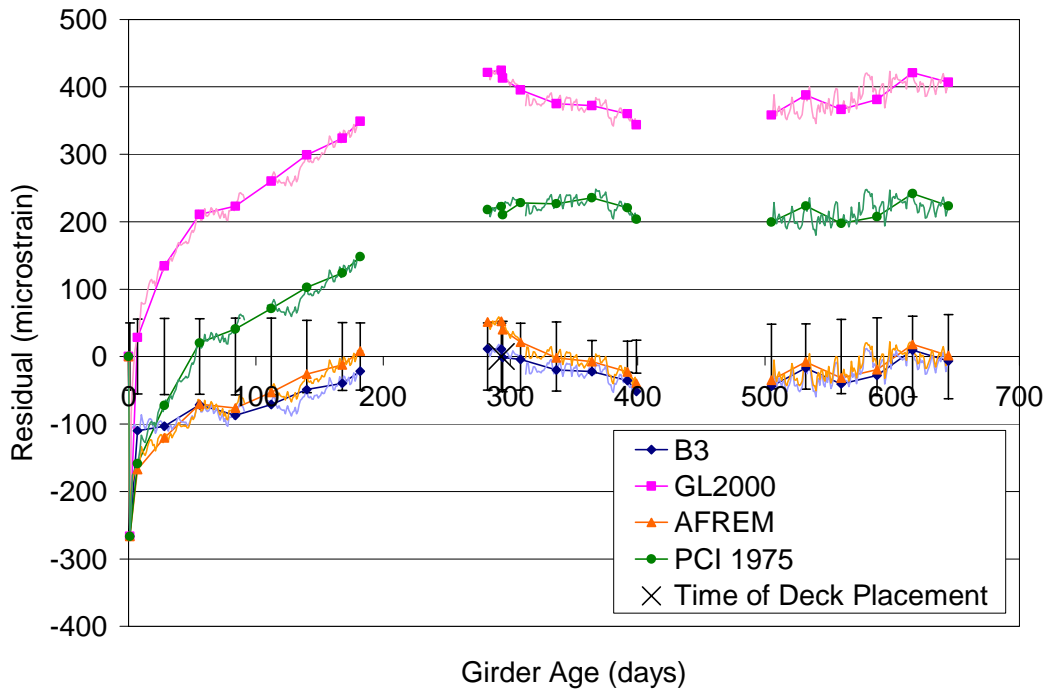


Figure 22 – Pinner’s Point Girders G, H, and J Residuals Strains for the B3, GL2000, AFREM, and PCI-1975 Models

As was the case for Pinner's Point Girders F, T, and U, each model over-estimates the contribution of creep recovery and differential shrinkage after deck placement with the exception of the PCI-1975 model. For the PCI-1975 model, creep recovery and differential shrinkage are not explicitly included as the creep over each time step which is simply determined by the stress at the centroid of the prestressing force at the beginning of that time step. Therefore, a new creep function for loads applied at the time the deck is placed is not determined, and the stress driving creep is simply reduced after the deck slab is cast. Girders G, H, and J do not show as dramatic an increase in the compressive strains after deck placement, as do Girders F, T, and U, and again, some of this increase in compressive strain is due to the removal of the deck forms over several weeks after the deck was cast. However, it is unlikely that the dead load of the deck forms is 65% to 70% of the dead load of the deck slab, as would be required for the increase in strain to be completely accounted for by the removal of the forms. It is also unlikely that the removal of the deck forms proceeded slowly over the 100 day period where the increase in compressive strain occurs. It is more likely that the girders experienced less tensile strains due to creep recovery and differential shrinkage than expected; however, the complete nature of the increase in compressive strains after deck placement, given the minimal changes in strain for the 100 days prior to the deck placement, is not completely understood.

In addition to the models presented previously, the model correlated to the laboratory study conducted by Townsend (2003), presented in Equations 9 and 10, was used to model Girders G, H, and J. This model was again corrected for the non-standard conditions of the bridge site using the factors for relative humidity and specimen size recommended by ACI-209 and the AASHTO LRFD Specification. Figures 23 and 24 show the predicted and residual strains, respectively, for these models. The difference between these models and those presented in Figures 15 and 16 is a result of the different modeled moduli of Girder G, H, and J and F, T, and U only. The factor for compressive strength was not used with the AASHTO LRFD corrections because the correction factor is based on the design strength and correcting the model to the higher design strength of Girders G, H, and J would be contradictory to the trend of the measured 28 day compressive strengths of the laboratory specimens and the bridge girders. Although the bridge girders had a higher design strength of 10,000 psi compared to 8,000 psi for the laboratory specimens, the laboratory specimens had a higher average 28 day compressive strength of 12,500 psi compared to 10,800 psi for the bridge girders.

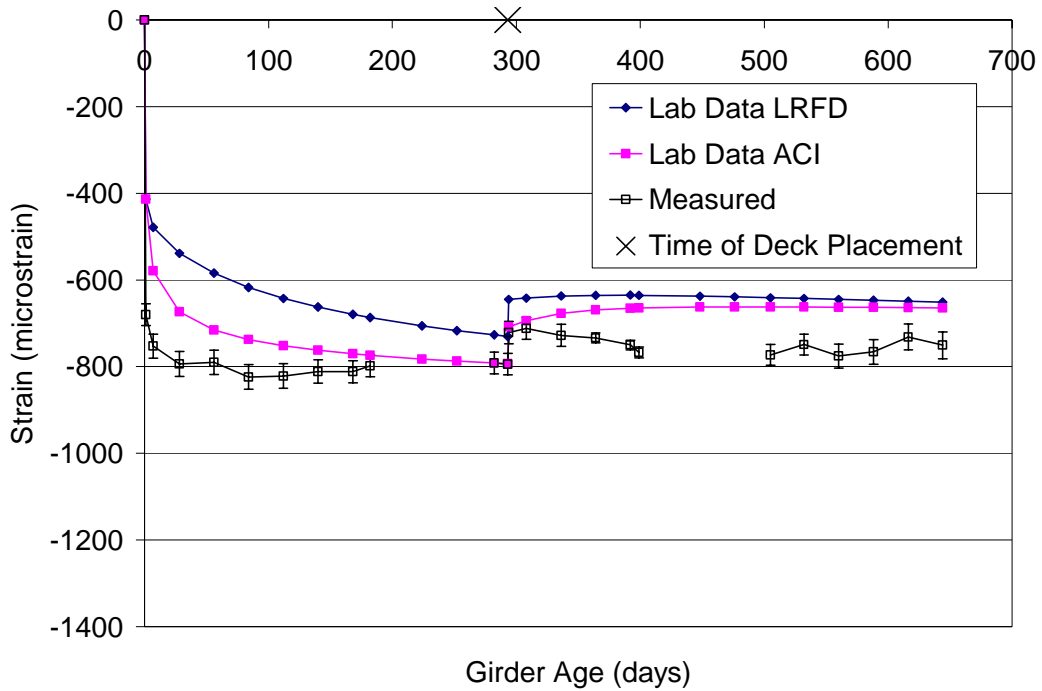


Figure 23 – Pinner’s Point Girders G, H, and J Predicted Strains for the Models Correlated to the Measured Creep and Shrinkage Properties

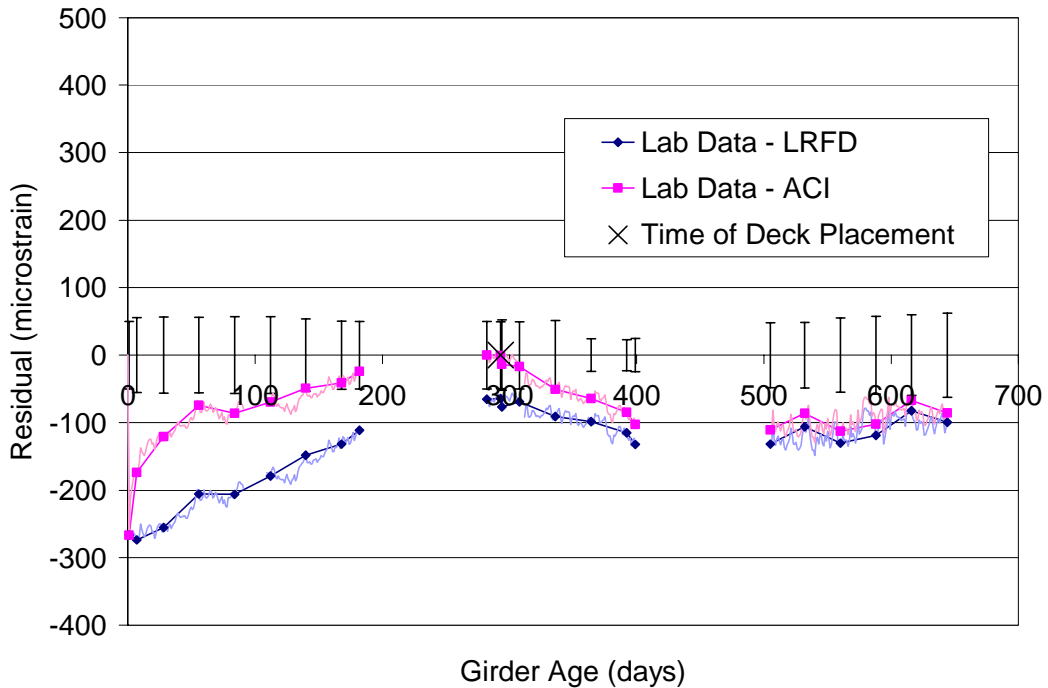


Figure 24 – Pinner’s Point Girders G, H, and J Predicted Strains for the Models Correlated to the Measured Creep and Shrinkage Properties

Both the models correlated to the measured creep and shrinkage properties under-predict the strains for the duration of the modeled period. Neither model predicts within the error bars for an extended period, but the model corrected using the factors from ACI-209 more closely

matches the magnitude and trend of the measured strains indicating that these factors for non-standard conditions more accurately represent the changes in creep and shrinkage behavior due to changes in environmental conditions and specimen size. The model corrected using the ACI-209 factors under-predicts by 40 to 180 microstrain between 7 and 200 days, while the model corrected using the AASHTO LRFD factors under-predicts by 110 to 280 microstrain during this same period. The ACI-209 corrected model under-predicts by 20 to 120 microstrain and AASHTO LRFD corrected model under-predicts by 70 to 130 microstrain between 300 and 400 days. Finally, both models under-predict by 80 to 150 microstrain between 500 and 650 days.

The under-prediction of the measured strains by the models is partly related to the higher compressive strength of the laboratory specimens due to the unintended lower water-cement ratio of these specimens reported by Townsend (2003). The water-cement ratio of the bridge girders was 0.33 while the water-cement ratio of the laboratory specimens was 0.30. This difference is due to the absorption of the aggregate. The concrete prepared at the casting yard was prepared with moist aggregates, approximately in the saturated surface dry (SSD) condition. The concrete prepared in the laboratory was prepared with oven dried aggregates and additional water to account for aggregate absorption was not included in the mixture, thus reducing the water available for hydration. However, the difference in compressive strength is not sufficient to account for the whole of the difference between the models and the measured strains. If the AASHTO LRFD factor for compressive strength were applied to these models, the ultimate creep coefficient would increase by 10%, and, the model curves would shift downward. However, at 650 days the residual strain for the AASHTO LRFD corrected model would only be reduced 20 microstrain from 100 to 80 microstrain, and the residual strain for the ACI-209 corrected model would only be reduced 10 microstrain from 100 microstrain to 90 microstrain. Therefore, the rest of the difference between the predicted and measured strains is the result of differences in the creep and shrinkage behavior of the laboratory specimens and bridge girders, and a result of inaccuracies in the correction factors for environmental conditions and specimen size.

### **Girders G, H, and J Residuals Squared Analysis and Model Ranking**

The final step in the analysis of the creep and shrinkage models for the Pinner's Point girders is to examine the sum of the daily residual strains squared to rank the prediction models. As before, for this analysis, the square of the residual strains are summed over the modeled period, and the resulting sums are used to rank the models. Table 9 shows the resulting ranking of the models, where models with similar sums are ranked equally. The B3 model is again the best predictor of the measured strains; however, unlike Girders F, T, and U, several of the models, including the AFREM, PCI-BDM, and NCHRP 496 models predict within the error bars for a portion of the modeled period, most notably after 500 days.

**Table 9 – Girders G, H, and J Model Ranking**

Ranking	Model
1	B3
1	AFREM
2	PCI-BDM
2	NCHRP 496
3	CEB-FIP MC90
3	Lab Data - ACI
4	AASHTO LRFD
5	Shams and Kahn
5	Lab Data – LRFD
6	ACI-209
6	PCI-1975
7	GL2000

### **Prestress Loss Calculations**

A comparison of the prestress losses estimated by the previously presented methods was performed for the six girders of the Pinner’s Point Bridge, and is presented in the following sections. Several methods account for compressive strength including the AAHSHTO LRFD Refined and Lump Sum, PCI-BDM, and NCHRP 496 Refined and Approximate methods.

### **Predicted Prestress Losses**

The predicted losses for Pinner’s Point Girders F, T, and U and Girders G, H, and J are presented in Table 10 and Table 11, respectively. The estimated total losses for Girders F, T, and U range from 31.3 ksi for the NCHRP 496 Refined method to 59.7 ksi for the AASHTO Standard Specification Lump Sum method, a difference of almost 100%, and the estimated losses for Girders G, H, and J range from 26.2 ksi for the NCHRP 496 Refined method to 58.4 ksi for the AASHTO Standard Specification Lump Sum method, a difference of over 100%. These large differences indicate the wide variation in the estimates of the various methods. Also, shown in Tables 11 and 12 are the predicted strains in the girders after all losses have occurred.

### **Comparison of Predicted and Measured Prestress Losses**

Table 12 and 13 present a comparison of the predicted and measured prestress losses for Girders F, T, and U and Girders G, H, and J, respectively. The losses are separated into losses occurring before and after deck placement for the models that allow the prediction of losses at any time (see Table 2), do not include steel relaxation losses. For the estimated losses to be compared to the losses determined from the measured strains, the measured strains must be adjusted to the end of service life for the bridge girders, which is assumed to be 75 years. To determine the approximate strain in the girders at the end of service life, a logarithmic curve is fit to the strains measured after deck placement and evaluated at 75 years (27,400 days). The estimated strain at the end of service life for Girders F, T, and U is 970 microstrain, and the estimated strain at the end of service life for girders G, H, and J is 960 microstrain. The measured total losses presented in Tables 13 and 14 are then determined from the estimated

**Table 10 – Predicted Prestress Losses for Pinner’s Point Girders F, T, and U**

Method	Initial Losses		Long-Term Losses			Total	P/S Centroid Strain
	Initial Rel.	ES	Shrinkage	Creep	Add'l Rel.		
	ksi	ksi	ksi	ksi	ksi		
AASHTO Standard General	1.7	13.0	5.8	23.1	3.4	47.0	-1,470
AASHTO Standard Lump Sum			45.0			59.7	-1,930 <sup>#</sup>
AASHTO LRFD Refined			11.2	12.4	3.0	41.3	-1,280
AASHTO LRFD General			5.8	23.1	2.7	46.3	-1,470
AASHTO LRFD Lump Sum			30.1			44.8	-1,420*
PCI-BDM			7.6	8.1	2.8	33.2	-1,010
NCHRP 496 Refined**			5.6	8.5	2.5	31.3	-947
NCHRP 496 Approximate			18.8			33.5	-1,030 <sup>+</sup>
PCI-1975			8.7	12.3	3.2	38.9	-1,190

<sup>#</sup> - Additional steel relaxation losses of 3.1 ksi assumed per AASHTO Standard General method

\* - Additional steel relaxation losses of 2.7 ksi assumed per AASHTO LRFD General method

<sup>+</sup> - Additional steel relaxation losses of 2.4 ksi assumed per Tadros et al., 2003.

\*\* - NCHRP 496 Refined shrinkage losses include the prestress gain due to differential shrinkage, and the creep losses include the elastic gain due to the deck slab.

**Table 11 – Predicted Prestress Losses for Pinner’s Point Girders G, H, and J**

Method	Initial Losses		Long-Term Losses			Total	P/S Centroid Strain
	Initial Rel.	ES	Shrinkage	Creep	Add'l Rel.		
	ksi	Ksi	ksi	ksi	ksi		
AASHTO Standard General	1.7	11.7	5.8	23.2	3.4	45.8	-1,430
AASHTO Standard Lump Sum			45.0			58.4	-1,870 <sup>#</sup>
AASHTO LRFD Refined			11.2	9.5	3.4	37.5	-1,140
AASHTO LRFD General			5.8	23.2	2.9	45.3	-1,430
AASHTO LRFD Lump Sum			28.5			41.9	-1,310*
PCI-BDM			6.8	6.4	3.1	29.7	-874
NCHRP 496 Refined**			4.6	6.2	2.0	26.2	-789
NCHRP 496 Approximate			15.9			29.3	-884 <sup>+</sup>
PCI-1975			8.7	12.8	3.4	38.3	-1,170

<sup>#</sup> - Additional steel relaxation losses of 3.4 ksi assumed per AASHTO Standard General method

\* - Additional steel relaxation losses of 2.9 ksi assumed per AASHTO LRFD General method

<sup>+</sup> - Additional steel relaxation losses of 2.4 ksi assumed per Tadros et al., 2003.

\*\* - NCHRP 496 Refined shrinkage losses include the prestress gain due to differential shrinkage, and the creep losses include the elastic gain due to the deck slab.

strains at the end of service life assuming strain compatibility between the concrete and the prestressing strands, or simply the strain at the end of service life times the estimated modulus of the prestressing steel.

**Table 12 – Comparison of Predicted and Measured Prestress Losses (excluding relaxation) for Pinner’s Point Girders F, T, and U.**

Method	Elastic Shortening	Loss From Transfer To Deck	Elastic Gain Due To Deck	Loss After Deck	Total Long-Term Loss	Total Loss	Ratio of Predicted to Meas.
	ksi	ksi	ksi	ksi	ksi	ksi	
AASHTO Standard General	13.0	--	-2.7	--	28.9 <sup>+</sup>	41.9	1.77
AASHTO Standard Lump Sum		--		--	41.9 <sup>+</sup>	54.9	1.98
AASHTO LRFD Refined		18.2		8.1	23.6	36.6	1.32
AASHTO LRFD General		--		--	28.9 <sup>+</sup>	41.9	1.51
AASHTO LRFD Lump Sum		--		--	27.4 <sup>+</sup>	40.4	1.46
PCI-BDM		18.0		0.4	15.7	28.7	1.04
NCHRP 496 Refined		17.5		-0.7	14.1	27.1	0.98
NCHRP 496 Approximate		--		--	16.4 <sup>+</sup>	29.4	1.06
PCI-1975		18.6		5.1	21.0	34.0	1.23
Measured		15.7		8.0	-2.3*	6.3	12.0

\* - The deck slab was cast over Girders T and U 5 days after Girder F, and 2.3 ksi is the sum of the changes in tendon stress during the two deck placements.

+ - The elastic gain due to the deck is implicitly included in the total long-term loss for these methods

**Table 13 – Comparison of Predicted and Measured Prestress Losses (excluding relaxation) for Pinner’s Point Girders G, H, and J.**

Method	Elastic Shortening	Loss From Transfer To Deck	Elastic Gain Due To Deck	Loss After Deck	Total Long-Term Loss	Total Loss	Ratio of Predicted to Meas.
	ksi	ksi	ksi	ksi	ksi	ksi	
AASHTO Standard General	11.7	--	-2.4	--	29.0 <sup>+</sup>	40.7	1.49
AASHTO Standard Lump Sum		--		--	41.6 <sup>+</sup>	53.3	1.95
AASHTO LRFD Refined		15.9		7.2	20.7	32.4	1.18
AASHTO LRFD General		--		--	29.0 <sup>+</sup>	40.7	1.49
AASHTO LRFD Lump Sum		--		--	25.6 <sup>+</sup>	37.3	1.36
PCI-BDM		13.5		2.1	13.2	24.9	0.91
NCHRP 496 Refined		13.9		-0.7	10.8	22.5	0.82
NCHRP 496 Approximate		--		--	13.5 <sup>+</sup>	25.2	0.92
PCI-1975		18.6		5.3	21.5	33.2	1.21
Measured		15.7*		7.0	-2.4	7.1	11.7

\* - Estimated from Girders F, T, and U as Girders G, H, and J were not monitored during the time when detensioning was completed until the girders were in final storage 2 hours later.

+ - The elastic gain due to the deck is implicitly included in the total long-term loss for these methods

The NCHRP 496 Refined method for estimating prestress losses is the only method examined that under-estimates the measured losses of Pinner’s Point Girders F, T, and U, predicting 98% of the measured losses. The other methods examined over-estimate the measured losses for Girders F, T, and U by 4% to 98%. The PCI-1975 method over-estimates the measured losses the least of the methods formulated for normal strength concrete, predicting 23% more losses than measured. When compared to the PCI-BDM and NCHRP 496 methods, which are formulated for high strength concrete, it is clear that the methods formulated for high strength concrete more accurately predict the losses of the 8,000 psi design strength Pinner’s Point girders, as expected.

Although the methods for estimating prestress losses that are correlated to high strength concrete predict the measured losses within 6% at the end of service life, the distribution of the losses over the life of the girders for these methods or the methods formulated using normal strength concrete data does not match the measured losses. The measured losses between transfer and deck placement are 8.0 ksi, which is less than half the lowest estimate of these losses (18.0 ksi for the PCI-BDM method). The losses after deck placement are 6.0 ksi, and are estimated reasonably by the AASHTO LRFD Refined and PCI-1975 methods; however, the methods formulated using high strength data over-estimate the contribution of creep recovery and differential shrinkage, and predict losses far below the measured losses. In fact, the NCHRP 496 method predicts a 0.7 ksi gain in the prestressing force after the deck is cast.

In addition to the difference in the measured and estimated long-term losses, there are significant differences in the measured and estimated elastic losses and gains. The estimated elastic shortening losses are 83% of the measured elastic shortening losses, indicating that either the elastic modulus at release or the prestressing force at release are not known with enough accuracy to better predict the initial losses. A modulus of 4,020 ksi at release is needed for the modeled losses to match the measured elastic shortening losses of 15.7 ksi; however, the estimated modulus at release of 4,850 ksi was determined using the ACI equation for modulus with a unit weight of 150 pcf, and this equation accurately modeled the elastic moduli measured by Townsend (2003). The measured elastic gain in the prestressing force is over-estimated by 17%. This result is not surprising, and is most likely due to a higher modulus at deck placement than estimated, a difference in the estimated and actual dead load of the slab due to the complex geometry of the bridge, or a combination of the two.

All three of the methods for estimating prestress losses formulated using data from high strength concrete under-predict the measured losses of Pinner's Point Girders G, H, and J, predicting between 82% and 92% of the measured total losses. Although Girders G, H, and J have a design compressive strength of 10,000 psi at 28 days, and achieved this strength, the concrete mixture used in these girders is virtually the same as the concrete mixture used in Girders F, T, and U. The only difference between the mixtures is the inclusion of five additional gallons of DCI in the mixture used for Girders G, H, and J. The additional DCI accelerated the mixture, producing 7,500 psi at release, as opposed to 6,570 psi for Girder F, T, and U and 10,800 psi at 28 days, as opposed to 8,560 psi at 28 days for Girders F, T, and U. However, this additional compressive strength did not significantly change the long-term behavior measured in the bridge girders, and the estimated total losses at the end of service life differ by only 0.3 ksi (27.4 versus 27.7 ksi) for the two sets of girders. Therefore, for the methods for estimating prestress losses formulated using data for high strength concrete, the estimates using a design strength of 8,000 psi more closely match the measured losses than do the estimates using a 10,000 psi design strength, since Girders G, H and J are produced using an 8,000 psi design strength concrete mixture only slightly modified to yield an design 28 day strength of 10,000 psi.

As was seen with girders F, T, and U, the trend of the estimated losses over the life of Girders G, H, and J does not match the trend of the measured losses. The measured losses between transfer and deck placement for Girders G, H, and J are 7.0 ksi, similar to the 8.0 ksi measured for Girders F, T, and U, and the lowest estimated losses over this time period are 13.5 ksi predicted by the PCI-BDM method. The measured losses for Girders G, H, and J between deck placement and the end of service life are 7.1 ksi, again similar to the losses of 6.3 ksi for

Girders F, T, and U over this time period, and while these losses are reasonably estimated by the AASHTO LRFD and PCI-1975 methods, the PCI-BDM and NCHRP 496 Refined methods significantly under-estimate these losses, with the NCHRP 496 Refined method again predicting a prestress gain over this time period due to creep recovery and differential shrinkage.

The estimated elastic shortening loss using the properties given in Appendix B is 75% of the measured loss of Girders F, T, and U. A direct comparison of the elastic losses of Girders G, H, and J is not possible because strains were not recorded at the completion of detensioning until several hours later after the girders were moved into storage. However, it is reasonable to assume that the elastic losses of Girders G, H, and J are similar to the elastic losses of Girders F, T, and U, since the measured strains in the two girders are similar at early ages. Finally, the elastic gain in the prestressing force due to the deck slab is accurately predicted for Girders G, H, and J. This indicates that the estimated elastic modulus of 6,060 ksi is closer to the modulus for both sets of girders than is the estimated modulus of 5,420 ksi for Girders F, T, and U, assuming the estimated dead load for the deck slab is representative of the actual dead load. However, considering the complex geometry of the bridge, most notably the varying girder spacing and girder spans, the true accuracy of the estimates for the elastic modulus cannot be inferred from comparing the elastic gain in the prestressing force due to the deck slab.

### **Dismal Swamp Bridge**

Three girders from the Dismal Swamp Bridge were instrumented with vibrating wire gages, with three gages across the bottom flange at the level of the centroid of the prestressing force, one gage at the girder centroid, and one gage in the top flange, all at midspan. The girders were monitored for 270 days while at the casting yard, then monitoring was ceased while the girders were shipped to the bridge site and erected. Girders A and C were reconnected at the bridge site 60 days later and monitored for another 70 days, yielding strain readings spanning 400 days. Girder B was not reconnected at the bridge site because the girder was placed in the wrong location in the bridge.

#### **Measured Strains**

Strains were recorded at least every two hours during the monitored periods, and the strain readings from each day were averaged to reduce the data. As was done for the Chickahominy River Bridge and the Pinner's Point Bridge, the time-step modeling procedure was used with the creep and shrinkage models and the variation of creep and shrinkage with time recommended by PCI (1975) to determine the girder strain predicted by each model. These predicted strains were then compared to the measured strains presented in the preceding section to determine which model is the best predictor of the behavior of the instrumented girders in the Dismal Swamp Bridge.

#### **Predicted Strains and Model Residuals**

Figures 25 through 30 present the predicted and residual strains for the various models for the Dismal Swamp Bridge, and the error bars in the figures represent plus and minus two standard deviations of the measured data. Figures 25 and 26 show the predicted and residuals

strains, respectively, for the ACI-209, PCI-BDM, and CEB-FIP MC90 models. Each model under-predicts the measured strains at early ages, with the ACI-209 model under-predicting for the first 50 days and the PCI-BDM and CEB-FIP MC90 models under-predicting for the first 100 days. After 40 days the PCI-BDM model predicts within the error bars; however, the model transitions from the lower limit at 40 days to the upper limit at 240 days and then back towards the lower limit again after deck placement with a maximum under-prediction of 80 microstrain and a maximum over-prediction of 90 microstrain during this period. The CEB-FIP MC90 model follows a trend similar to the PCI-BDM model over-predicting by a slightly larger margin (140 microstrain maximum) after 150 days. The ACI-209 model does not consistently predict within the error bars during the observed period and under-predicts the measured strain by as much as 210 microstrain and over-predicts the measured strain by as much as 340 microstrain after 7 days.

Figures 27 and 28 show the measured and residual strains, respectively, for the AASHTO LRFD, Shams and Kahn, and NCHRP 496 models. Again, each model under-predicts the measured compressive strains at early ages with the AASHTO LRFD model under-predicting for the first 140 days and the NCHRP 496 model under-predicting for the first 60 days. The Shams and Kahn model under-predicts the measured strains for the entire observed period, except for immediately before and after deck placement. The maximum under-prediction of the model is 290 microstrain. The AASHTO LRFD model transitions from the lower two standard deviation limit to the upper two standard deviation limit between 90 and 230 days, and remains near or above the upper limit after 230 days with a maximum over-prediction of 140 microstrain. The NCHRP 496 model follows a trend similar to the AASHTO LRFD model and transitions from the lower to the upper two standard deviation limit between 40 and 120 days. The model then predicts outside the error bars until after deck placement with a maximum over-prediction of 140 microstrain, but over-predicts by only 20 microstrain at 400 days.

Figures 29 and 30 show the predicted and residual strains, respectively, for the B3, GL2000, AFREM, and PCI-1975 models. The B3 and PCI-1975 models over-predict the measured strains after 100 days, the GL2000 model over-predicts the measured strains after 7 days, and the AFREM model always under-predicts the measured strains. The B3 model predicts within the error bars for the majority of the observed period over-predicting by at most 250 microstrain. The GL2000 over-predicts outside the error bars after 14 days, over-predicting by as much as 440 microstrain. The PCI-1975 model predicts within the error bars between 50 and 270 days; however, the model over-predicts outside the error bars by as much as 150 microstrain after deck placement. The AFREM model provides a good lower-limit on the compressive strains for the majority of the observed period, predicting near the lower limit between 100 and 270 days and after deck placement. Just prior to and immediately after deck placement, the AFREM model predicts within 5 microstrain of the measured strains.

As was seen with the Chickahominy River Bridge and the Pinner's Point Bridge, each model over-estimates the gain in prestress after deck placement due to creep recovery and differential shrinkage as evidenced by the predicted decrease in the compressive strain for a short period following deck placement. A decrease in compressive strain due to creep recovery and differential shrinkage is expected due to the nearly constant strains just prior to deck placement indicating that the creep and shrinkage of the girders has nearly stopped. However, the girders

show an increase in compressive strain during the 50 days following deck placement, the reason for which is not completely understood. In the absence of creep and shrinkage in the girder due to the prestressing force, the creep recovery due to the deck weight and the differential shrinkage of the deck concrete should induce a downward movement of the girder and, therefore, a net decrease in the compressive strain at the bottom of the girder; however, this is not the case for the three instrumented bridges.

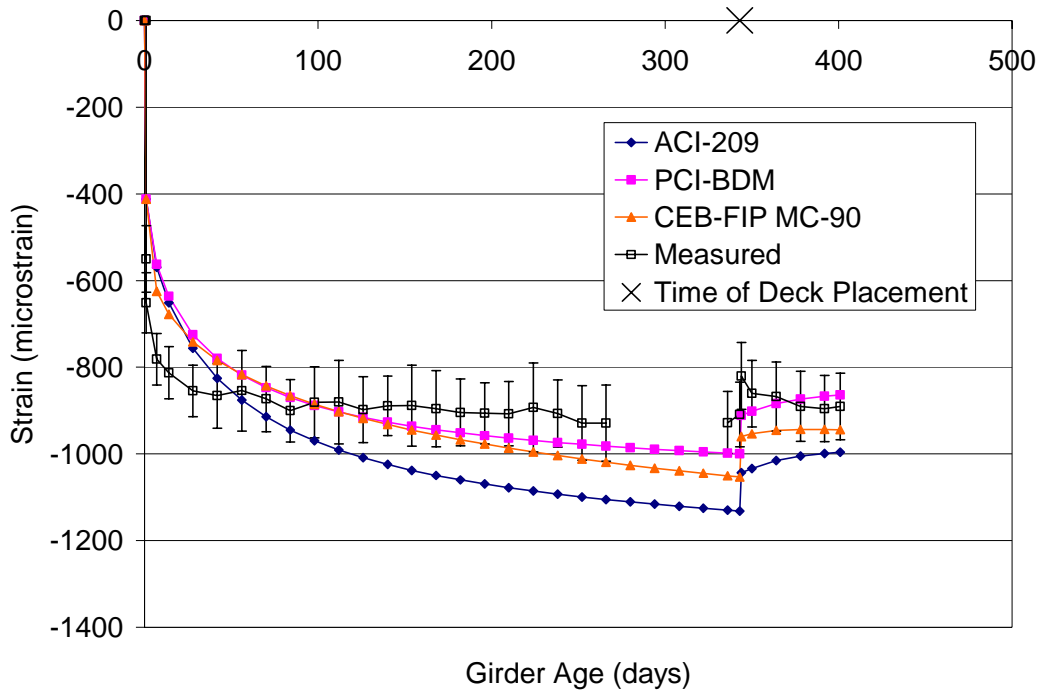


Figure 25 – Dismal Swamp Bridge Predicted Strains for the ACI-209, PCI-BDM, and CEB-FIP MC90 Models

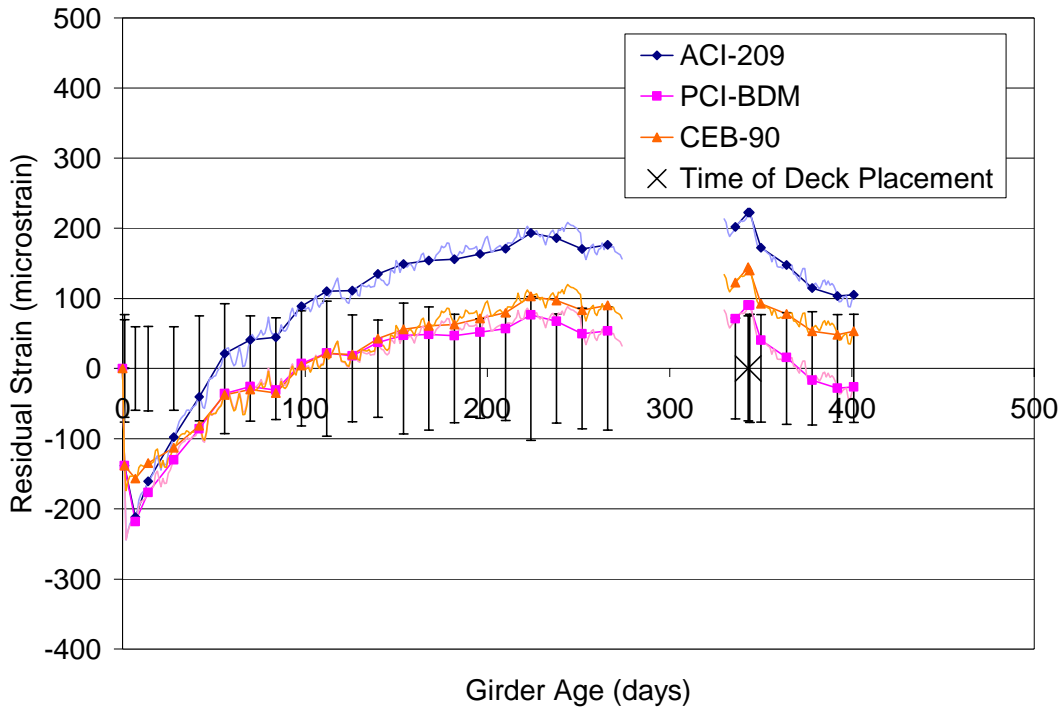


Figure 26 – Dismal Swamp Bridge Residual Strains for the ACI-209, PCI-BDM, and CEB-FIP MC90 Models

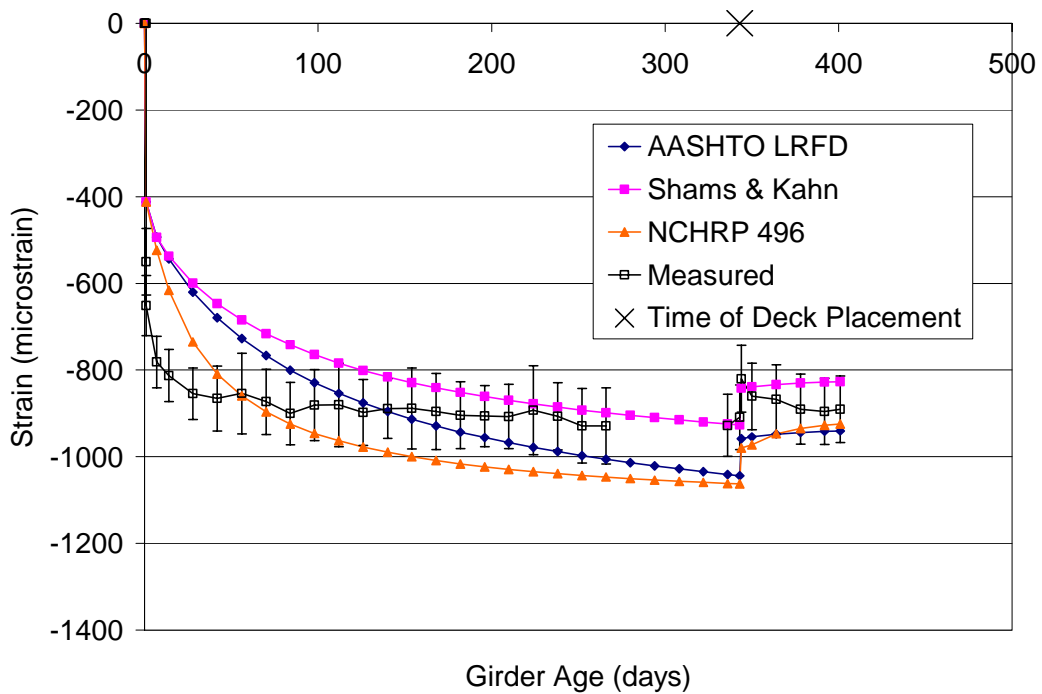


Figure 27 – Dismal Swamp Bridge Predicted Strains for the AASHTO LRFD, Shams and Kahn, and NCHRP 496 Models

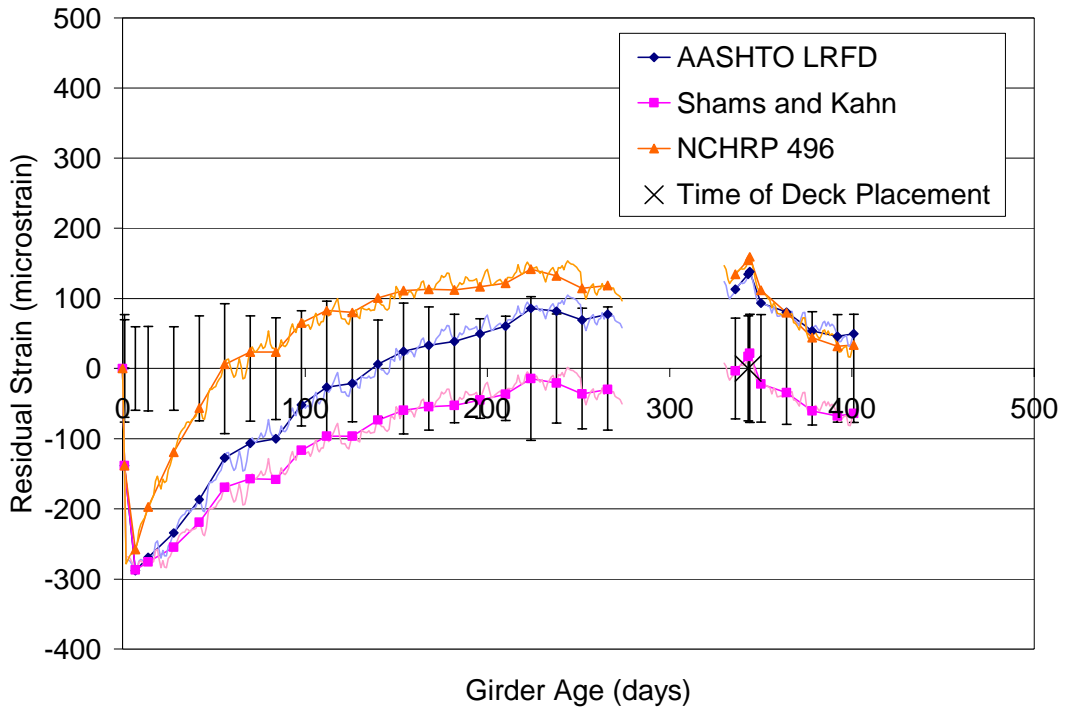


Figure 28 – Dismal Swamp Bridge Residual Strains for the AASHTO LRFD, Shams and Kahn, and NCHRP 496 Models

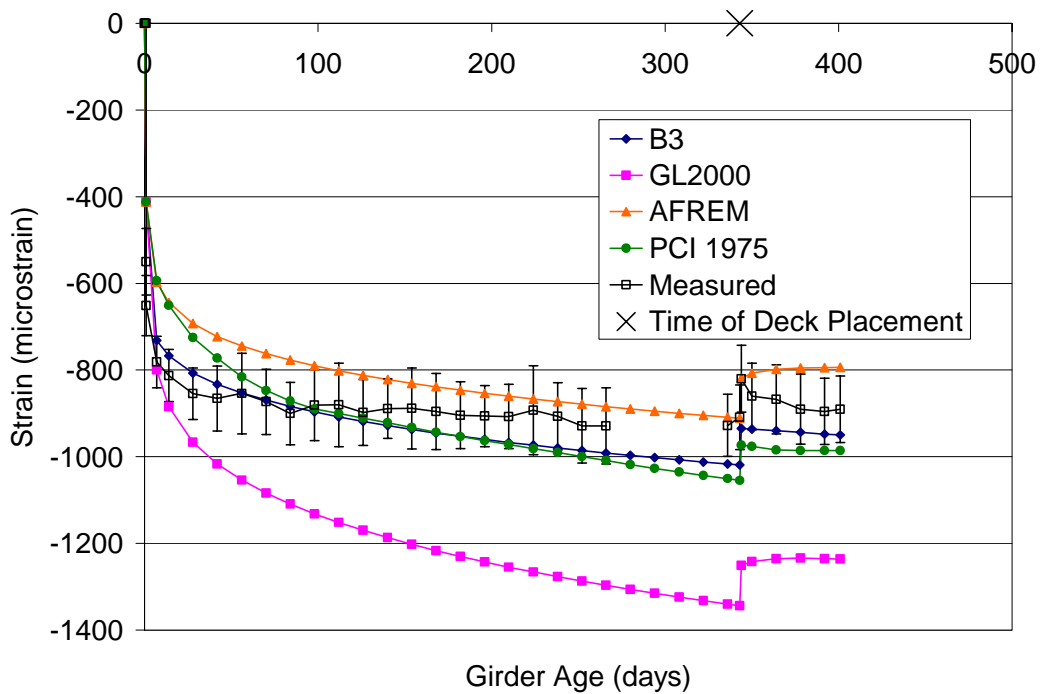
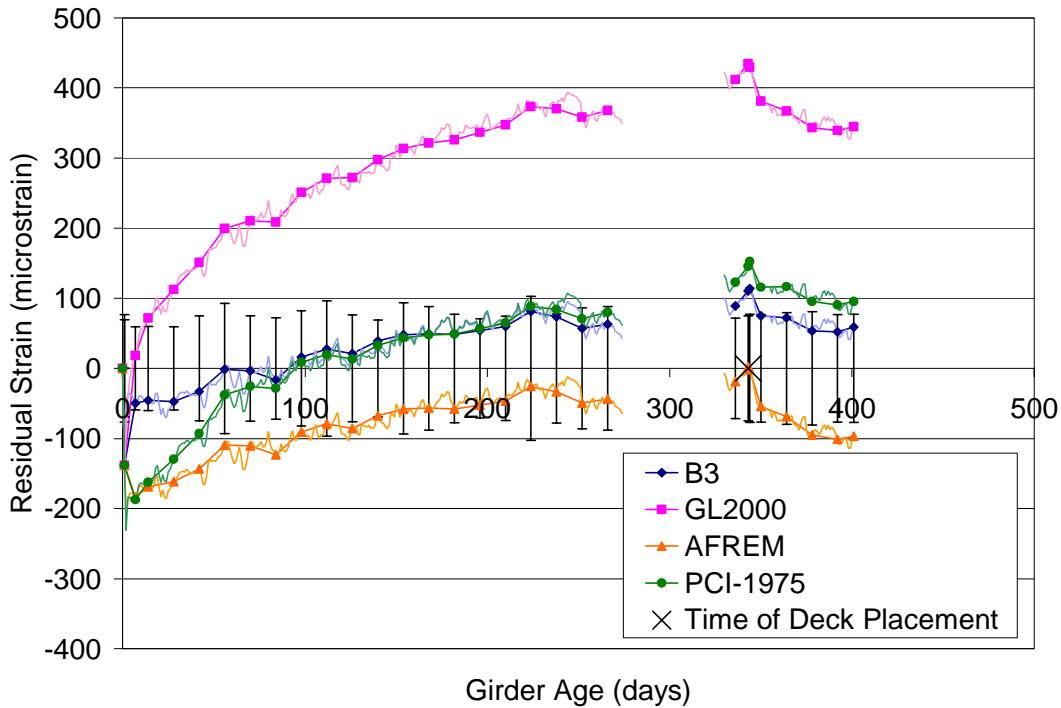


Figure 29 – Dismal Swamp Bridge Predicted Strains for the B3, GL2000, AFREM, and PCI-1975 Models



**Figure 30 – Dismal Swamp Residual Strains for the B3, GL2000, AFREM, and PCI-1975 Models**

In addition to the existing creep and shrinkage models, models based on the results of the creep and shrinkage testing were constructed. These models were again constructed by performing a nonlinear regression analysis on the laboratory creep coefficient and shrinkage strain to determine the parameters of Equations 5 and 6 that minimize the sum of the square of the residuals between the data and the model. The resulting models and correlation coefficients for the creep coefficient and shrinkage strain are given in Equations 11 and 12, respectively. The ultimate creep coefficient for the Dismal Swamp HPC is between the ultimate creep coefficients for the HPLWC and the Pinner’s Point HPC, and the ultimate shrinkage strain is the highest of the concretes investigated. The development of creep and shrinkage with time is the slowest for the Dismal Swamp concrete, as indicated by the higher constants in the denominator of Equations 11 and 12, as compared to Equations 7 through 10.

$$v_t = 1.73 \frac{t^{0.58}}{8.13 + t^{0.58}}, R^2 = 0.9904 \quad \text{Eq. 11}$$

$$(\epsilon_{sh})_t = 725 * (10^{-6}) \frac{t^{0.42}}{9.70 + t^{0.42}}, R^2 = 0.9875 \quad \text{Eq. 12}$$

Equations 11 and 12 were used with the factors for humidity and size given by the ACI-209 and AASHTO LRFD models to predict the strains of the bridge girders. Figures 31 and 32 show the predicted and residual strains, respectively, for these models. The model corrected using the ACI-209 factors more closely matches the measured strains than does the model corrected using the AASHTO LRFD factors before 100 days, while the opposite is true after 100 days, with the exception of just before and just after deck placement. The model corrected using

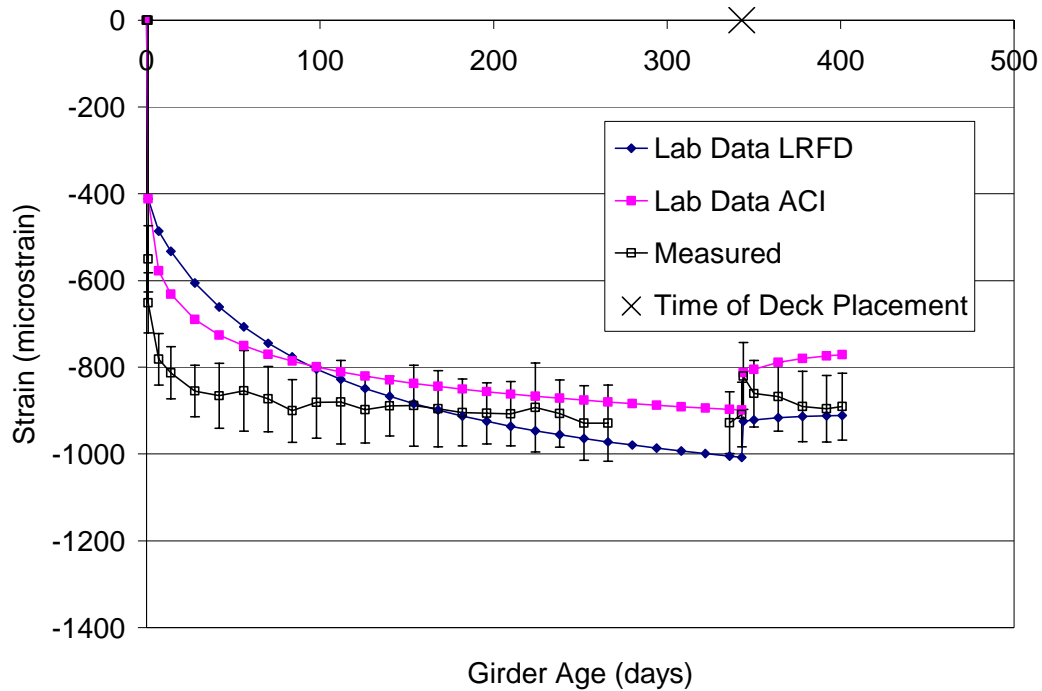


**Figure 31 – Dismal Swamp Bridge Predicted Strains for the Models Correlated to the Measured Creep and Shrinkage Properties**

the ACI-209 factors predicts within the error bars, under-predicting by 20 to 80 microstrain, between 100 days and deck placement; however, prior to 100 days the model under-predicts by as much as 200 microstrain, and after deck placement, the model under-predicts by as much as 130 microstrain. The model corrected using the AASHTO LRFD factors predicts within the error bars after 100 days, with the exception of just prior to and just after deck placement, under-predicting by as much as 80 microstrain and over-predicting by as much as 100 microstrain during this period. However, the model over-predicts by only 20 microstrain at 400 days, and between 7 days and 140 days, under-predicts by as much as 300 microstrain.

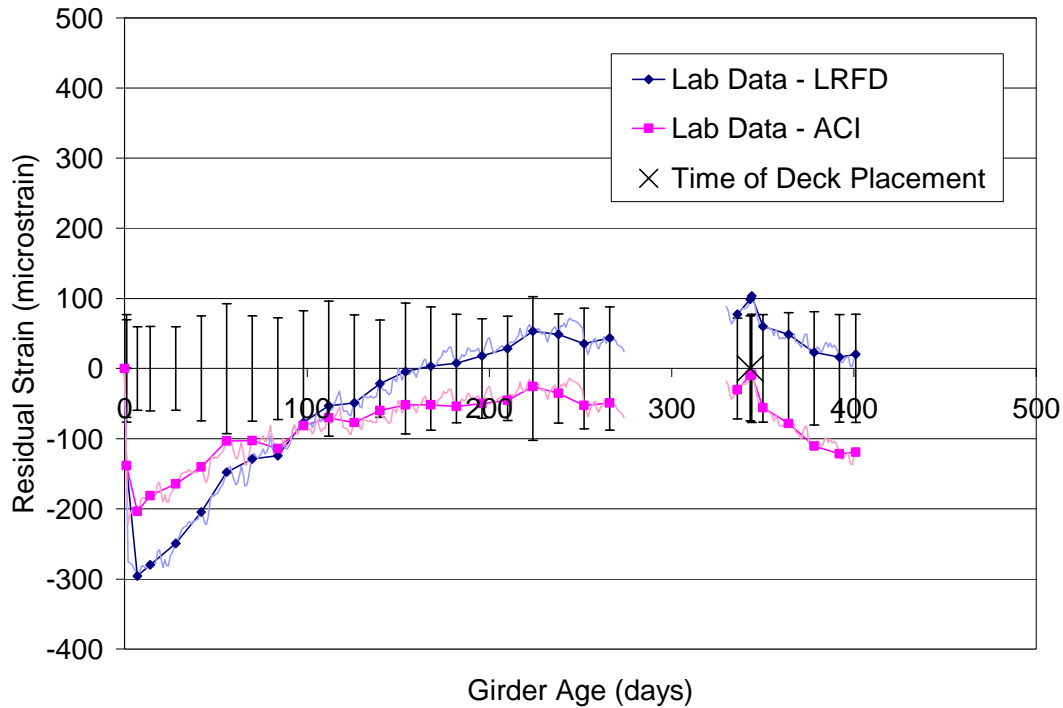


**Figure 32 – Dismal Swamp Bridge Residual Strains for the Models Correlated to the Measured Creep and Shrinkage Properties**

Unlike the creep and shrinkage studies conducted by Vincent (2003) and Townsend (2003), the concrete specimens for the creep and shrinkage study conducted for the Dismal Swamp Bridge were cast and steam-cured alongside the instrumented girders to minimize the difference between the creep and shrinkage specimens and the bridge girders. Still, the predicted strains correlated to the measured creep and shrinkage properties under-predict the measured strains. This is further indication that the factors for non-standard conditions recommended by the ACI-209 and the AASHTO LRFD Specification do not accurately represent the changes in the behavior of the bridge girders due to varying environmental and geometric conditions. The primary difference between the creep and shrinkage specimens and the instrumented girders is the age at loading of the specimens. The bridge girders were loaded immediately after steam-curing, but the creep and shrinkage specimens were not loaded until approximately 24 hours after the end of the steam curing period because of the transporting and preparation time required. Therefore, the shrinkage during the first 24 hours after steam curing was not measured for the laboratory specimens, and considering that the instrumented girders exhibit considerable changes in strain at very early ages, it is possible that the early shrinkage is significant for steam-cured concrete and contributes to the under-prediction of the measured strains at early ages by the models correlated to the measured creep and shrinkage properties.

## Residuals Squared Analysis and Model Ranking

Table 14 shows the resulting ranking of the models. The B3 model is the best predictor of the measured strains over the observed period; however, the AFREM model exhibits the most consistent residual after 100 days, under-predicting by no more than 100 microstrain during this period and providing an approximate to the lower bound of the measured compressive strains. The other models, with the exception of the model correlated to the measured creep and shrinkage properties and adjusted using the ACI-209 factors for non-standard conditions, cross from under-predicting to over-predicting at least once during the observed period.

**Table 14 – Dismal Swamp Model  
Ranking**

Ranking	Model
1	B3
2	PCI-BDM
2	CEB-FIP MC90
3	PCI-1975
3	AFREM
3	Lab Data – ACI
4	NCHRP 496
4	Lab Data – LRFD
4	AASHTO LRFD
4	Shams and Kahn
5	ACI-209
6	GL2000

## Prestress Loss Calculations

A comparison of the prestress losses estimated by the methods was performed for the Dismal Swamp Bridge girders, and the results are presented in the following sections. As discussed previously, the AASHTO LRFD Refined and Lump Sum, PCI-BDM, and NCHRP 496 Refined and Approximate methods account for compressive strength, and Table 2 relates the methods for estimating prestress losses to the appropriate creep and shrinkage models.

## Predicted Prestress Losses

The predicted losses for the Dismal Swamp Bridge are presented in Table 15. The estimated total losses range from 31.3 ksi for the NCHRP 496 Approximate method to 58.7 ksi for the AASHTO Standard Specification Lump Sum method, however the AASHTO Standard Specification Lump Sum method estimates losses significantly higher than the next highest estimation of 43.6 ksi for the AASHTO LRFD Specification Lump Sum method. In addition, the PCI-BDM and NCHRP methods, which are correlated to high strength concrete, predict lower losses than do the other traditional methods. The last column in Table 16 gives the predicted strains in the girders after all losses have occurred for comparison to the measured strains.

**Table 15 – Predicted Prestress Losses for the Dismal Swamp Bridge**

Method	Initial Losses		Long-Term Losses			Total	P/S Centroid Strain
	Initial Rel.	ES	Shrinkage	Creep	Add'l Rel.		
	ksi	ksi	ksi	ksi	ksi		
AASHTO Standard General	1.7	12.0	5.8	19.5	3.6	42.6	-1,308
AASHTO Standard Lump Sum			45.0			58.7	-1,873 <sup>#</sup>
AASHTO LRFD Refined			12.9	11.7	3.1	41.4	-1,283
AASHTO LRFD General			5.8	19.5	3.0	42.0	-1,308
AASHTO LRFD Lump Sum			30.0			43.7	-1,368 <sup>*</sup>
PCI-BDM			8.3	8.3	2.8	33.1	-1,003
NCHRP 496 Refined <sup>**</sup>			6.7	9.8	2.5	32.7	-999
NCHRP 496 Approximate			17.6			31.3	-954 <sup>+</sup>
PCI-1975			9.8	12.7	3.3	39.5	-1,210

<sup>#</sup> - Additional steel relaxation losses of 3.6 ksi assumed per AASHTO Standard General method

<sup>\*</sup> - Additional steel relaxation losses of 3.0 ksi assumed per AASHTO LRFD General method

<sup>+</sup> - Additional steel relaxation losses of 2.4 ksi assumed per Tadros et al., 2003.

<sup>\*\*</sup> - NCHRP 496 Refined shrinkage losses include the prestress gain due to differential shrinkage, and the creep losses include the elastic gain due to the deck slab.

### Comparison of Predicted and Measured Prestress Losses

Table 16 presents a comparison of the predicted and measured prestress losses for the Dismal Swamp Bridge. The losses are broken into losses occurring before and after deck placement for the models that allow the prediction of losses at any time (see Table 2), and the long-term prestress losses presented in Table 16 do not include steel relaxation losses. For the estimated losses to be compared to the losses determined from the measured strains, the strain at the end of service life for the bridge girders, which is assumed to be 75 years, must be estimated. The limited strain data collected after deck placement is insufficient to fit a logarithmic curve and yield a reasonable estimate of the strain at 75 years. Using this technique results in an estimated strain at 75 year of over 2,000 microstrain, which correlates to total losses of over 60 ksi, and this is certainly not the case for the Dismal Swamp Bridge. Instead, it is assumed that the Dismal Swamp Bridge girders will undergo a change in strain between deck placement and 75 years similar to Girders F, T, and U from the Pinner's Point Bridge since the measured losses of the two bridges are similar, and the strain behavior shortly after deck placement is similar. Therefore, the change in strain between deck placement and 75 years for the Dismal Swamp Bridge is estimated to be 260 microstrain, which when added to the strain after deck placement of 820 microstrain, results in a strain at 75 years of 1,080 microstrain. A change in strain of 260 microstrain between deck placement and 75 years is determined by setting the ratio of the change in strain for the Dismal Swamp Bridge to the change in strain for Pinner's Point Girders F, T, and U after deck placement equal to the ratio of the change in strain for the two bridges prior to deck placement. This produces proportional losses between transfer and deck placement and deck placement and 75 years for the Dismal Swamp Bridge and Girders F, T, and U of the Pinner's Point Bridge. The measured losses presented in Table 17 are then determined from the measured strains and the estimated strain at the end of service life as the change in strain times the elastic modulus of the prestressing strand.

**Table 16 – Comparison of Predicted and Measured Prestress Losses (excluding relaxation) for the Dismal Swamp Bridge**

Method	Elastic Shortening	Loss From Transfer To Deck	Elastic Gain Due To Deck	Loss After Deck	Total Long-Term Loss	Total Loss	Ratio of Predicted to Meas.
	Ksi	ksi	ksi	ksi	ksi	ksi	
AASHTO Standard General	12.0	--	-2.3	--	25.3	37.3	1.21
AASHTO Standard Lump Sum		--		--	41.4	53.4	1.73
AASHTO LRFD Refined		21.2		5.7	24.6	36.6	1.19
AASHTO LRFD General		--		--	25.3	37.3	1.21
AASHTO LRFD Lump Sum		--		--	27.0	39.0	1.27
PCI-BDM		16.7		2.2	16.6	28.6	0.93
NCHRP 496 Refined		19.5		-0.7	16.5	28.5	0.93
NCHRP 496 Approximate		--		--	15.2	27.2	0.88
PCI-1975		20.0		4.8	22.5	34.5	1.12
Measured		15.7*		10.2	-2.5	7.4	15.1

\* - The elastic shortening losses are estimated from strain measurements taken 4 to 6 hours after the transfer of prestress because the data logger was disconnected prior to transfer so the girder side forms could be stripped

The PCI-BDM and NCHRP 496 methods for estimating prestress losses, which are correlated to high strength concrete, under-estimate the measured losses of the Dismal Swamp Bridge, predicting between 88% and 93% of the measured losses, and the PCI-BDM and NCHRP 496 Refined methods are the only methods that predict the total losses within 10% of the measured losses. The other methods examined over-estimate the measured losses by 12% to 73%, with the AASHTO LRFD Lump Sum method as the only method that over-estimates the losses by more than 27%. Of the methods formulated for normal strength concrete, the PCI-1975 method most accurately predicts the total losses, predicting 12% more losses than measured. However, the limited strain measurements after deck placement provide only a rough estimate of the total losses, and more time must pass before the estimate can be refined.

Although the PCI-BDM and NCHRP 496 Refined methods predict the measured losses within 7% at the end of service life, the distribution of the losses over the life of the girders for these methods and the methods formulated using normal strength concrete data does not match the measured losses. The measured losses between transfer and deck placement are 10.2 ksi, which is 40% less than the lowest estimate of these losses (16.7 ksi for the PCI-BDM method). The estimated losses after deck placement are 7.4 ksi, and are estimated within 3 ksi by the AASHTO LRFD Refined and PCI-1975 methods; however, the methods formulated using high strength concrete over-estimate the contribution of creep recovery and differential shrinkage, and predict losses far below the measured losses between deck placement and the end of service life. The NCHRP 496 method, in fact, predicts a 0.7 ksi gain in the prestressing force between deck placement and the end of service life due to creep recovery and differential shrinkage.

In addition to the difference between the measured and estimated long-term losses, there is a significant difference in the measured and predicted elastic loss at detensioning. The estimated elastic shortening losses (12.0 ksi) are only 76% of the measured elastic shortening losses (15.7 ksi), indicating that either the elastic modulus or the prestressing force at release are not known with enough accuracy to better predict the initial losses. Elastic shortening losses of 15.7 ksi indicate a modulus of 3,300 ksi at release; however, the estimated modulus at release of

4,450 ksi was determined using a unit weight of 150 pcf and a compressive strength of 6,500 ksi, which modeled the elastic moduli measured during the laboratory testing of the concrete creep and shrinkage characteristics within 3%. The estimated gain in the prestressing force due to deck placement is 92% of the measured gain in prestressing force. This indicates that the estimates of the elastic modulus of the girder at the time of deck placement and the estimate of the deck weight moment are reasonable for this bridge. ASTM C469 indicates that the expected variation in the elastic modulus between different batches of the same concrete is 5%, and a similar variation, if not more, is expected in the determination of the deck weight moment due to variations in the unit weight of the deck concrete and in the slab geometry.

### Summary of Long-Term Strain and Prestress Loss Predictions

The preceding sections present the results of long-term strain measurements for one HPLWC bridge and two HPC bridges in Virginia. Tables 17 and 18 summarize the creep and shrinkage models and methods for estimating prestress losses, respectively. Tables 17 and 18 also indicate which models include lightweight concrete, which models were developed for high strength concrete, and which models include concrete strength. Table 2 also summarizes the methods for estimating prestress losses and indicates which creep and shrinkage model, if any, is used by each method.

**Table 17 – Summary of Creep and Shrinkage Models**

Model	Includes LWC	Developed for HPC	Concrete Strength Factor
ACI-209	Yes	No	None
PCI-BDM	No	Yes	Creep and Shrinkage
CEB-FIP MC90	No	No	Creep and Shrinkage
AASHTO LRFD	No	No	Creep
Shams and Kahn	No	Yes	Creep
NCHRP 496	No	Yes	Creep and Shrinkage
B3	No	No	Creep and Shrinkage
GL2000	No*	No	Shrinkage
AFREM	No	No	Creep <sup>+</sup> and Shrinkage
PCI-1975	Yes	No	None

\* - Aggregate stiffness is included

<sup>+</sup> - Only for concrete that include microsilica

**Table 18 - Summary of Prestress Loss Methods**

Method	Includes LWC	Developed for HPC	Concrete Strength Factor
AASHTO Standard General	No	No	No
AASHTO Standard Lump Sum	No	No	No
AASHTO LRFD Refined	No	No	Yes*
AASHTO LRFD General	No	No	No
AASHTO LRFD Lump Sum	Yes	No	Yes
PCI-BDM	No	Yes	Yes*
NCHRP 496 Refined	No	Yes	Yes*
NCHRP 496 Approximate	No	Yes	Yes
PCI-1975	Yes	No	No

\* - Included in the creep and/or shrinkage model

The HPLWC shows different behavior when compared to the creep and shrinkage models than does the normal weight HPC investigated. The models all over-estimate the measured strains of both the HPLWC test girders and the Chickahominy River Bridge girders. The Shams and Kahn model is the best predictor of the strains measured in the HPLWC bridge girders, predicting the average strain of the bridge girders reasonably well. The PCI-1975 model predicts strains that produce a reasonable lower bound for the measured strains for the HPLWC bridge girders, and is the best overall predictor of the strains for the HPLWC test girders.

For the three sets of normal weight HPC girders investigated, the models tend to under-predict the measured strains at early ages and over-predict the measured strains at later ages, with the exception of the GL2000 model which consistently over-predicts the measured strains throughout the modeled period by a large margin. The B3 and AFREM models are the best predictors for both sets of the Pinner's Point girders, and in general, the models that account for compressive strength predict the strains of the 10,000 psi girders better than the strains of the 8,000 psi girders. In addition, since both sets of girders from the Pinner's Point Bridge exhibit similar strains, it is likely that the models accounting for compressive strength would predict the strains of the 8,000 psi girders better by assuming a 10,000 psi compressive strength. This indicates that compressive strength is not the best property to use to adjust the long-term models for HPC; however, it is a simple parameter to measure and is generally known at the design stage, which is why it is used by each of the recently developed models. Finally, for the Dismal Swamp girders, the B3 model is the best predictor of the measured strains.

Overall, when examining the girders from all three bridges no one model consistently predicts the strains of each set of girders. The PCI-BDM model is the only model to be ranked in the top half of the 10 models for each of the four sets of bridge girders, indicating that it is the most consistent predictor of the measured strains over the whole observed period. Examining the strains at the end of the modeled period as an approximation of the strains at the end of service life, the PCI-BDM and NCHRP 496 models are the best predictors for the three sets of normal weight HPC girders and the Shams and Kahn and PCI-1975 model are the best predictors for the HPLWC girders. It is clear from this comparison that a single model is not well suited to both lightweight and normal weight HPC without some modification for lightweight concrete.

As important as the strain predictions, if not more important, are the prestress loss estimations examined and compared to the measured losses. The traditional methods of prestress loss estimation provided in the AASHTO Standard and LRFD Specifications all over-predict the measured losses for the three bridges by as little as 18% and as much as 98%. The PCI-1975 method also over-predicts the measured losses by 12% to 23%, but provides the closest estimate to the measured losses for the HPLWC bridge girders. The methods correlated to high strength concrete, in general, predict the long-term losses better than the traditional methods. For the three sets of normal weight girders, the PCI-BDM is the most consistent predictor of the long-term losses, and is the only method that estimates losses within 10% of the measured losses for all three sets of girders. The NCHRP 496 Refined method under-predicts the long-term losses for all three sets of girders, estimating between 82% and 98% of the measured losses, and the NCHRP 496 Approximate method under-estimates the losses of the Dismal Swamp and 10,000 psi Pinner's Point girders by 12% and 8%, respectively, and over-estimates the long-term losses of the 8,000 psi Pinner's Point girders by 6%. Finally, the PCI-BDM and NCHRP 496 Refined

and Approximate methods over-estimate the losses of the HPLWC bridge by 18%, 20%, and 22%, respectively.

Although the PCI-BDM and NCHRP 496 methods provide the best estimates for the total losses, the distribution of the long-term losses throughout the life of the girder is not estimated accurately. The losses between transfer and deck placement are over-estimated by these methods, and the traditional methods. The estimated losses between transfer and deck placement are more than three times the measured losses for the HPLWC girders, two times the measured losses for the Pinner's Point girders, and one-and-a-half times the measured losses for the Dismal Swamp girders. The PCI-BDM and NCHRP 496 methods are then able to predict the total losses with better accuracy because they under-estimate the measured losses after deck placement by a similar margin. In fact, the NCHRP 496 Refined method predicts a small prestress gain between deck placement and the end of service life for the Pinner's Point Bridge and the Dismal Swamp Bridge, which is not observed in the measured strains.

## **CONCLUSIONS AND RECOMMENDATIONS**

The following conclusions and recommendations are made based on the results and analyses presented in the preceding chapters.

### **Creep and Shrinkage Modeling Conclusions**

- The Shams and Kahn model is the best overall predictor of strain for the HPLWC bridge girders and is also the best predictor of strain at the end of the observed period.
- The PCI-1975 model yields similar results to the Shams and Kahn model for the HPLWC bridge girders, and is the best predictor of strain for the HPLWC test girders.
- The B3 model is the best predictor of strain for the normal weight HPC investigated. However, this model is not well suited to design since it requires significant knowledge of the concrete proportions, including the cement content, the aggregate-to-cement ratio, and the water-to-cementitious materials ratio.
- The AFREM model yields similar results to the B3 model without significant knowledge of the concrete mixture proportions.
- The PCI-BDM and NCHRP 496 models also predict the strains reasonably well at the end of the observed period for the normal weight HPC.
- The PCI-BDM model is the most consistent predictor of strain when analyzing both the HPLWC and the normal weight HPC.
- In general, the models correlated to HSC, Shams and Kahn, PCI-BDM, and NCHRP 496, predict the girder strains better than the traditional models.

- Curve fitting the laboratory data and adjusting the developed model for the average humidity at the bridge site and size of the bridge girders, shows that these correction factors do not fully account for the changes in creep and shrinkage behavior as measured in the field. However, the factors used by the ACI-209 model more accurately represent the changes in behavior of the normal weight HPC of this study than do the factors contained in the AASHTO LRFD Specification (AASHTO, 1998)

### **Prestress Loss Estimation Conclusions**

- The methods for estimating prestress losses presented in the AASHTO Standard (AASHTO, 1996) and LRFD (AASHTO, 1998) Specifications, over-estimate the measured total losses for each set of girders by 18% (5 ksi) to 98% (27 ksi).
- The PCI-1975 method for estimating prestress losses is the best predictor of the measured total losses for the HPLWC girders, over-estimating the measured losses by 17% (6 ksi).
- The PCI-BDM method for estimating prestress losses is the most consistent predictor of the measured total losses, estimating within  $\pm 10\%$  (3 ksi) for the normal weight HPC and over-estimating the measured total losses of the HPLWC by 18% (6 ksi).
- The NCHRP 496 Refined and Approximate methods for estimating prestress losses predict within  $\pm 18\%$  (5 ksi) for the normal weight HPC and over-predict the measured total losses of the HPLWC by less than 22% (8 ksi).

### **Recommendations and Future Research**

- The NCHRP 496 Refined and Approximate methods for estimating prestress losses are recommended for estimating the prestress losses at the end of service life for girders utilizing normal weight HPC similar to that used in this study. Continued use of the AASHTO Standard and LRFD Specifications is overly conservative but acceptable until the NCHRP 496 methods are adopted by AASHTO.
- It is recommended that VDOT begin using the NCHRP 496 method for prestress loss calculations as soon as AASHTO adopts it as part of the AASHTO LRFD Fourth Edition or as an interim specification. This may allow VDOT to avoid adopting the AASHTO LRFD method for prestress loss calculation for a short period of time.
- The NCHRP 496 methods are recommended because they predict similar losses to the PCI-BDM method, are no more than 5 ksi unconservative (2.5% of the jacking stress), and are scheduled for inclusion into the next revision of the AASHTO LRFD Specification.
- Further investigation of the HPLWC is needed. The measured strains in the HPLWC girders varied by approximately 200 microstrain from girder to girder, which is more than twice the variation between girders seen with the normal weight HPC. This is

likely due to variations in the concrete batches because of the precasters' unfamiliarity with the lightweight aggregates used in the concrete mixture.

- In the interim, the NCHRP 496 Refined and Approximate methods can be used to conservatively estimate the total losses for girders utilizing the HPLWC analyzed in this study.
- Further investigation of the early age behavior of the normal weight HPC analyzed in this study is needed. For the normal weight HPC considerably more strain was measured prior to 30 days after transfer than predicted by the models. The elastic shortening strains (determined from measurements taken two to four hours after detensioning) were also larger than the elastic strains estimated from the measured concrete properties.
- Further investigation of the behavior of the bridge girders after deck placement is also needed. Each instrumented girder exhibited a nearly flat strain curve prior to deck placement indicating that creep and shrinkage had nearly ceased. However, after deck placement instead of exhibiting decreasing compressive strains, as would be caused by creep recovery and differential shrinkage, the girders showed increasing compressive strains for a period of approximately 100 days following deck placement.
- The effect of continuity on the strains and prestress losses in the girders after deck placement also should be investigated. The time step procedure in this research modeled the girders as simply supported throughout the observed period, and as a result, the effect of differential shrinkage on prestress loss was likely over-estimated.
- Finally, the Dismal Swamp Bridge should continue to be monitored to better estimate the total losses at the end of service life. There is currently not enough data after deck placement to reasonably extrapolate the total losses at 75 years using a logarithmic curve fit.
- A method for verifying vibrating wire gage data should be employed.

## **COSTS AND BENEFITS ASSESSMENT**

The two types of bridge super-structures used by VDOT in short and medium span bridges are structural steel and pre-tensioned, prestressed girders with reinforced concrete decks. This report evaluates methods (one presently used by VDOT and two proposed methods) for calculating prestress losses in pretensioned, prestressed bridge girders. The method presently used by VDOT is found in the AASHTO Standard Specification for Highway Bridges but VDOT will be transitioning to the AASHTO LRFD Specification for Highway Bridges over the next two years. AASHTO is in the process of adopting NCHRP 496 as part of the AASHTO LRFD Specification. The findings of this report show that both the AASHTO Standard Specification method and the AASHTO LRFD method for calculation of prestress losses are overly

conservative which in many cases will lead to overly conservative designs of prestressed bridge girders. However, the findings also show that the NCHRP 496 method yields conservative designs but not overly so. By adopting the NCHRP 496 method as soon as it is adopted by AASHTO, VDOT can begin producing more efficient prestressed girder designs.

## REFERENCES

- American Association of State Highway and Transportation Officials (AASHTO), (1996). *Standard Specification for Highway Bridges: Sixteenth Edition*. Washington, D.C.
- American Association of State Highway and Transportation Officials (AASHTO), (1998). *LRFD Specification for Highway Bridges: Second Edition*. Washington, D.C.
- American Concrete Institute (ACI), (1992). Prediction of creep, shrinkage, and temperature effects in concrete structures. *Manual of Concrete Practice, ACI 209R-92*, Farmington Hills, MI.
- Ahlborn, T. M., French, C. E., and Leon, R. T., (1995). Applications of high-strength concrete to long-span prestressed bridge girders. *Transportation Research Record*, 1476, 22-30.
- Alexander, M. G., (1996). Aggregates and the deformation properties of concrete. *ACI Materials Journal*, 93(6), 569-577.
- American Society for Testing and Materials (ASTM), (2001). "C 469 – 94: Standard test method for static modulus of elasticity and Poisson's ratio of concrete in compression. *Annual Book of ASTM Standards*, 04.02, 248-251.
- Bazant, Z. P. and Baweja, S., (1995a). Creep and shrinkage prediction model for analysis and design of concrete structures-model B3, RILEM recommendations. *Materials and Structures*, 28, 357-365.
- Bazant, Z. P. and Baweja, S., (1995b). Justification and refinements of model B3 for concrete creep and shrinkage 1. Statistics and sensitivity. *Materials and Structures*, 28, 415-430.
- Bazant, Z. P. and Baweja, S., (1995c). Justification and refinements of model B3 for concrete creep and shrinkage 2. Updating and theoretical basis. *Materials and Structures*, 28, 488-495.
- Chern, J. C. and Chan, Y. W., (1989). Deformations of concretes made with blast furnace slag cement and ordinary portland cement. *ACI Materials Journal*, 86(4), 372-382.
- Collins, M. P. and Mitchell, D., (1991). *Prestressed Concrete Structures*, Prentice Hall, Englewood Cliffs, NJ.

- Collins, T. M., (1989). Proportioning high strength concrete to control creep and shrinkage. *ACI Materials Journal*, 86(6), 567-580.
- Comite Euro-Internationale du Beton (CEB), (1990). CEB-FIP model code 1990. *Buletin D'Information No. 213/214*, Lausanne, Switzerland.
- Gardener, N. J. and Lockman, M. J., (2001). Design provisions for drying shrinkage and creep of normal-strength concrete. *ACI Materials Journal*, 98(2), 159-167.
- Gross, S. P. and Burns, N. H., (1999). Field performance of prestressed high performance concrete bridges in Texas. *Research Report 580/589-2*, Center for Transportation Research, University of Texas at Austin, Austin, TX.
- Greuel, A., Rogers, B. T., Miller, R. A., Shahrooz, B. M., and Baseheart, T. M., (2000). Evaluation of a high performance concrete box girder bridge. Research Report, University of Cincinnati, Cincinnati, OH.
- Kahn, A. A., Cook, W. D., and Mitchell, D. (1997). Creep, shrinkage, and thermal strains in normal, medium, and high strength concrete during hydration. *ACI Materials Journal*, 94(2), 156-163.
- Kebraei, M., Luedke, J., and Azizinamini, A. A., (1997). High performance concrete in 120<sup>th</sup> and Giles Bridge, Sarpy County, Nebraska. University of Nebraska, Lincoln, NE.
- Le Roy, R., De Larrard, F., and Pons, G. (1996). The AFREM code type model for creep and shrinkage of high-performance concrete. Proceedings of the 4<sup>th</sup> International Symposium on Utilization of High-Strength/High-Performance Concrete, Paris.
- Lopez, M., Kahn, L. F., Kurtis, K. E., and Lai, J. S., (2003). Creep, shrinkage, and prestress losses of high-performance lightweight concrete: final report – lightweight concrete for high strength/high performance precast prestressed bridge girders. Structural Engineering, Mechanics, and Materials Research Report No. 00-1, Georgia Institute of Technology, Atlanta GA.
- Mak, S. L., Foster, G., Chirgwin, G., and Ho, D. W. S., (1997). Properties of high-performance heat-cured slag cement concrete for bridge structures. Proceedings of the 3<sup>rd</sup> CANMET/ACI International Conference, Kuala Lumpur, Malaysia, 821-830.
- McHenry, D. (1943). A new aspect of the creep in concrete and its applications to design. *ASTM Proceedings*, 43, 1069-1084.
- Mokhtarzadeh, A. and French, C., (2000). Time-dependent properties of high-strength concrete with consideration for precast applications. *ACI Materials Journal*, 97(3), 263-271.

- Mossiosian, V. and Gamble, W. L., (1972). Time-dependent behavior of non-composite and composite prestressed concrete. Federal Highway Administration, Illinois State Division of Highways, Urbana, IL.
- Nassar, A., (2002). Investigation of transfer length, development length, flexural strength, and prestress losses in fully bonded high strength lightweight prestressed girders. Master's Thesis, Via Dept. of Civil and Environmental Engineering, Virginia Polytechnic Institute and State University, Blacksburg, VA.
- Neville, A. M., (1970). *Creep of Concrete: Plain, Reinforced, and Prestressed*. North-Holland Publishing Company, Amsterdam, Holland.
- Neville, A. M., Dilger, W. H., and Brooks, J. J., (1983). *Creep of Plain and Reinforced Concrete*. Construction Press, New York.
- Ozyildirim, C. and Gomez, J., (1999). High-performance concrete in a bridge in Richlands, Virginia. *Virginia Transportation Research Council Report No. FHWA/VTRC00-R6*, VTRC, Charlottesville, VA.
- Pessiki, S., Kaczinski, M., and Wescott, H. H., (1996). Evaluation of effective prestress force in 28-year old prestressed concrete bridge beams. *PCI Journal*, 41(5) 78-89.
- Precast/Prestressed Concrete Institute (PCI), (1997). *Bridge Design Manual*, Chicago, IL.
- Precast/Prestressed Concrete Institute (PCI) Committee on Prestress Losses, (1975). Recommendation for estimating prestress losses. *PCI Journal*, 20(4), 43-75.
- Roller, J. J., Russell, H. G., Bruce, R. N., and Martin, B. T., (1995). Long-term performance of prestressed, pretensioned high strength concrete bridge girders. *PCI Journal*, 40(6), 48-59.
- Seguirant, S. J., and Anderson, (1998). New deep WSDOT standard sections extend spans of prestressed concrete girders. *PCI Journal*, 43(4), 92-119.
- Shah, S. P. and Ahmad, S. H., (1994). *High Performance Concrete: Properties and Applications*. McGraw-Hill, New York.
- Shams, M. K. and Kahn, L. F., (2000). Time-dependent behavior of high-strength concrete: task 3, use of high strength/high performance concrete for precast prestressed concrete bridges in Georgia. Structural Engineering, Mechanics, and Materials Research Report No. 00-1, Georgia Institute of Technology, Atlanta GA.
- Shenoy, C. V. and Frantz, G. C., (1991). Structural test of 27-year old prestressed concrete bridge beams. *PCI Journal*, 36(5), 80-90.

- Stanton, J. F., Barr, P., and Eberhard, M. O., (2000). Behavior of high-strength HPC bridge girders. Research Report, University of Washington, Seattle, WA.
- Smadi, M. M., Slate, F. O., and Nilson, A. H., (1987). Shrinkage and creep of high, medium, and low strength concretes, including overloads. *ACI Materials Journal*, 84(3), 224-234.
- Tadros, M. K., Al-Omaishi, N., Seguirant, S. J., and Gallt, J. G., (2003). Prestress losses in pretensioned high-strength concrete bridge girders. *NCHRP Report 496*, National Cooperative Highway Research Program, Transportation Research Board, National Research Council.
- Townsend, B. (2003). Creep and shrinkage of a high strength concrete mixture. Master's Thesis, Via Dept. of Civil and Environmental Engineering, Virginia Polytechnic Institute and State University, Blacksburg, VA.
- Vincent, E. C. (2003). Compressive creep of a lightweight concrete mixture. Master's Thesis, Via Dept. of Civil and Environmental Engineering, Virginia Polytechnic Institute and State University, Blacksburg, VA.
- Waldron, C. J. (2004). Investigation of Long-Term Prestress Losses in Pretensioned High Performance Concrete Girders. PhD Dissertation, Via Dept. of Civil and Environmental Engineering, Virginia Polytechnic Institute and State University, Blacksburg, VA.